Published in final edited form as:

Chem Rev. 2015 June 10; 115(11): 4571–4606. doi:10.1021/cr400659h.

Organic−Inorganic Hybrid Nanocomposite-Based Gas Sensors for Environmental Monitoring

Ajeet Kaushik[*,†,‡], **Rajesh Kumar**[*,‡,§], **Sunil K. Arya**[‖], **Madhavan Nair**[†], **B. D. Malhotra**[⊥], **Shekhar Bhansali**[‡]

[†]Center for Personalized Nanomedicine, Institute of Neuroimmune Pharmacology, Department of Immunology, Herbert Wertheim College of Medicine, Florida International University, Miami, Florida 33199, United States

[‡]Bio-MEMS Microsystems Laboratory, Department of Electrical and Computer Engineering, College of Engineering, Florida International University, Miami, Florida 33174, United States

[§]Department of Physics, Panjab University, Chandigarh 160014, India

[‖]Bioelectronics Program, Institute of Microelectronics, A*Star, 11 Science Park Road, Singapore Science Park II, Singapore

[⊥]Department of Biotechnology, Delhi Technological University, Shahbad Daulatpur, Delhi 110042, India

Graphical Abstract

[*]**Corresponding Authors:** ajeet.npl@gmail.com (A.K.), rajeshbaboria@gmail.com (R.K.).

The authors declare no competing financial interest.

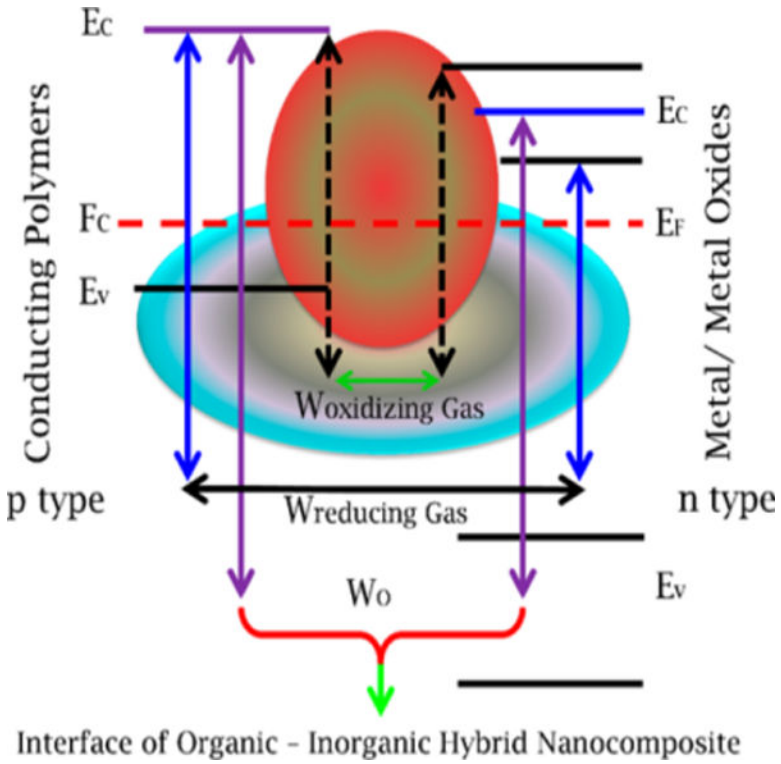

1. INTRODUCTION

Rapidly increasing environmental pollution has been recognized as a major concern, and its monitoring has become a priority area for human health.[1–4] This fact has led efforts to find new and user-friendly techniques for the detection of gases hazardous to the environment and human health.[5] Gas sensors (Figure 1) have become one of the key technologies for rapid, selective, sensitive, and e*ffi*cient detection of gases (at ppt level), chemical vapors (at ~1 ppb), and explosives (at ~5 ppm).[6,7] The commercialization of gas sensors for environmental and personalized health monitoring is growing rapidly.[8] The field of gas sensing device development remains an area of active research interest due to the urgent need for reliable, miniaturized, low-cost, and portable sensing systems for health care and security.[9] The current state of the art in chemical sensors for gas detection has been discussed in reviews by Janata,[10] Korotcenkov,[11] and Stetter.[12]

Gas sensors based on organic conducting polymers (such as polyaniline (PANI),[13,14] polypyrrole (PPy),[15] polythiophene (PTh),[16] etc.) of desired functionality and conductivity continue to improve gas sensing performance.[17–24] However, due to the high a*ffi*nity of conducting polymers toward volatile organic compounds (VOCs) and moisture present in the environment, they are sometimes unstable and exhibit poor sensitivity.[25,26] On the other hand, gas sensors made from inorganic metal oxides, such as tungsten oxide (WO_3), zinc oxide (ZnO), tin oxide (SnO_2), titanium oxide (TiO_2), iron oxide (Fe_2O_3/Fe_3O_4), silicon oxide (SiO_2), etc., show improved sensing characteristics due to changing oxygen stoichiometry and electrically active surface charge.[27–31] However, these gas sensors usually

operate at very high temperatures (~300–400 °C), frequently leading to baseline drift and oxidation of analytes.[32] In spite of the high sensitivity, the use of such gas sensors for practical applications is very limited.

Issues related to low conductivity and poor stability of organic materials, and the high-temperature operation and complicated processability of inorganic materials, hinder their use in gas sensor fabrication. The use of hybrid nanocomposites of these two classes of materials may result in gas sensors with improved and e*ffi*cient gas sensing characteristics. It has been predicted that host−guest chemistry combined with the use of organic and inorganic counterparts in hybrid nanocomposite forms may help to eliminate their particular drawbacks due to synergetic/complementary effects, leading to development of improved gas sensing devices. These nanocomposite materials have recently aroused extensive interest in gas sensing applications. This review focuses on organic−inorganic hybrid nanocomposite-based gas sensors for environmental monitoring. Additionally, efforts have been made to discuss the gas sensing mechanism of organic−inorganic hybrid nanocomposites and humidity sensing applications. However, better control is required for commercialization of nanostructure-based gas sensors.[33,34]

2. ORGANIC−INORGANIC HYBRID NANOCOMPOSITES: SMART ADVANCED FUNCTIONALZED MATERIALS FOR GAS SENSING

The field of organic−inorganic hybrid nanocomposites is a rapidly growing area of research in advanced functional materials science (Figure 2). These materials are made of nanoscaled organic and inorganic counterparts, wherein the interaction at molecular level generates unique properties at the interface. In nanocomposites, inorganic nanostructures can be three-dimensional, two-dimensional, one-dimensional, or zero-dimensional nanomaterials. Since 1995, the research group of Sanchez has been exploring the origin, fundamentals, advancements, prospects, and possible applications of organic−inorganic hybrid nanocomposites.[35–47] This group has explored transition-metal-based hybrid organic−inorganic structures and proposed this area of research as a multidisciplinary field.[35,36] Design of organic−inorganic hybrid nanocomposites using fundamental nanobuilding blocks (NBB), studies of their properties (i.e., optical, electrical, mechanical, and electrical) along with their nanophotonics application have also been explained.[38,39,48–50] The controlled and improved properties generated at the interfaces via molecular and supramolecular dynamics of hybrid organic−inorganic nanocomposites and formation of various mesoporous hybrid nanocomposites have been studied by this research group.[41,42,47,51] In 2005, the various applications of hybrid organic−inorganic nanocomposites were reported by Sanchez et al.[43] These authors proposed a number of organic−inorganic composite systems and advanced hybrid platforms along with their prospects from laboratory to market.[45] The molecular and surface engineering of organic−inorganic hybrid nanocomposite systems in order to improve the properties needed for various applications has also been highlighted by this research group.[44–47]

The properties of hybrid nanocomposite materials depend not only on the properties of their individual constituents, but also on their morphology and interfacial characteristics.[52–56]

Comprehensive studies of organometallic compounds have led to increased interest in understanding the interactions of organic and inorganic moieties, and have generated unique properties at interfaces. Further, heterogeneous or homogeneous mixing, suspension, and cross-linking of organic and inorganic components produce interesting composite materials with commercial prospects. Significant efforts have been focused on the ability to obtain nanostructures of desired shape, size, and properties using innovative synthesis approaches.[57] The surface modification and functionalization of nanoparticles, covalent attachment, self-assembly, and ease of organization on the surfaces provide a means to generate nanocomposite materials with tunable surface properties.[52,57] Efforts are continuing toward the preparation of new nanocomposite materials to obtain novel properties.[53,57–59] There is a strong interest in using nanometal or metal oxides as additives in the functionalization of polymers (conducting/biopolymer), and significant research has been undertaken in nanocomposite science for device applications.[60,61] Experimental studies have shown that incorporation of inorganic nanomaterials into polymer matrices leads to organic–inorganic nanocomposites with enhanced and improved properties. Nanocomposites offer diverse properties that are absent in their precursors materials, e.g., flexible-mechanical and superconducting properties due to interfacial interactions between the two phases.[39,62–68] Therefore, nanocomposites have been predicted to have a wide range of applications, e.g., high-energy radiation shielding materials, microwave absorbers, optical limiters, polarizers, and hydrogen storage systems.[57,63–68]

A promising and demanding area of research relates to the utilization of organic−inorganic hybrid nanocomposites as gas sensing materials.[69,70] Many reports pertaining to adsorption of gas molecules onto mesoporous ordered organic−inorganic nanocomposite frameworks have been explored since 1990.[68] The effects of parameters such as surface area, pore volume, and pore size on the properties of these materials are still a matter of considerable interest, in order to achieve selective and sensitive detection. Other than interfacial interactions, control of nanostructure morphology is an important aspect that influences the nanocomposite performance. Hence, in a nanocomposite development effort, a long-term goal is to develop new synthetic strategies to control the size, shape, morphology, and composition. This control allows the tuning of nanocomposite properties.[61] The adopted methods to synthesize hybrid nanocomposites of desired properties and application are discussed below.

2.1. Preparation Methods of Organic−Inorganic Nanocomposites

Depending on the nature of the metal or metal oxide and polymer structure, these processes are likely to result in the incorporation of inorganic nanomoieties into the polymer backbone via different electrostatic interactions.[61] Recently, it has been demonstrated that it is possible to develop suitable techniques for these materials, which are often sufficient to yield high-quality nanocomposite films.[61,63,65] The hybrid nanocomposite thin films containing metal or semiconductor nanocrystals and polymers exhibit porous structures.[64] This enables gaseous molecules from the environment to readily penetrate into the polymer matrix and be adsorbed onto the nanocrystals of the nanocomposite film, resulting in strong sensing behavior.[52,58,61,68]

Many techniques such as sol−gel, self-assembly, evaporation deposition, chemical and electrical techniques can be used to fabricate organic−inorganic hybrid nanocomposite thin films.[71–74] Sanchez et al.[40] have described in detail the various strategies (A−E, Figure 3) to synthesize organic−inorganic hybrid nanocomposites of desired architecture and properties for a variety of applications with possible commercial market prospects. Well-defined nonaggregated nano-objects/NBBs were synthesized using path A via controlled reactivity of molecular precursors (metal alkoxides, metal−organic or organometallic compounds, inorganic salts, etc.). The controlled reactivity allows the understanding of nucleation, growth, and aggregation among precursors in water, organic solvents, inorganic molten salts, ionic liquids, gels, xerogels, etc. NBBs are nanoparticles, nanolamellar compounds (clays, layered double hydroxides, lamellar phosphates, oxides, chalcogenides, etc.) with strong molecular interactions. The composition of NBBs can be fully inorganic or hybrid with organic moieties either included in the framework or located at the nano-object surface. For the last two decades, nanosized metals, metal oxides, metal chalcogenides, metal phosphides, and their hybridized associated derivatives with controlled shape, size, and tailored morphology have been synthesized by adopting path A.[39,45,46,51]

Soft chemistry based routes such as sol−gel chemistry have been followed using specific bridged and poly functionalized precursors such as silsesquioxanes $X_3Si\text{-}R'\text{-}SiX_3$ (R′ being an organic spacer, X = Cl, Br, −OR) for the synthesis of hybrid nanocomposites (path B). In this method, “sol” is prepared by dissolving an inorganic precursor in an appropriate solvent (e.g., various alcohols) and controlled addition of water under acidic or basic conditions to initiate the condensation reactions leading to oligomeric molecules or colloids that form a three-dimensional network by chemical reaction.[37,56,73,75–78] The condensation reactions, evaporation of a solvent, and aggregation of a species in the sol result in the formation of a gel that transforms into films on the desired substrate via spin coating, dipping, or spraying techniques. Next, the deposited film is cured at low temperature or annealed. The heat treatment is designed to remove any organic residues and water through evaporation, pyrolysis or combustion, as well as to provide densification. The tunable supramolecular chemical interactions yield hybrid materials with higher degrees of polymerization. For the deposition of an organic−inorganic hybrid film, care must be taken to heat the film below the decomposition point of the organic component.

Path C corresponds to hydrothermal or solvothermal synthesis routes generally performed in polar solvents to obtain crystallized material. In this method, the utilization of organic templates results in microporous hybrid materials such as organically templated zeolites.[34] These materials have already led to extensive applications in the fields of adsorbents and catalysts.[34] Recently, metal organic frameworks (MOFs), crystalline hybrids of polymers built from telechelic or polyfunctional spacers that coordinate metallic centers or metal-containing small oligomers have been developed.[51]

NBBs predicted to provide nanostructured hybrid networks with better structural definition can be synthesized using assembly or intercalation and/or dispersion (path D). The step-by-step preparation of nanobuilding components that are nanometric, monodispersed, and have well-defined structures and shapes, usually allows for a high level of control over their structure and properties. The NBB molecules retain their integrity in the

hybrid nanocomposites, wherein these can be preserved or capped using polymerizable ligands or connected through organic spacers of telechelic molecules, polymers, or functional dendrimers. Different assembling methods were used to synthesize various organic−inorganic hybrids of tunable electrical and optical properties which depend on the nature, structure, and functionality of the nanobuilding blocks.[51]

Path E explores the template-assisted organization and assembly of inorganic or hybrid networks grown using micelles, lyotropic liquid crystals, latex, or silica beads for the fabrication of mesostructured organic−inorganic hybrid composites. In practice, self-assembly of molecular or polymeric amphiphilic components coupled with sol−gel polycondensation reactions or with other colloidal-chemistry-based approaches can be used for growth. Periodically organized mesoporous hybrid silica with organic functionality within the walls was synthesized using path E, and exhibited a high degree of order. The presence of mesoporosity is an added advantage for further organic functionalization. These hybrids can be synthesized by the combination of self-assembly and NBB approaches.[45,46,51] Due to the use of NBBs, a large variety of organic−inorganic hybrid nanocomposites of tunable functionalities and properties can be synthesized via various chemical/molecular interactions (Figure 4). The synthetic approaches discussed above allow control of the shape, size, and properties of the organic–inorganic hybrid nanocomposites. The hybrid nanocomposites are currently being patterned or integrated in devices for applications that demand easy and effective synthesis and processing pathways (Figure 5).

Organic−inorganic hybrid films have recently been prepared via deposition under vacuum conditions, e.g., thermal evaporation and pulse polymerization techniques. The vacuum-deposited hybrid nanocomposite films can be used for fabrication of novel optoelectronic devices due to good repeatability and identical optical, electrical and molecular properties.[52,58,79–82] Organic−inorganic hybrid nanocomposite thin films are fabricated by the aforementioned techniques and can be used as sensing materials for various sensor configurations.[61,83,84] However, the problems pertaining to nanostructure fabrication using expensive sophisticated tools and thermal or temporal incompatibility between the organic and inorganic components during evaporation are still unresolved issues.

Electrical polymerization (Figure 6) is a widely used technique for thin film fabrication of conducting polymer (PANI, PPy, etc.)-metal (Au, CNT, Pt, graphene, etc.)/metal oxide (ZnO, TiO_2, ZrO_2, etc.) hybrid nanocomposites.[85] The heterogeneous electrochemical polymerization of monomers in the presence of an oxidant, dopant, and metal oxide nanoparticles has been performed using cyclic voltammetry.[86] During polymerization, the presence of metal oxide nano-particles inhibits the polymer-related oxidation process and diminishes the degradation products in the composite materials. Good adhesion of composite materials on the conducting substrate results in superior electro-active repetitive properties compared to that of a pure polymer. However, the problem pertaining to variation in optical and electrical properties continues to exist. To overcome this limitation, the electrophoretic deposition technique (two-step process) has been used, wherein the charged particles in a liquid first migrate toward an electrode under an electric field (electrophoresis).[80,87] In the second step, the particles are deposited on the electrode

surface from a homogeneous film via coagulation. The electrophoretic technique has recently gained prominence. It has been found to yield uniform, dense, and pinhole-free conducting polymer−metal/metal-oxide-based nanocomposite films. Electrochemically deposited nanocomposite films have been utilized for fabrication of organic light-emitting diodes, display devices, artificial fingerprint devices, photovoltaic applications, sensors, etc.[88,89]

The preparation of a hybrid nanocomposite sensing material with desired properties is dependent on the selection of the synthesis method. Thus, selection of an appropriate preparation technique is crucial to prepare a 3S, i.e., a stable, selective, and sensitive gas sensor. Optical,[90–94] field effect transistor (FET),[95,96] surface acoustic wave (SAW),[97–99] quartz crystal microbalance (QCM),[100] and electrochemical[92,101–104] (i.e., chemoresistor,[105,106] potentiometric,[107,108] and amperometric[12,109]) based gas sensors have contributed significantly to the state-of-the-art of environmental monitoring. The selection of sensor fabrication method and transduction technique is crucial to achieve desired sensing abilities. For example, electrochemical gas sensing techniques are suitable for miniaturized and wearable sensor fabrication.

It has been found that the electrical, optical, and molecular properties of organic−inorganic hybrid nanocomposites can be changed or tuned using an appropriate synthetic route and varying precursors/operational parameters. Moreover, these nanostructures have potentially been used for various technological applications. We herein focus on the gas sensing applications for environmental monitoring. Figure 7 illustrates the organic−inorganic hybrid nanocomposites used to detect gases. The next section focuses on the gas sensing mechanism of the organic−inorganic hybrid nanocomposites.

3. GAS SENSING PRINCIPLE OF ORGANIC−INORGANIC HYBRID NANOCOMPOSITES

The gas sensing behavior of organic−inorganic hybrid nanocomposite sensors obtained by estimating time dependent change in the magnitude of resistance as a function of gas concentration at room temperature is illustrated in Figure 8. It has been found that exposure of reducing/oxidizing gas molecules onto nanocomposite film results in a change of resistance. Simultaneously, gas flow is cut off and fresh air is introduced into a test chamber, thus leading to restoration of the original resistance value.[52] The observed change in the resistance is due to physical adsorption of the gaseous molecules onto the surface of the nanocomposite film. The interaction of gaseous molecules with a π electron network of a polymer that has embedded metal/metal oxide nanoparticles results in capture/donation of electrons, depending upon the nature of gaseous molecules, leading to the decrease/increase of the resistance.

The n-type metal oxide nanoparticles form a barrier layer with a polymer matrix leading to the formation of the depletion region. The interaction of the nanocomposite film surface with target gas molecules causes a change in the width of the depletion region (W_0) and therefore modulates the conductivity of the sensing element. The space charge region (W_{gas}) varies with the decrease or increase of electrons (by adsorption of gas molecules) in the

polymers, which in turn results in a conductivity change.[52] The modulation of the space charge region at the interface of the metal oxide nanoparticles with the polymer matrix results in enhanced sensitivity for the desired gas. On the basis of the energy band gap diagram (Figure 8), the gas sensing behavior of organic−inorganic nanocomposites can be understood with respect to the analyte.[52,110] The next section focuses on the application of these hybrid nanocomposites to detect toxic gases for environmental monitoring.

4. ORGANIC−INORGANIC HYBRID NANOCOMPOSITE-BASED GAS SENSORS FOR ENVIRONMENTAL MONITORING

The gas sensing potential of organic−inorganic hybrid nanocomposite sensors is discussed in this section. Advancement in sensing materials science and improvement in gas sensing parameters, such as detection limit, sensing range, response/recovery time, repeatability, and stability, are also briefly and critically discussed. Sensor fabrication using organic−inorganic systems for commercial prospects to improve environmental monitoring are also highlighted.

4.1. Organic−Inorganic Hybrid Nanocomposites for Volatile Organic Compounds (VOCs)

The evaluation of indoor air quality is presently a widespread environmental issue.[111,112] Indoor pollutants consisting of VOCs may cause environmental illness.[113,114] The effect of VOCs on human health was brought to the fore during 2007–2009, due to illnesses caused by poorly made residential/commercial dry walls.[115–118] However, the presence of low concentrations and the large diversity of VOCs has made their detection a challenging task.[2,3] Thus, there is increased demand for the development of a continuous real-time technique to monitor indoor VOCs. Recently, nanocomposites fabricated using electrochemical or self-assembly of metal/metal oxide nanoparticles on top of functionalized conducting polymer film surfaces, has enabled the selective sensing of VOCs.[119] In these hybrid nanocomposites, the selectivity is achieved by assembling different metal nanoparticles on the same conducting polymer film. This eliminates the need to develop different polymer chemistries and device configurations for each specific analyte. The utilization of organic−inorganic nanocomposite-based VOC sensors are described briefly in this section. The aspects of nanocomposite material science resulting in sensing performance and the related sensing mechanism are also discussed.

For the detection of hydrocarbon vapors, Li et al.[120] used a PANI-MWCNT (mass ratio 4:1) hybrid nanocomposite prepared by an in situ electrochemical polymerization technique. This sensor exhibited a response in the 200–1000 ppm range of aromatic hydrocarbon vapors due to an increase in conductivity, and the maximum response (0.31%) was measured at 1000 ppm. The increase in conductivity of PANI after gas exposure has been attributed to physical interactions due to dipole−dipole interactions that uncoil the polymer chain and decrease the hopping distance for the charge carriers. Electrochemically fabricated PANI/aluminum (Al) nanocomposite-based Schottky barrier diodes have been used by Campos et al.[121] to detect methanol (CH_3OH). The current−voltage (I– V) and capacitance− V characteristics of the diodes were studied with different concentrations of gas for different time intervals at room temperature. The presence of CH_3OH resulted in a decrease in the forward

and reverse-bias current and an increase in the barrier height, i.e., increase in resistance. However, the effects of different concentrations and sensitivity were not explained and thus need more investigation. An optical CH_3OH sensor has been fabricated by Stevens et al.[93] using a mesoporous coumarin 481 (C481) dye-doped hybrid composite film of nonionic surfactant Pluronic P123 and silica by sol−gel methods. The composite films were found to be capable of CH_3OH detection at a concentration of ~150 ppm via changes in the fluorescence intensity. An energy transfer complex formed via interaction between dye and nanocomposite exhibited enhanced response to methanol vapor, but only for the first few sensing cycles. The observed decrease in fluorescence intensity is attributed to an excited state interaction between methanol and C441. However, key parameters of these films, such as sensitivity, long-term photostability, and specificity to methanol, need further optimization to fabricate commercially viable optical sensors. Sadek et al.[122] described a surface acoustic wave (SAW)-based gas sensor to detect H_2 using a nanocomposite film of PANI-WO_3 nanofiber fabricated onto a layered ZnO/64°YXLiNbO_3 SAW transducer via chemical oxidative polymerization. It was observed that, during sensing, the analyte adsorbed onto the WO_3 surface and generated free electrons, resulting in a decreased depletion region and leading to increased surface conductivity. The sensor response was found to be 7 kHz toward 1% of H_2 in synthetic air at room temperature with a response time of 40 s, recovery time of 100 s, and repeatability in a stable baseline condition. A hybrid nanocomposite of plasma-polymerized acrylonitrile (PP-AN)-ZnO nanobelt (NB) has been used to detect O_2, and its sensing characteristics have been compared with bare ZnO nanobelt based sensors.[123] The nanocomposite showed better O_2 sensing than bare ZnO-NB. The obtained sensing performance enhances on UV exposure. UV exposure increases the conduction in the nanocomposite due to generation of a photocurrent, resulting in a direct increase of electron−hole pairs. Moreover, desorption of charge species with a related reduction in the electron depletion region near the ZnO-NB surface leads to modified surface potential. It was observed that nanocomposite-based sensors exhibited response enhancements from 0 to 25.3% (minimum sensitivity at 150 °C is 16.6 ppm in 300 s) at low temperature. Also, the sensor can avoid structural deterioration and caused stability in the obtained response. However, the effects of O_2 desorption/adsorption in PP-AN on the electron depletion region in the ZnO were significant for sensing phenomena.

Solvents such as propanol ($CH_3CH_2CH_3OH$), toluene ($C_6H_5CH_3$), ethanol (CH_3CH_2OH), hexane, (C_6H_{14}) and chloroform ($CHCl_3$) were detected using array-based gas sensors using hybrid composite films of polyvinyl butyrl (PVB), Fe_2O_3 and manganese dioxide (MnO_2) by Arshak et al.[124] The response of the sensors $\Delta R = \{(R_{gas} - R_{air})/R_{gas}\} \times 100$ (R_{gas} and R_{air} are the magnitude of resistances in the presence of target gas and air, respectively) was seen to increase with increasing gas vapor concentration and was found to be dependent on film compositions and the number of layers. The PVB containing 1.5 wt % carbon black exhibited a response to CH_3CH_2OH (43.27%) and $C_6H_5CH_3$ (19.43%) at 5000 ppm. In contrast, the response of a sensing layer comprised of Fe_2O_3/MnO_2 to the same concentration of $CH_3CH_2CH_3OH$ and $C_6H_5CH_3$ at room temperature was found to be 62.57% and 45.95%, respectively. Further, authors investigated the application of nickel oxide (NiO)/Fe_2O_3 (75/25, 50/50, and 25/75) and PVB nanocomposite films for gas sensor a p plications to detect CH $_3$ OH, CH $_3$ CH $_2$ OH, CH3CH_2CH_2OH, $C_6H_5CH_3$, acetone

(CH_3COCH_3), and tetrahydrofuran (THF, C_4H_8O) at room temperature (25 °C).[125] For each composition tested, the highest response was displayed for $C_6H_5CH_3$ and CH_3CH_2OH. The fastest response and recovery times of each device were recorded after their exposure to 4000 ppm of $C_6H_5CH_3$ and CH_3CH_2OH at room temperature. Sensors fabricated using composition 75/25 M wt % of NiO to Fe_2O_3 showed response/recovery times of 30/45 s for CH_3CH_2OH and 40/48 s for $C_6H_5CH_3$.

The detection of acetone (CH_3COCH_3) and $C_6H_5CH_3$ at ppm level is achieved by covalent assembly of Ni and Pd metal nanoparticles on top of poly(3,4-ethylenedioxythiophene-*co*-thiophene-3-acetic acid), poly(EDOT-*co*-TAA), films using 4-aminothiophenol linker molecules (Figure 9).[126] These authors explained the effect of Ni/Pd-poly(EDOT-*co*-TAA) hybrid film thickness on the sensitivity to $C_6H_5CH_3$ and CH_3COCH_3. The initial changes in resistance of Pd/poly(EDOT-*co*-TAA) and Ni/[poly(EDOT-*co*-TAA)] hybrid films (50 nm) were at 10 ppm with a response time of 60 s to CH_3COCH_3 and at 2 ppm with a response time of 200 s to $C_6H_5CH_3$, respectively. The observed enhanced performance was attributed to the improved interactions between precursors due to covalent binding. However, Pd/poly(EDOT-*co*-TAA) films were found to be selective for CH_3COCH_3, and Ni/poly(EDOT-*co*-TAA) films were shown to be selective for toluene. The observed sensing was thickness-dependent, and the optimized thickness of the sensor was estimated at ~50 nm.

A SAW gas sensor (Figure 10) based on nanocomposites of MWCNT with polyepichlorohydrin (PECH) and polyetherurethane (PEUT) as sensitive layers was investigated to detect octane (C_8H_{18}) and $C_6H_5CH_3$. The effect of MWCNT concentration on the response of sensors has been studied.[127] It was observed that the introduction of small percentages (~1%) of MWCNT into the polymer increased the adsorption of toluene, but no change has been observed for C_8H_{18} (Figure 10A). The fabricated sensor shows no response on exposure of nitrogen dioxide (NO_2), ammonia (NH_3), H_2, or carbon monoxide (CO), confirming its selectivity. The detection limits of C_8H_{18} and toluene were found to be 7.4 and 1.7 ppm, respectively (Figure 10B). The stability and repeatability of the sensor responses have been confirmed by testing the sensors periodically for 5 months.

Chloroform ($CHCl_3$), one of the most widely used solvents, has been detected using quantum dot (QD) nanocomposite-based gas sensors. QDs of cadmium selenide/zinc sulfide (CdSe/ZnS) were added and encapsulated within polystyrene (PS)−polystyrene-*co*-maleic anhydride (PSMA); PS−PSMA polymer nanofibers using electrospinning techniques to fabricate nanocomposite sensing films to detect chloroform and THF.[128] Change in electrical conductivity due to interactions between the QDs and the PSMA side-chains were used to detect organic solvents with a response time of less than 1 s and with high durability. The fabricated sensor exhibited a shelf life of 6 months and was found to be more sensitive to chloroform (0.001% to 0.99%) than to THF. Olive oil capped QDs of CdSe (~6 nm) and poly(3-hexylthiophene) nanocomposite sensors have been used for selective detection of chloroform at room temperature.[129] This nanocomposite sensor exhibited a linear range from 100 to 1200 ppm and a detection limit of 100 ppm. The sensor was found to be selective to chloroform vapors in comparison to VOCs such as toluene, propanol, and acetone with concentrations of 1000 ppm. The recovery time of the sensor improved from

8 to 4 min on illumination with monochromatic light (600 nm), due to photoinduced enhancement of charge transfer in the nanocomposite under the incident light.[129] Sharma et al.[130] reported Cu-PANI nanocomposite-based gas sensors for chloroform detection at the ppm level, wherein the response time in terms of increase in DC electric resistance on exposure to chloroform vapor was observed. In comparison to the pure PANI, the nanocomposite exhibited good, reversible response for a comparatively low concentration of chloroform ($CHCl_3$, ~100 ppm) with a relative sensitivity range of 1.5–3.5. This gas sensing mechanism mainly involves the adsorption−desorption of $CHCl_3$ on a Cu nanocluster surface. Chemisorption of the analyte vapor induces charge redistribution in the metal nanoparticles and changes their work function. The conjugated linker molecule responds to the change in the work function of the embedded nanoparticles and reflects the changes in the electronic states of the underlying conducting polymer films, resulting in a measurable change in the resistance of the hybrid nanocomposite.

Ma et al.[131] deposited nanocomposite thin films of PANI-TiO_2 onto interdigitated carbon paste electrodes via a spin-coating and immersion method for detection of trimethylamine at room temperature. This nanocomposite film exhibited gas-sensitivity to trimethylamine [$N(C_2H_5)_3$, 5.14×10^{-7} mol mL^{-1}], which increases further by 3–5 orders of magnitude within 3 min and was selective to analogous gases. The sensing film exhibited reproducibility, stability, and easy recovery with high-purity N_2 at room temperature. The nanocomposites of polysiloxanes containing 3-heptafluorobutanoyl camphorates of metal ions, e.g., Zn(II), Ni(II), and Eu(Ill), have been used by Hierlemann et al.[132] as sensitive layers for thickness-shear mode resonators (TSMRs) for the monitoring of various VOCs. Sensing layers provided pronounced selectivity in detecting VOCs in the gas phase and in particular analytes containing heteroatoms, such as O and N. The selectivity resulted from coordinative binding between the electronically unsaturated metal complexes and the heteroatom-containing analytes. The detection of analyte in the concentration range 60–100 ng L^{-1} or 20–40 ppb and a detection limit of 1 ng L^{-1} were achieved for p yr idin e (C_5H_5N) and *n* -bu tylamine ($CH_3CH_2CH_2CH_2NH_2$). The drawback of long response and recovery times can perhaps be compensated by applying an evaluation method based on the response slope.

Wang et al.[133] reported fabrication of nanocrystalline antimony-doped tin oxide (ATO ~ 5 nm) with an amphiphilic block copolymer [poly(ethylene-*co*-butylene)-*block*-poly-(ethylene oxide] template via the sol−gel method. It was found that polymers not only provide favorable sites for the growth of the particulate assemblies, but they also influence the formation process, including the nucleation, growth, coagulation and flocculation. Formaldehyde (HCHO, 10–50 ppm) gas sensing devices were fabricated using ATO nanoparticles on alumina tubes with Au electrodes and Pt wires, and showed quick response to HCHO gas (0 to 10%) at an operating temperature of 136 °C. This sensor exhibited a sensitivity coefficient of 3.44 and a low detection limit of 130 ppb. However, there is considerable scope to improve the sensing parameters of this sensor. To detect aldehydes at room temperature, Wang et al.[134] explored ion-exchange reactions between PANI and MoO_3 to prepare $(CH_3CH_2CH_3)$-$(PANI)_xMoO_3$ nanocomposite films. The fabricated nanocomposite film exhibited an increase of 8% in electrical resistivity for 500 ppm formaldehyde and a change of 3.8% for 500 ppm acetaldehyde within 600 s at 30 °C.

However, no response was observed for toluene and xylene. Authors suggested that, in the nanocomposite, PANI amplified the signal and the analyte affected the charge conduction between the host and guest.

Itoh et al.[135,136] explored layered organic−inorganic hybrid nanocomposite films of molybdenum oxide (MoO_3) with poly(*N*-methylaniline) (PNMA), PANI, and poly(*o*-anisidine) (PoANIS) formed by a modified intercalation process to investigate the effect of aldehyde such as HCHO and acetaldehyde (CH_3CHO). The $(PNMA)_xMoO_3$ hybrid nanocomposite thin film exhibited increased resistivity (S = 2.8%) to approximately 1–10 ppm for aldehyde gases with reproducibility. However, $(PANI)_xMoO_3$ and $(PoANIS)_xMoO_3$ hybrid thin films exhibited enhanced response magnitude (S = 6%) as a function of resistance when exposed to HCHO and CH_3CHO in the range of 25–400 ppb at 30 °C.[136] The obtained high sensitivity and low quantity detection using $(PANI)_xMoO_3$ and $(PoANIS)_xMoO_3$ nanocomposite-based sensors is due to the modified sensor fabrication approach used, which removes insoluble polymer content and enhances interlinking between polymer and MoO_3 nanoparticles. Additionally, the sensitivity of the (PNMA)xMoO_3 hybrid thin film was found to be suitable and selective for CH_3CHO. It was reported that $(PNMA)_xMoO_3$ hybrid composites possess interlayer spaces equal to the size of methyl group, which assist in adsorption of CH_3CHO.[135]

Lu et al.[137] fabricated a layer-by-layer nanocomposite film of PANI nanoparticles and multiwall carbon nanotubes (MWCNT) onto interdigitated electrodes for fabrication of stable chemiresistive sensors for CH_3OH, CH_3CH_2OH, and $C_6H_5CH_3$ detection with reproducible response upon chemical cycling. Double percolated conductive networks in PANI (1%)-MWCNT (0.005%) hybrids resulted in both higher sensitivity (relative amplitude ~1.1%) and selectivity than other formulations, demonstrating a positive synergy. These features make them attractive for integration with electronic noses to balance the stability and sensitivity. The present report was mainly focused on the effect of precursor concentrations on sensing characteristics. Hence, efforts should be made to improve selectivity and sensitivity of this sensor.

Optical gas sensors based on Au-polyimide nanocomposite films fabricated by glow discharge vapor deposition polymerization for CH_3OH and CH_3CH_2OH detection using the SPR technique have been reported by Fernandez et al.[138] It was observed that a pure polyimide film does not show any absorption change in the presence of alcohol vapors, but good response was observed in the case of Au-polyimide (5×10^{16} Au^+/cm^2), which exhibited a dynamic optical absorption sensing response for CH_3OH (6000 ppm) and CH_3CH_2OH ethanol (6000 ppm) in the spectral range corresponding to the SPR peak of the Au nanoparticles. The SPR technique has been found more suitable for gas sensing; however, limitations regarding the suitable film thickness for SPR excitation are yet to be overcome. The reported sensitivity is low and shows low selectivity. Nanocomposites of MoO_3 and PPy have been prepared using the vapor polymerization technique for application to CH_3CH_2OH sensing.[139] It was observed that at room temperature the MoO_3−PPy composite exhibited an improved sensing response when compared to that of a MoO_3 or PPy based system. The magnitude of the resistance of the composite was found to decrease with increasing concentration of CH_3CH_2OH (0.3%), and this was due to catalytic reaction

of CH_3CH_2OH on the MoO_3 surface. A hybrid nanocomposite of PANI-silver (Ag, ~15 nm) prepared using ultrasound-assisted in situ mini-emulsion polymerization has been used for ethanol sensing by recording changes in electrical conductivity.[140] The sensing ability and response time of the PANI-Ag nanocomposite-based sensor was found to be dependent on addition of the Ag nanoparticles into the polymer matrix. This nanocomposite exhibited a detection range of 50–225 ppm, a response time of 2100 s, and a maximum response at 100 ppm.

For CH_3OH sensing, the layer-by-layer technique has been used by Kumar et al.[141] to fabricate conductive bionanocomposites of chitosan (CH)-CNT with good chemical and electrical properties. CH−CNT nanocomposites exhibited a chemical nanoswitching mechanism in promoting tunneling conduction. Using this bionanocomposite, the authors described the chemical and electronic behavior of the nanocomposite after diffusion of a gas molecule, resulting in enhanced tunneling conductance. This hybrid bionanocomposite-based transducer showed high sensitivity toward water and CH_3OH (0 to 100%) and showed low response to $C_6H_5CH_3$. Athawale et al.[142] prepared a PANI-palladium (Pd) nanocomposite using oxidative polymerization to fabricate a chemiresistive gas sensor to detect different aliphatic alcohol vapors such as CH_3OH, CH_3CH_2OH, and isopropanol [$(CH_3)_2CHOH$]. Due to its high polarity, the fabricated sensor showed higher selectivity and sensitivity ($8.9 \times 10^5\ \Omega\ ppm^{-1}$) to CH_3OH (10 ppm) vapors than that of CH_3CH_2OH and $(CH_3)_2CHOH$, which causes more efficient interaction on sensing surfaces. However, these sensors exhibited high response time (~2 s) due to the competition arising between the different molecules adsorbed over the nanocomposite surface, wherein the presence of bulkier molecules resulted in a barrier diffusing toward the sensor, compared with the smaller CH_3OH molecules. A flow-through sensor was designed by Han et al.[143] Authors fabricated a SWCNT-poly(methyl methacrylate) (PMMA) nanofiber hybrid composite onto IDE using electrospinning techniques, which was used as a flexible sensing material to detect CH_3OH (600–3500 ppm). Ag contacts printed on nanofiber structures using printing techniques were used for measurements. It was observed that this flexible flow-through sensor design shows 1 order of magnitude higher sensitivity than that of a nanofiber deposited on a conventional IDE (Figure 11).

A 3D sensing platform has been developed by Feller et al.[144] via assembling MWCNT onto PMMA microbeads using spray-coated layer-by-layer (LBL) techniques to fabricate a chemiresistive VOC (CH_3OH, H_2O, $C_6H_5CH_3$, and $CHCl_3$) sensor.[144] It was found that, in this hybrid nanocomposite, the system had an original hierarchical architecture with a segregated network of MWCNT bridging PMMA (Figure 12, inset A). The sensors showed an increase in resistance when exposed to vapor stream, i.e., with target gases adsorption, and also showed a decrease in resistance when exposed to dry nitrogen, i.e., desorption of analyte. This behavior was attributed to the fact that the diffusion of solvent molecules results in disconnection of the conducting network of CNTs, because the energy required for electron circulation by tunneling increases exponentially with the CNT-CNT junction gap. The MWCNT-PMMA hybrid nanocomposite exhibited selective response on exposure to CH_3OH (Figure 12A). The effect of analyte concentration on MWCNT-PMMA response amplitude for CH_3OH, H_2O, $C_6H_5CH_3$, and $CHCl_3$ vapors were studied (Figure 12A), and the curves were fitted with the Langmuir−Henry clustering (LHC) electro-sorption

model described in the inset of Figure 12 B. The outcome of sensing results showed that the sensitivity of 3D assemblies of the MWCNT network increased by a factor of 2 and selectivity for CH_3OH vapor by a factor of 5 relative to other VOCs. This sensor can be used as an “electronic nose”, which requires a balance between stability and sensitivity.

To detect 1-butanol, Lvova et al.[145] utilized SWCNTs modified with porphyrin (Pr) hybrid composites as sensing materials in quartz microbalance (QMB) sensors with an integrated preconcentration unit. A CNT-Pr hybrid composite was fabricated following two different strategies (Figure 13). Two methodologies were adopted to prepare QCM sensing materials. First, the electropolymerization of pyrrole-substituted Pr monomers, wherein negatively charged carboxylic acid (COOH)-functionalized SWCNTs acted as a dopant. Second, SWCNT−Pr composites were synthesized chemically and then entrapped in PPy/SWCNT-COOH films. SWCNT-Pr was utilized both as the preconcentrator adsorbing phase and QMB coating f or sensitive detection of 1-butanol ($CH_3CH_2CH_2CH_2OH$), in concentrations close to the odor threshold. Five different QMB sensors were fabricated using preconcentration procedures to detect low concentrations of $CH_3CH_2CH_2CH_2OH$. QMB 1 (PPy/SWCNT-COOH), QMB 2 (PPy/PPy-Porph-2/SWCNT-COOH), and QMB 3 (PPy/SWCNT-COOH/SWCNT-TPP) exhibited higher responses than QMB 4 (PPy-Porph-1/ClO_4) and QMB 5 (PPy-Porph-2/ClO_4) due to the presence of SWCNTs (Figure 13). The results exhibited detection of 1-butanol from 46 to 500 ppb using the QMB 3 sensor.

4.2. Organic−Inorganic Hybrid Nanocomposites for Hydrochloric Acid (HCl) Detection

Hydrochloric acid (HCl) is known to be a level III hazardous air pollutant. HCl is the most commonly used acid in the semiconductor and chemical industries.[146,147] It is excreted in incineration plants, chlorofluorocarbon (CFC) atmospheres, and accidental emissions. HCl is a source of the well-documented pollutants acid rain and dioxin, and has also been identified as a workplace hazard with a short-term exposure limit of 5 ppm. The toxic nature of HCl in both gaseous and aqueous forms has led to increased demand for detection of HCl at ppm levels.[1] It is therefore essential to fabricate sensors to monitor the presence of HCl at site using a fast, user-friendly, safe, and economical method.[146,147] Recently, there has been remarkable growth in the development of electro-active semiconducting polymer thin-film-based sensors for detection of HCl gas.

Nanocomposite polymeric combinations have been found to play an important role in the development of efficient sensors for detection of HCl and other hazardous gases. Jang et al.[148] fabricated carbon nanofiber (CNF ~50 nm)-PPy (~22 nm) coaxial nanocables (~75 nm) via one-step vapor deposition polymerization (VDP) to detect ammonia (NH_3) and HCl. The PPy-coated CNF exhibited an enhanced response signal (from 1 to 3.5, estimated using $\Delta R/R_0$) due to the presence of the thin and uniform conducting polymer layer. The observed response was found to be dependent on the PPy layer thickness. The electrical conductivity of the sensor was found to decrease upon NH_3 exposure due to an increase in the fraction of neutral polymer chains through electron donation to oxidize the polymer chain. The conductivity increased after HCl exposure because Cl^- ions embedded in the polymer backbone lead to the formation of polarons/bipolarons. The response of the PPy-coated CNF upon interaction with NH_3 (10 ppm) and HCl (20 ppm) was reversible and

reproducible. However, there is scope to improve the selectivity, sensitivity, and detection limit of these materials. An optically transparent nanocomposite thin film of tetracationic porphyrin (TMPyP) and TiO_2, fabricated using glancing-angle physical vapor deposition techniques, exhibited direct monitoring of HCl.[149] The fabricated sensor had a recovery period of 300 s, a response time of 50.7 s, a detection limit (0.1 ppm), and a shelf life of 30 days. The obtained detection of 0.1 ppm is remarkable; however, this fabricated sensor operates at 80 °C.

A selective, rapid and sensitive HCl gas sensor was fabricated by Mishra et al.[82] using nanocomposites of copolymers of aniline and formaldehyde synthesized with a metal complex of Fe−Al (95:05) via thermal vacuum evaporation deposition techniques. This sensor detects HCl (0.2 to 20 ppm) within 8–10 s. These nanocrystalline composite films exhibited high sensitivity (400–800) and a response time of 10 s (Figure 14). During sensing, exposure of HCl reduces the barrier height at the metal−polymer interface, which increases the charge transport across the interface and enhances output current. The selectivity was achieved by suitable doping of PANI during synthesis (Figure 14). The sensor was reusable, as there was no chemical reaction between PANI film and the gas. Furthermore, the sensor operated at room temperature and possessed an extended lifetime.

4.3. Organic−Inorganic Hybrid Nanocomposites for Ammonia (NH_3) Detection

Ammonia (NH_3) is an important gas to be monitored when studying air pollution. High dosages of NH_3 are easy for humans to detect due to the strong odor of the gas. However, small quantities need to be determined using highly sensitive and selective sensors. Some traces of NH_3 found in drinkable water indicate decomposition of organic matter that may be harmful to human health.[150] In contrast, farmers frequently use ammonia-based fertilizers, which at high doses alter the acidity of the soil, creating an ecological imbalance.[151,152] These factors have motivated researchers to expand their efforts for the development of a selective and sensitive gas sensor to monitor NH_3 at room temperature.

Ammonia, along with VOCs, has been detected using an organic−inorganic hybrid nanocomposite based gas sensor. A hybrid nanocomposite of PANI and 3-mercapto-1-propanesulfonate-functionalized Au nanoparticles has been prepared using a new and facile method based on osmosis. The PANI and Au NPs were dissolved together in dimethylformamide (DMF) in a dialysis bag and immersed in water.[153] The nanocomposite has been tested for sensing of NH_3 and other VOCs. The sensitivity toward H_2O was 0.00055% ppm^{-1}, whereas it was 1.9% ppm^{-1} for NH_3. The doped PANI-Au NPs nanocomposite shows a low detection limit of 10.8 ppm at room temperature. The NH_3 gas sensing properties of five PANI based materials were studied by Lobotka et al.: thick and thin PANI films, PANI-MWCNT and PANI-SWCNT nanocomposite films, and PANI nanogranules embedded in a polyvinylpyrrolidone matrix fabricated onto an Au integrated microelectrode.[154] These sensing systems were tested for NH_3, H_2, ethanol, methanol, and acetone. It was observed that, at low concentration, PANI thin films (~100 nm thick) showed sensitivity to NH_3 below 0.5 ppm, which is higher than that of nanocomposite films. A nanocomposite thin film of PANI-TiO_2 was fabricated via the self-assembly method by Tai et al.[155] onto a silicon substrate covered with IDE for NH_3 (23–141 ppm) and CO gas

sensing applications at 60 °C. The results have shown that the response, reproducibility, and stability of the PANI-TiO_2 thin film to NH_3 is superior than CO gas with a much smaller effect of humidity on the resistance of the PANI/TiO_2 nanocomposite film. Further, sensing parameters of PANI-TiO_2 nanocomposite thin films have revealed faster response (30 s) and recovery rates (40 s), with stabilities of 30 days. This may be due to the presence of TiO_2 nanoparticles, which influence the morphology of the nanocomposite film, resulting in variation of the sensor response-recovery behavior. This group also fabricated hybrid nanocomposites of PANI with TiO_2, SnO_2, and indium oxide (In_2O_3) using the in situ self-assembly technique for NH_3 sensing (23–141 ppm).[156] The results of sensing studies showed that all PANI-based nanocomposite systems had faster response (2–3 s) and recovery (23–50 s) times with better reproducibility (4 cycles) and long-term stability (15 days). The effect of humidity on the response of all these sensors was also investigated. However, PANI-TiO_2 nanocomposite-based sensors showed optimum NH_3 gas-sensing characteristics, due to the compatible energy band gap.

The NH_3 sensors discussed above have limited selectivity and poor detection limits. To fabricate an efficient NH_3 sensor, A PPy-SWCNT hybrid nanocomposite synthesized via chemical polymerization has been used to fabricate a sensitive NH_3 gas sensor.[157] These authors also studied the effect of film thickness, annealing temperature, and SWCNT concentration on the gas sensing characteristics of nanocomposite thin films. Sensors under optimized conditions exhibited a response of 26–276% upon NH_3 exposure ranging from 10 to 800 ppm, with response and recovery times of 22 and 38 s, respectively. Thermal dynamic refluxing and vapor-phase polymerization techniques have been used to encapsulate Pd nanoclusters with PPy to fabricate a nanocomposite film for rapid (14 s) NH_3 sensing.[158] The optical, electrical, and gas sensing properties of a PPy-Pd nanocomposite system have been found to be dependent on the Pd nanoparticle size (15–35 nm), Pd concentration, reaction time, and the morphology of the nanocomposite film. The fabricated sensor exhibited a reversible and reproducible electrical signal with response and recovery times of 14 and 148 s for 1000 ppm. The magnitude of sensor response was 13.9–58.9% for detection from 50 to 2000 ppm at room temperature. The obtained sensing characteristics were better than those of PPy-based NH_3 sensors. The fabricated sensors were also tested for various VOCs and were found to be very selective.

Lim et al.[159] investigated the electrical and NH_3 gas sensing properties of PANI−SWNTs using temperature-dependent resistance and FET transfer characteristics. The sensing response due to the deprotonation of PANI was found to be positive for NH_3 (25–200 ppb) and negative to NO_2 and H_2S. This sensor exhibited sensitivities of 5.8% (NH_3), 1.9% (NO_2), and 3.6% (H_2S) with lower detection limits of 50, 500, and 500 ppb, respectively. However, the poor selectivity of this fabricated sensor limits its further application. Jian et al.[160] reported poly(3,4-ethylenedioxythiophene)/poly-(styrenesulfonate) (PEDOT/PSS) and O_2 plasma-treated SWCNT nanocomposite films as materials of high gas sensing capability at the ppb level. The sensor has been prepared through dielectrophoretic assembly of nanostructured layers of PEDOT/PSS-(SWCNTs) on Au IDEs (Figure 15A,B). The $\pi-\pi$ interactions and electrostatic attraction between PEDOT chains and the SWCNTs result in uniform dispersion of SWCNTs in the PEDOT matrix (Figure 15 C). This gas sensor showed stable and reversible response to NH_3 in the range 2–300 ppm and trimethylamine

from 6 to 1000 ppb at room temperature (Figure 15D). The gas sensing properties were found to be dependent on the concentration and alignment of SWCNTs in the PEDOT matrix.

A 2D-ordered, large effective surface area, free-standing and patterned hybrid nanocomposite platform of PANI nanobowl-Au nanoparticles (15 nm) was self-assembled onto polystyrene (PS) spheres at the aqueous/air interface as a template and used for NH_3 detection (0–1600 ppm) by Jiang et al.[161] The sensor with a thickness of ~100 nm exhibited a fast response time of 5 s with recovery time of 7 s at 100 ppm of NH_3. A one-pot synthesis approach has been used to fabricate Au/CNT-PANI nanocomposites for online monitoring of NH_3 gas.[162] The fabricated Au/CNT-PANI nanocomposite-based sensors showed repeatability upon repeated exposure to NH_3. The improved properties were attributed to fast charge transfer between the electron-donating molecule and CNTs, resulting in a change in conductivity of the system. The sensor exhibited a linear detection range from 200 ppb to 10 ppm, a mean sensitivity of 0.638 (at 25 ppm), a response time of 10 min, and a recovery time of 15 min. Zhang et al.[163] prepared a camphorsulfonic acid (CSA)-doped PANI−SWCNT nanocomposite-based (diameter 17–25 nm) gas sensor using electropolymerization for the selective and sensitive detection of NH_3. The sensor was fabricated using electropolymerization for 2 min. However, the sensor-to-sensor variability was found to be ~±30% due to batch-to-batch processing. This sensor showed humidity-independent NH_3 sensing responses ranging from 10 to 80 ppb, while the relatively high sensitivity of the sensor to NH_3 concentrations of 400 ppm was demonstrated. The obtained high sensitivity is due to the coordinating roles of the nitrogen atoms of NH_3 gas and the nanocomposite and the deprotonation/protonation process due to the adsorption–desorption of NH_3. The selectivity of the sensor was studied using 1 ppm of NO_2, 3000 ppm of H_2O, and 1 ppm of H_2S. The resistance of SWCNTs increases upon H_2O adsorption, because H_2O molecules donate electrons to hole charge carriers of p-type SWCNTs. Contrary to SWCNTs, the resistance of CSA-doped PANI films decreased upon exposure to H_2O, which was explained by the proton exchange-assisted conduction of electrons mechanism. Thus, the opposite electrical responses of SWCNTs and PANI(CSA) toward H_2O made it possible to eliminate the effect of RH by having just the right balance of PANI(CSA) functionalization. These researchers demonstrated that the effect of cross-interference can be eliminated by accurate control of precursor concentration. Such novel nanoengineered sensing materials are capable of overcoming the shortcomings of conventional sensors.

A highly sensitive (at ppt level) NH_3 sensor was fabricated by Gong et al.[164] P-type conductive PANI nanograins were prepared onto an electrospun n-type semiconductive TiO_2 fiber surface (Figure 16). The structure resulted in two p−n junctions at PANI/TiO_2 interfaces. The forward resistance R1 and bulk resistance R2 are very small compared to the reverse resistance R3. Due to the fact that PANI is much more conductive than the TiO_2 microfiber, the current flows preferably through the conductive PANI particle, when the electric field applied to the reverse bias of the p−n junction is higher than the breakdown voltage. When exposed to NH_3, the bulk resistance of the PANI, R2, increases due to its dedoping, and the current flows solely through the TiO_2 microfibers rather than the PANI nanograins. Therefore, the I–V response changes from nonohmic to ohmic after exposure to NH_3. The resistance of the p-n heterojunctions combined with the bulk resistance of

the PANI nanograins can function as electric current switches when NH_3 gas is absorbed by PANI nanoparticles. As a result, the sensor sensitivity can be significantly improved. The detection of 50 ppt of NH_3 gas in air were observed with a sensitivity of 0.004. The repeatability and recovery of the sensor was tested using 10 ppb of NH_3. However, the selectivity of this sensor was not tested, and the observed sensitivity was very low.

4.4. Organic−Inorganic Hybrid Nanocomposites for Hydrogen Disulfide (H_2S) Detection

Hydrogen sulfide (H_2S) is a hazardous toxic gas. At low concentrations, it can lead to personal distress, whereas in a concentration higher than 250 ppm, it may result in loss of consciousness, permanent brain damage, and may cause death. Although a number of techniques have been reported for the estimation of H_2S concentrations, new advanced techniques with high sensitivity, fast response, easy operation, and low cost are still desirable.[165]

Geng et al.[166] prepared PPy/γ-Fe_2O_3 nanocomposites for NH_3 and H_2S gas sensing. It was found that the PPy exhibited maximum sensitivity of 48.5 for NH_3 and 31.4 for H_2S at room temperature. However, a PPy/γ-Fe_2O_3 hybrid nanocomposite annealed at 150 °C showed a maximum sensitivity of 68 for NH_3 and of 406.8 for H_2S, whereas PPy exhibited decreased gas sensitivity at this temperature. The results revealed that PPy/γ-Fe_2O_3 had higher sensitivity and stability than that of PPy, and the working temperature was lower than that of γ-Fe_2O_3. Furthermore, PPy/γ-Fe_2O_3 showed superior properties to those of pure PPy and r-Fe_2O_3. A CSA-doped PANI-CdS nanocomposite prepared using chemical polymerization was used for the selective detection of H_2S (10–100 ppm). This sensor exhibited a maximum response of 76% at 100 ppm and 97.34% stability after 10 days for 40% doping of CSA in the PANI-CdS nanocomposite. The CSA-PANI-CdS sensor exhibited negligible response (2–5%) to NO_2, CH_3OH, C_2H_5OH, and NH_3. Unfortunately, however, this sensor possesses a high recovery time of ~205–413 s.[167]

Due to the fact that PPy and oxide nanoparticles have lower conductivity, Shirsat et al.[168] used metal nanoparticles to decorate synthesized polymer nanowires to achieve higher conductivity and higher sensing surface area. To prepare hybrid networks, PANI nanowires bridging the 3 μm gap between two Au IDEs were synthesized using a two-step galvanostatic electrochemical polymerization technique. These nanowire networks were then functionalized by controlled growth of Au nanoparticles of size ~70–120 nm.[168] The PANI-based sensor exhibited a detection limit of ~500 ppm due to lower conductivity. However, a PANI-Au nanocomposite chemiresistive sensor exhibited an enhanced detection range of 0.1–100 ppb and a detection limit of 0.1 ppb with good selectivity and reproducibility. The improved sensing response has been ascribed to the formation of AuS by the reaction $H_2S + Au \rightarrow AuS + H^{2+}$ and enhanced doping of PANI. The electron transfer from PANI (donor) to Au (acceptor) increases the conduction of PANI (Figure 17).

4.5. Organic−Inorganic Hybrid Nanocomposites for Detection of Nitrogen Oxides (NO_x)

As a result of industrialization, harmful gases such as nitrogen oxides (NO_x), carbon monoxide, and hydrocarbons are of serious concern because of increasing atmospheric pollution and increasing automobile density. The monitoring of these gases is important

in order to control their emission from automobiles and industrial plants. NO_x is evolved during the formation of ground-level ozone in the atmosphere, contributes to acid rain, and is an active ingredient in global warming.[52,169] It is also involved in various nitration processes with biomolecules, causing certain forms of cancer and other diseases. Among several oxides of nitrogen present in air, NO and NO_2 are considered the most harmful in terms of both health risk and environmental damage. NO_2 is produced together with NO by oxidation of nitrogenous compounds in fuel combustion.[169] A NO_x sensor that can be attached to the exhaust systems of automobiles could play an important role in monitoring the level of NO_x.[170,171] Therefore, there is an urgent need for efficient sensors to detect NO_x in the ambient environment.

Kaushik et al.[52] and Prakash et al.[172] used WO_3−PANI and hemin/ZnO-PPy nanocomposite thin film sensors, respectively, to detect NO_x gases. The NO_x gas sensing characteristics of the sensors were studied by measuring the change in resistance with respect to time. The studies suggested that hemin/ZnO-PPy/Pt electrodes exhibited 3-fold-enhanced electrochemical activity toward detection of NO_x compared to hemin/PPy/Pt electrodes. This sensor exhibited a linear range of 0.8–2000 μM, a sensitivity of 0.04 μM^{-1}, and a detection limit of 0.8 μM at room temperature. Geng et al.[173] reported the application of PPy-ZnO nanocomposites for the sensing of toxic gases such as NH_3, H_2S, and NO_x at different operating temperatures (30, 60, and 90 °C) at gas concentrations of 1000, 1500, and 2000 ppm. PPy-ZnO nanocomposites showed superior selectivity and reversibility to NO_x compared to PPy. Furthermore, the working temperature of the PPy-ZnO composites was much lower than the reported working temperature of ZnO (350–450 °C). PPy-ZnO (10%) showed the maximum sensitivity to NO_x in identical experimental conditions.

The nanocomposites discussed above were prepared by mechanical mixing, which leads to inferior attachment and interaction at the interface. Xu et al.[174] used in situ chemical oxidative polymerization methods to fabricate a SnO_2 hollow sphere (20%)-polythiophene hybrid composite system for NO_2 sensing (10–200 ppm). It was observed that a strong synergetic interaction existed between the SnO_2 hollow spheres and polythiophene, resulting in higher sensitivity with good thermal stability. This gas sensing system showed enhanced sensor response (S = 6), selectivity and a short response time (2 min), but a longer recovery time (~24 h) at a working temperature of 90 °C. These results were attributed to the high surface area of the hybrids and the p-n heterojunction formed between p-type polythiophene and n-type SnO_2 hollow spheres. Sadek et al.[175] used the highly sensitive SAW technique to fabricate sensors for the detection of toxic gases. Nanofibers of PANI/indium oxide (InO_3) composites were deposited onto a layered ZnO/64° YX $LiNbO_3$ SAW transducer. This sensor was tested to detect H_2 (1.1% in 30 s), NO_2 (500 ppm in 24 s), and CO (2.12 ppm in 30 s) gases at 11, 2, and 2.5 kHz, respectively.[175] The observed reproducibility was 1.12% for H_2, 125 ppm for CO, and 510 ppb for NO_2. The sensor exhibited repeatability for H_2 and CO. However, repeatability at higher concentrations of NO_2 is presently an issue due to nanocomposite poisoning.

The deposition of in situ self-assembled LBL (layer-by-layer) films has been adopted by Ram et al.[110] LBL assembly, based on electrostatic or molecular forces, is a unique approach for the formation of molecular architectures by adsorption of consecutively

alternating polyelectrolytes. The most substantial advantage of LBL is the accurately controlled layer thickness, wherein the macroscopic properties of the molecular film can be controlled by the size of the microscopic structure of the repeat unit. Ultrathin films of polyhexylthiophene (PHTh), regioregular PHTh (RRPHTh), (PEDOT), PHTh−PEDOT copolymer, sulfonated PANI, PANI−SnO_2, PPy−SnO_2, PEDOT-SnO_2, PHTh−SnO_2, and copolymer (HTh-PEDOT)−SnO_2 were deposited using layer-by-layer self-assembly for NO_2 gas sensing (Figure 18). The results of these studies suggest that the PHTh and its nanocomposite (6 layered films) provide good platforms for NO_2 recognition (10–800 ppb). These nanocomposites were also studied for selectivity by exposing these films to two or more gases at the same time. Among these, the RRPHTh-SnO_2 nanocomposite-based sensor was found to be the most suitable platform for NO_2 gas sensing applications due to its excellent change in conductivity (ΔR changes from 0 to 120 KΩ at 200 ppm) at room temperature.

The sensing response of the nanocomposite can be enhanced by increasing the conductivity, which can be achieved by (i) replacing oxide nanostructures with metallic nanostructures of better conductivity, or (ii) doping of polymer or oxide nanostructures. Fabrication of a PANI/Au/Nafion hybrid nanocomposite film using the CV technique and its application to amperometric NO_2 gas detection was reported by Doet al.[176] NO_2 diffusion into a porous polymer resulted in reduction of mass transfer resistance with increment in cathodic reduction of NO_2. The sensor exhibited a sensitivity of 3.04 μA ppm^{-1} with a switching effect for 0 and 100 ppm concentrations. It was observed that nanocomposites with higher effective surface area and electrochemical activity could be obtained using electrochemical techniques. Hohercakova et al.[177] prepared Au-PVC nanocomposite electrodes by dispersing Au nanoparticles in a highly plasticized PVC matrix containing a hydrophobic electrolyte, for application to solid-state electrochemical NO_2 sensors. The fabricated Au-PVC nanocomposite electrode, in an array of microelectrodes, exhibited a high catalytic activity. The fabricated sensor showed a linear detection in the 0.6–2.6 ppm (v/v) range with a sensitivity of 400 nA ppm^{-1}, a detection limit of 50 ppb, and a response time of 50 s. The obtained sensing performance was better than that of the Nafion-only NO_2 sensor.

Cha et al.[109] fabricated an amperometric sensor for direct real-time detection of NO produced by cells cultured within the microdevices. The electrochemically deposited Au-hexacyanoferrate layer on the ITO substrate was used to catalyze NO oxidation to nitrite at lower applied potential (0.65–0.75 vs Ag/AgCl) and to obtain a stable current output. The stepwise fabrication of gas sensing architecture is shown in Figure 19A.[109] Furthermore, use of a gas-permeable membrane to separate internal sensor compartments from the sample phase imparts NO selectivity over common interfering agents present in culture media and biological fluids, such as ascorbate, NH_3, etc. (Figure 19B). This reversible amperometric sensor exhibited a linear range of 0–250 nM, a detection limit of ~1 nM (in stirred buffer), a sensitivity of ~10 pA/nM, and stability of 4 weeks. The amperometric response studies as a function of NO concentration were performed using a flow rate of 50 μL min^{-1} at 350, 100, 200, and 40 nM of NO (Figure 19C).[109] This sensor has applications in mechanistic studies and drug testing.

Nguyen et al.[178] prepared an interpenetrated network of MWCNT-poly(1,5-DAN) on IDE for NO_2 sensing (Figure 20). The MWCNT dispersed in Nafion was drop-coated onto Pt-IDE, followed by electro-polymerization of poly(1,5-DAN). Three interpenetrated networks of MWCNT-poly(1,5-DAN) were obtained by operating the electrochemical process voltage between 0.1 and 0.95 V at a scan rate of 50 mV s^{-1} for 5, 10, and 15 cycles. Under NO_2 exposure, the polymerized MWCNT network showed large resistance change while the non-polymerized MWCNT network showed no significant change.

The gas sensing mechanism has been attributed to the removal of unoccupied electrons from the NH_2 groups in the poly(1,5-DAN) backbone by NO_2 gas molecules. The removal of electrons induces the formation of NO^- ions and polarons on the polymer which in turn leads to the formation of new double bonds in neighboring positions. The formation of polarons and bipolarons assist charge migration across the backbone, resulting in decreased resistance. It was observed that the sensitivity and selectivity improves with an increase in polymer film thickness, but the response and recovery time is better for films of lower thickness. The observed drawback in this work is that the resistance change did not recover fully in the observed recovery time period. Thus, more efforts are required to obtain improved response-recovery times.

4.6. Organic−Inorganic Hybrid Nanocomposites for Carbon Dioxide (CO_2) Detection

Detection of carbon dioxide (CO_2) concentration has been recognized as very important to preserve a clean environment in an airtight room to control agricultural and biological processes.[179,180] In this context, infrared spectroscopic and gas chromatographic techniques have been found to be unsuitable because the available apparatus is expensive and large in size. Hence, a number of simplified CO_2 sensors have been proposed that permit the routine measurement of CO_2 gas. The principle of CO_2 sensing depends mainly on the basis of the change in the electrical response of sensing materials as a function of CO_2 concentration; e.g., the electromotive force and capacitance were measured in electrolyte and capacitance type CO_2 sensors, respectively.[181]

Kim et al.[182] studied the gas-sensing properties of organic–inorganic hybrids of poly(amide-6-β-ethylene oxide) (PEBAX) and silica (SiO_2) prepared via in situ polymerization of tetraethoxysilane (TEOS) using sol−gel processes. Gas permeation measurements were conducted at various temperatures with helium, CO_2, O_2, and N_2. The activation energy of CO_2 and its permeation through the hybrid membranes was found to be decreased due to the large contribution of the heat of sorption, while that of N_2 increased resulting from the increase of tortuosity and restricted chain mobility. This was attributed to the strong interaction between CO_2 molecules and SiO_2 domains, which resulted in blocking of additional sorption sites of the polyamide in PEBAX and the organic/inorganic interface. The PEBAX-SiO_2 composite membrane exhibited higher gas permeability coefficients and permselectivity than those of PEBAX, particularly at an elevated temperature: $\alpha CO_2/N_2$ = 72 at 25 °C with PCO_2 = 205 bar and $\alpha CO_2/N_2$ = 44 at 85 °C with PCO_2 = 507 bar for P8S2. There is considerable scope to prepare organic−inorganic hybrid nanocomposites for application to rapid, sensitive, and selective detection of CO_2.

Moreover, organic−inorganic hybrid nanocomposites were used to separate CO_2 from gas mixtures for practical applications.[183,184] A membrane of a metal−organic framework consisting of copper 1,4-benzenedicarboxylate based on a bottom-up approach was prepared to separate CO_2 from CO_2/CH_4 gas mixtures (Figure 21).[183] A free-standing membrane of polysilsesquioxanes (PSSQs), an organic/inorganic hybrid, was also developed for gas separation (He, H, CO_2, O_2, N_2, and CH_4) applications.[184] These membranes were found to show maximum permeability for CO_2 only.

4.7. Organic−Inorganic Hybrid Nanocomposites for Carbon Monoxide (CO) Detection

Carbon monoxide (CO) is a colorless, odorless, and tasteless gas that can inhibit the transportation of oxygen in human blood. CO is one of the most common and dangerous pollutants present in the environment due to its emission from automated vehicles, aircraft, natural gas emission, industrial waste, sewage leaking, mines, etc.[185] Its deleterious effect on human life is well-known.[186] When the level of CO rises beyond the minimum level in the environment, it becomes life-threatening and hazardous.[4] It is thus essential to continuously monitor the CO level in the surroundings and places of work in real time.

The currently available techniques such as gas chromatography, chemical analysis, infrared absorption, electronic noses, and semiconducting oxides, which depend upon sample drawing and analysis using light sources, laser beams, etc. are sophisticated, time-consuming, temperature dependent, and expensive. Recently, several selective, cost-effective, and stable gas sensors using nanocomposites have been reported for CO detection. For CO sensing (7.8 to 1000 ppm), Densakulprasert et al.[187] measured the electrical conductivity of PANI-zeolite nanocomposites as a function of precursor concentration, pore size, and the ion exchange capacity of zeolite. The highest electrical conductivities and sensitivities were obtained with the 13X zeolite, followed by the Y zeolite, and the AlMCM41 zeolite. Zeolite AlMCM41 exhibited poor sensitivity due to large pore size and the lowest Cu^{2+} exchange capacity. Y zeolite and 13X zeolite, however, are known to have similar pore sizes; however, the latter has a greater pore free volume and appropriate location distribution of the Cu^{2+} ions. The observed response time was found to increase with the amount of zeolite in the composites but was inversely related to the amount of ion-exchange capacity. A stable resonance of +C≡ O− with the positive charge at the carbon atom withdraws a lone pair of electrons at the amine nitrogen: −NH−. The positive charge at the carbon atom then becomes neutral, and the amine nitrogen then possesses a positive charge and becomes a polaron $-NH^{\bullet+}-$. This amine-to-polaron conversion results in a net increase of the number of positive charge carriers and, therefore, an increase in conductivity.

Ram et al.[188] and Jin et al.[189] have reported improved lower detection limits of 1.7 and 1 ppm for CO, respectively. PANI-MWCNT-based nanocomposites have been used to fabricate an electrochemical gas sensor for CO detection. This sensor works on the basis of bifunctional catalysis and shows enhanced catalytic oxidation and reduction of CO. The observed results revealed detection of CO in the linear range 0.01 to 0.7 mM (Pt/PAN-MWCNTs/WGE) and 10–50 μM (Pt−Ni/PAN-MWCNTs/WGE), respectively, along with a detection limit of 1.7 ppm and 0.1 mM at a scan rate of 50 mV s^{-1}. A response time of 90 s was observed (Figure 22).[189] The ultrathin conducting PANI-SnO_2 and PANI-TiO_2 hybrid

nanocomposite films were deposited onto interdigitated electrodes for CO gas (0–1000 ppm) detection, as a function of resistivity change at room temperature. The sensor showed response and recovery times of 20 and 250 s, respectively, at 1 ppm of CO gas.

The rapid and selective detection of CO at ppb level was reported by Mishra et al.[81] using vacuum-deposited PANI-Fe:Al (80:20) nanocomposite thin films. Using these sensors, CO could be detected in the range 0.006 to 0.3 ppm at room temperature. These sensors showed very high sensitivity of the order of 400–600, and response times of 10 s at room temperature. During sensing, CO gas resulted in a reduction of the barrier height at the intercrystallite grain boundary, thus lowering the intercrystallite barrier and increasing the current flow through the sensor. Figure 23 shows the gas sensing behavior of hybrid nanocomposite materials upon exposure to CO gas concentrations. The increase in current output of the sensor was directly proportional to the amount of the exposed gas on the sensor surface. It was observed that vacuum-deposited PANI-Fe:Al thin film sensors were suitable for online detection and continuous monitoring of CO.

5. ORGANIC−INORGANIC HYBRID NANOCOMPOSITES FOR HUMIDITY DETECTION

Next to temperature, humidity is the second most important parameter to monitor in industry. Humidity monitoring is of paramount importance in a number of areas, such as in moisture-sensitive products, storage areas, computer rooms, hospitals, museums, libraries, high-voltage engineering, and accelerator systems.[190,191] Recently, there has been a considerable increase in demand for humidity control in various fields, such as air conditioning systems, electronic devices, the tire industry, the sugar industry, and drying processes for ceramics/food. Moreover, the monitoring of humidity is also important for the fabrication of highly sophisticated integrated circuits (semiconductor industry).[192] A large number of nanostructures ranging from ceramics, semiconductors, and polymer hybrid nanocomposites have been utilized for humidity detection.

Humidity is the most ubiquitous interferent in any realistic environmental sensing situation. Most sensing reports only describe the sensing of gases in the absence of water and likewise, sensing of humidity is done in the absence of any other potentially interfering species. Recently, efforts have been made to prepare gas sensors that will remain unaffected by humidity[193,194] or only selective to humidity, i.e., that remain unaffected by other gases.[195] However, more extensive efforts are required to address this issue. The potential of organic–inorganic hybrid nanocomposites to fabricate humidity sensors is discussed here.

Tandon et al.[196] fabricated conductive nanocomposites of PPy−Fe_3O_4 using an emulsion polymerization method in aqueous solution, for use as gas sensors. This nanocomposite exhibited fairly high sensitivity (980) to relative humidity (80%) and some commonly used gases (N_2, O_2, and CO_2). The sensitivity of PPy-Fe_3O_4 gas sensors increases almost linearly, but the rise is steeper for CO_2 gas, due to the smaller kinetic diameter (0.33 nm) of the CO_2 molecule in comparison to 0.345 nm for O_2 and 0.364 nm for N_2. The fabricated sensor exhibited a response time of 10–15 s and a recovery time of ~25 s. However, this sensor was not found to be selective. Power et al.[197] fabricated a poly(vinyl alcohol)−Ag

nanoparticle (~22 nm) nanocomposite onto Pt-IDE and utilized it as a sensor to detect humidity selectively. At constant potential, the fabricated nanocomposite exhibited a change in current as a function of %RH from 10% to 60%. The sensor was found to be reversible, selective, and rapid. The authors also proposed the sensor response mechanism, and it correlated well with a second-order Langmuir adsorption model using second-order $S = S/S_s$ ($K_bC/1 + K_bC$), where S_s is relative signal at saturation, K_b is the binding constant, and C is the relative %RH.

Since the chemistry of polymers influences the sensing mechanism, further research focused on tailoring materials with good sensitivity, detection range and detection limits is likely to be very beneficial for device applications. Su et al.[198] described fabrication of a hybrid nanocomposite thin film of PPy-TiO_2 onto an Al substrate using the in situ electrochemical polymerization technique for humidity detection. The sensing behavior and its related mechanism were investigated by measuring the activation energy and by impedance spectroscopy. PPy-TiO_2 hybrid nanocomposite (TiO_2 nanoparticles ~0.0012 g) thin-film-based sensors (at 15 to 35 °C) exhibited lower hysteresis, sensitivity and good linearity ($Y = -0.306X + 0.84$; $R^2 = 0.94$) with response and recovery times of 20 and 40 s, respectively. The sensing characteristics of this sensor were improved by adding poly[3-(methacrylamino)propyl]-trimethylammonium chloride (PMAPTAC) to a PPy-TiO_2 (0.048 g) nanocomposite using photopolymerization. Enhanced flexibility, sensitivity, linearity ($Y = -0.0665X + 9.57$; $R^2 = 0.997$), hysteresis, a fast response time, a shorter recovery time, and a smaller temperature effect between 15 and 30 °C were obtained.[199] The gas sensing performance of PMAPTAC-PPy-TiO_2 nanocomposite films was not affected by CO and CO_2 gases.

Humidity sensing properties of poly(*o*-anisidine)-WO_3 (POA/WO_3) nanocomposite sensors as a function of resistance versus relative humidity and humidity hysteresis was explored by Patil et al.[200] The humidity sensing properties of the POA were also studied for comparison. Parvatikar et al.[201] prepared WO_3 nanoparticle-based hybrid nanocomposites with PANI for humidity sensing. Patil et al. prepared nanocomposites by mechanical mixing, whereas Parvatikar et al. used the “in situ” deposition technique by placing fine-grade WO_3 nanoparticles in a polymerization mixture of aniline. It was observed that the composite prepared by mechanical mixing of 30 wt % WO_3 in POA showed the maximum response factor of 353 at 85% RH, with narrow hysteresis (6%). The nanocomposites prepared by the in situ method showed better sensing performance. High-temperature conductivity measurements showed thermally activated behavior with a change in resistance with respect to % RH. The almost linear response (10 to 95% RH) of the PANI-WO_3 nanocomposite (50 wt % of WO_3 in PANI) to a broad range of humidity conditions suggested it to be an interesting and competent material for use as a humidity sensor. The superior sensing performance of in situ-prepared nanocomposites over mechanically mixed nanocomposites can be understood in the terms of improved interaction at the interface between inorganic nanoparticles and polymers. The improved interaction at the interface perhaps results in easy and efficient charge transfer and better sensing performance of the nanocomposites.

The impedance spectroscopy technique has been used to investigate humidity sensing and electrical properties of SiO_2 and poly[3-(methacrylamino)propyl]trimethylammonium

chloride (poly-MAPTAC)-based nanocomposite sensors.[202] A sensor based on a SiO_2-poly-MAPTAC nanocomposite film showed satisfactory resistance at high humidity atmospheres ~97% RH with high sensitivity (three orders), better linearity over a wide humidity range (10–90% RH), negligible hysteresis, and response and recovery time (humidification: 60 s, desiccation: 120 s). The activation energy for conduction reduced with water adsorption. Further, different response mechanisms of SiO_2-poly-MAPTAC nanocomposite sensors were suggested at low and high relative humidity. Highly electro-active CNTs were incorporated into polydimethyldiallylammonium chloride (PDDA) to fabricate nanocomposite films between IDEs on a Si/SiO_2 substrate using the layer-by-layer self-assembly technique.[203] The resistance of CNT-PDDA nanocomposite films was found to increase exponentially with an increase in humidity (RH ~ 20%–98%). In sensing, CNT junctions played an important role in the overall resistance change for water molecule absorption. The sensor exhibited a high sensitivity of 80%, a fast response time of 8 s, and good reversibility (5 cycles). Another impedance-based humidity sensor was reported by Li et al.[204] using nanocomposite thin films of sodium polystyrenesulfonate (NaPSS) and ZnO nanoparticles. The impedance response (as a function of humidity concentration) of the sensor was found to increase by 4 orders of magnitude, over a humidity range of 11–97% RH. The NaPSS-ZnO nanocomposite sensors exhibited sensitivity (2–90% RH), better linearity, low hysteresis (~2% RH), and a quicker response (2 s for absorption and desorption) than the NaPSS-based sensor. It has been proposed that the improved sensing properties were due to the addition of ZnO nanoparticles to NaPSS.

An optical-fiber-based humidity sensor containing Ag (diameter ~15 nm)-PANI nanocomposite has been fabricated onto optical fiber clad (length ~6 mm) using evanescent wave absorption spectroscopy and tested in the range of 5–95% RH.[205] It was observed that reduction of the Ag nanoparticle size leads to improved sensitivity and response time. The fabricated sensor exhibited reversible response with a standard deviation of 1% and response time of ~30 s with a high recovery time of 90 s. This report focused on the effect of Ag nanoparticle concentration in nanocomposites for sensing phenomena. Liu et al.[206] and Timm et al.[207] used IDEs to fabricate sensors of lower dimensions with enhanced sensing performance. Liu et al.[206] deposited MW/SWCNT-PDDA hybrid nanocomposite films onto $IDE/Si/SiO_2$ substrates by the layer-by-layer self-assembly technique for the sensing of humidity (20–98%). The resistance stability of composite films was found to be improved by thermal annealing. The resistance of composite films increased exponentially with increases in humidity. The sensitivity [$S = (\Delta R/R_{20\%}) \times 100$] was improved with the increase in the number of layers in the sensor (8 layers). An eight-layered MWCNT-PDDA humidity sensor exhibited a response time of 8 s and a recovery time of 35 s, while in the case of a SWCNT-PDDA sensor, the observed response and recovery times were 8 and 40 s, respectively. A MWCNT-modified sensor showed better sensitivity than SWCNT-based sensors in higher RH ranges (80%). The humidity sensing in CNT-PDDA composite films has been attributed to the junction resistance of CNTs. The sensors were reversible, and temperature was observed to affect the sensitivity of CNT-PDDA composite film humidity sensors.

A nanocomposite film of meso(3/4-pyridyl)porphyrinate Co(III) species coordinated to four $[Ru(bipy)_2Cl]^+$ complexes and vanadium pentoxide (V_2O_5) was deposited onto an Au IDE

(Figure 24).[207] This nanocomposite exhibited interesting electrical and electrochemical properties for application to resistive sensors for humidity detection at room temperature. The sensitivity of the fabricated sensor decreased exponentially as a function of water concentration in the ethanol/water system. The sensing phenomenon is based on reversible adsorption/desorption processes involving a defined number of interaction sites, according to the Langmuir equation. These devices were found to be more sensitive toward a lower concentration range (0–10%, v/v) of humidity and allowed quantification of the water content in commercial anhydrous ethanol and hydrated ethanol used as fuel (Figure 24 D). The improved sensing properties have been attributed to the use of IDE in fabrication of sensors. The use of IDE enhances the collection or transfer of charges to the electrode due to the smaller gap between the successive electrodes.

6. CHALLENGES IN ORGANIC−INORGNIC HYBRID NANOCOMPOSITE-BASED GAS SENSING

The applications of organic−inorganic hybrid nanocomposites for environmental monitoring require urgent solutions related to materials processing science and sensor fabrication. Inorganic nanoparticles have a tendency to become agglomerated in solvents, which decreases the effective surface area. This shortcoming can be overcome using different surfactants to modify the surface of nanoparticles for uniform dispersion. Another approach is to use nanostructures with aspect ratios higher than unity, as the agglomeration is reduced in these nanostructures in comparison to spherical nanoparticles. For the fabrication of an efficient sensor, organic−inorganic hybrid nanocomposites need to be deposited or transferred onto an electronically conducting substrate. The challenge is to improve binding of nanocomposites with electrode/conducting platforms and the tuning of energy barrier at the interface for facile charge transport that is required for improved sensing. Depending upon the nature of the electrode and hybrid nanocomposite, various electrode treatments (such as hydrogen/nitrogen/plasma treatment, higher temperature annealing, self-assembled monolayer modification, etc.) have been introduced for efficient sensor platform development. These treatments are likely to result in better attachment of hybrid nanocomposite films to electrodes, along with the lowering of the energy barrier (reduction in the depletion region).

Gas detection at the ppt level requires good analyte adsorption at the nanocomposite sensing surface that can be achieved by developing a better sensing nanomaterial for a given target analyte. The charge carriers generated by the adsorption of the target gas analyte should migrate easily and be collected at the electrode. Due to the low conductivity of organic materials in nanocomposites, fewer charge carriers reach the electrodes. This can perhaps be resolved by doping a suitable dopant (mainly surfactant and metal nanostructures, e.g. graphene, Pt, Ni, Au, Ag, etc.) that may improve the charge migration toward electrodes. Another approach adopted by many researchers is to perhaps deposit the nanocomposite sensing thin film onto IDEs (comb like microstructures). These successive electrodes in IDEs are separated by a spacing of a few microns, which may enhance the collection of charge, resulting in better sensing performance. With fast-advancing engineering and technology, it is now possible to fabricate IDEs with electrode interspacing in the range

of tens of nanometers. The application of these IDEs in sensing can enhance the signal significantly and sensing at the ppt level can be achieved.

Organic−inorganic hybrid nanocomposites have bright prospects for application in environmental monitoring, but selectivity is still a major concern. The development of optimized target-analyte-specific hybrid nanocomposites is required. Studies and modifications targeted at the interface between organic host materials and guest inorganic nanostructures hold the key for nanocomposite sensing performance. Thus, the science of interfaces needs more clarity and understanding. Due to abundant humidity in the environment, the effect and interference of humidity on sensing needs to be systematically investigated. Hydrophobic organic conducting materials can be used to overcome the problem of humidity. Table 1 summarizes the sensing characteristics of organic−inorganic hybrid nanocomposite-based sensors for environment monitoring.

7. CONCLUSIONS

This article reviews recent developments in the fabrication of organic−inorganic hybrid nanocomposites based gas sensors for environmental monitoring. These materials have been found to be an excellent alternative to conventional gas sensing materials due to their unusual optical, electrical, and morphological properties that are advantageous for gas sensor development, which can easily be tailored by variation of their synthetic routes or precursors. Among the various hybrid nanocomposite systems, conducting polymers and metal/metal oxide nanocomposite sensors are reviewed in greater detail due to their promising abilities as a platform for environmental gas monitoring. This interesting class of hybrid nanocomposite shows interesting optical, electrical and molecular properties that can be easily and cost-effectively tuned. The review clearly demonstrates that sensing characteristics depend both on the composition of the hybrid materials and the geometrical characteristics of the structures produced. The compositions of the materials, in conjunction with their structural morphology and geometrical characteristics, are under further investigation with an aim to optimize materials and overall performance. The review also highlights the urgent need for making measurements in the presence of humidity to establish the ability of the sensors to function in a real world environment.

ACKNOWLEDGMENTS

This work was supported by NIH Grants RO1-DA027049, R21-MH101025, RO1-MH085259, and RO1-DA034547 and NSF Grant ERC-ASSIST No. 1160483. DST (DST/TSG/ME/2008/18 and DBT (DBT/GAP070832) is also acknowledged. R.K. acknowledges the UGC, India for the award of Raman Fellowship (ID 1001, 2013–14).

Biographies

Ajeet Kaushik received his Ph.D. (chemistry, biosensors; 2010) in collaboration with the National Physical Laboratory and Jamia Milia Islamia, New Delhi, India. Presently, he is a faculty at Centre of Personalized Nanomedicine, Institute of NeuroImmune Pharmacology, Department of Immunology, of Florida International University (FIU), USA. He is exploring smart electro-active magnetic nanocarriers for on-demand site-specific delivery and controlled release of therapeutics across BBB to prevent HIV; a new approach towards neuroAIDS. He has worked as a Post-Doctoral Research Associate in the area of fabrication of BioMEMS-based electrochemical biosensors for biomarker detection using nanostructures at the Department of Electrical and Computer Engineering of FIU. He has also worked at Chungnam National University, Deajeon, Korea as a Visiting Researcher and at Dublin City University, Dublin, Ireland as a Research Assistant. He has published over 70 international research papers jointly in the area of nanostructured platforms for biosensor and drug delivery applications. His main research interest is the fabrication of nanomedicines and wearable sensors for personalized health care.

Rajesh Kumar is an Assistant Professor in the Department of Physics at Panjab University, Chandigarh, India. He was born in Gurdaspur district of Punjab, India. He received his Ph.D. from the National Physical Laboratory in collaboration with University of Delhi and the Indian Institute of Technology, Delhi, India in the area of Materials Science (2010). He was awarded the prestigious Raman Fellowship by University Grant Commission, India, in 2013 to undertake research in U.S.A. for 1 year. Presently he is working as a Visiting Assistant Professor in the Department of Electrical and Computer Engineering, Florida International University, Miami, Florida. He has published ca. 20 international papers in the area of synthesis and applications of nanomaterials and organic−inorganic hybrid nanocomposites. His research focus is in interface modification of hybrid nanocomposites for energy-harvesting device development.

Sunil K. Arya received his B.Sc. in chemistry in 2002, MSc. in organic chemistry in 2004, and Ph.D. in chemistry and biosensors in 2008 from the University of Delhi, Delhi, India. He is currently a scientist at the Institute of Microelectronics, A*star, Singapore. He has completed Post-Doctoral research at University of South Florida, Tampa, Florida, and at the National Institute of Nanotechnology and University of Alberta, Edmonton, Alberta, Canada. He has published ca. 45 papers in international journals. His primary interests are in the synthesis and applications of nanomaterials, monolayers, and MEMS for use

in gas sensors and electrochemical biosensors. His research focus is in the areas of micro/nanofabrication, materials science, and thin film sensors/biosensors.

Madhavan Nair received his Ph.D. from Tata Memorial Cancer Center, Bombay University, India, in cancer immunology and trained at the Memorial Sloan Kettering Cancer Center, New York City. He then joined the faculty of the Department of Pediatrics at the University of Michigan, Ann Arbor and subsequently worked at the Department of Medicine and Microbiology at SUNY, Buffalo, New York as a Tenured Professor and Director of Research in Allergy and Immunology. He is a certified Clinical Nutrition Specialist (CNS), Fellow of American College of Nutrition (FACN), and Fellow of the American Academy of Allergy, Asthma and Immunology (FAAAI). Recently, Dr. Nair was named Distinguished Professor and Founding Chair of the Department of Immunology, and Director of the Institute of Neuro-Immune Pharmacology at the FIU College of Medicine, and Associate Dean, Biomedical Research, FIU, Miami, Florida. Nair has published more than 100 research papers, chaired a number of scientific sessions and served in various NIH study sections and committees as chair/member since 1980. His recent research mainly involves the role of different drugs of abuses such as alcohol, morphine, cocaine, and methamphetamine on neuro-AIDS and therapeutic approaches to control neuro-AIDS by specific drugs capable of targeting the brain using nanotechnology.

B. D. Malhotra received his Ph.D. degree from the University of Delhi, Delhi, India in 1980. He has published more than 260 papers in peer-reviewed journals, filed 10 patents, and edited/coedited books on biosensors and polymer electronics. After his stint as Chief Scientist and Head of the DST Centre on Biomolecular Electronics at the National Physical Laboratory, New Delhi, India, he moved to the Delhi Technological University (DTU), India and is currently Professor at the Department of Biotechnology at DTU. He has nearly 30 years of research experience in the field of biomolecular electronics and has guided 24 Ph.D. students to date. His current activities include biosensors, nanobiomaterials, conducting polymers, and ordered molecular assemblies including Langmuir−Blodgett films and self-assembled monolayers among others. Dr. Malhotra is a Fellow of the Indian National Science Academy (INSA), the National Academy of Sciences, India (NASI), and an Academician of the Asia-Pacific Academy of Materials (APAM).

Shekhar Bhansali is an Alcatel-Lucent Professor and Chair at the Department of Electrical and Computer Engineering at Florida International University. He received his Ph.D. in Electrical Engineering (1997) from the Royal Melbourne Institute of Technology, Melbourne, Australia. His research interests are in the areas of Bio-MEMS, sensors, nanostructures, and microsystems. He is the recipient of an NSF CAREER Award, an Alfred P. Sloan Foundation Outstanding Mentor Award, FGLSAMP Outstanding Mentor Award, FEF Outstanding Mentor Award, and USF Outstanding Researcher Award. He holds 16 patents in the area of biosensors, nanostructures, and microsystems technologies; has coauthored over 200 journal articles and conference publications; and is the editor of the book “MEMS for Biomedical Applications”.

GLOSSARY

$(CH_3)_2CHOH$	isopropanol
[A]	analyte
[DL]	detection Limit
[FT]	fabrication technique
[L]	linear range
[NSP]	nanostructured platform
[R]	response
[Rm]	remarks
[Rs]	response time
[Rv]	recovery time
[S]	sensitivity
[SL]	shelf life
AN	acrylonitrile
ATO	antimony-doped tin oxide
$C_2H_5CH_3$	toluene
C_4H_8O	tetrahydrofuran
C_5H_5N	pyridine

C_6H_{14}	hexane
C_8H_{18}	octane
CdSe	cadmium selenide
CeO_2	cerium oxide
CFC	chlorofluorocarbon
CH	chitosan
$CH_3(CH_2)_3NH_2$	n-butylamine
$CH_3CH_2CH_3$	propane
CH_3CH_2OH	ethanol
CH_3CH_2OH	propanol
CH_3CHO	acetaldehyde
CH_3COCH_3	acetone
CH_3OH	methanol
CH_4	methane
$CHCl_3$	chloroform
ClO_4	perchlorate
CLPANI	cross-linked polyaniline
CNF	carbon nanofiber
CNT	carbon nanotube
CO	carbon monoxide
$CoCl_2$	cobalt chloride
COOH	carboxylic acid
CSA	camphorsulfonic acid
CuPc	copper phthalocyanine
DMF	dimethylformamide
EDOT-*co*-TAA	3,4-ethylenedioxythiophene-co-thiophene-3-acetic acid
EPA	environment protection agency
Fe_3O_4/Fe_2O_3	iron oxide
FET	field effect transistor

GO	graphene oxide
H_2O_2	hydrogen peroxide
H_2S	hydrogen sulfide
HCHO	formaldehyde
IDEs	interdigitated electrodes
In_2O_3	indium oxide
ITO	indium−tin-oxide
MAcoBMA	methacrylic acid-*co*-*tert*-butyl methacrylate
MAPTAC	[3 - (methacrylamino) propyl] - trimethylammonium chloride
MnO_2	manganese oxide
MoO_3	molybdenum oxide
$N(C_2H_5)_3$	triethylamine
NaPSS	sodium polystyrenesulfonate
NBB	nanobuilding block
NH_3	ammonia
NiO	nickel oxide
NIR	near-infrared
NO_x	nitrogen oxides
OTFT	organic thin-film transistor
P3HT	poly(3-hexylthiophene)
PANI	polyaniline
PDDA	polydimethyldiallylammonium
PDDAC	polydiallyldimethylammonium chloride
PEBAX	poly(amide-6-*b*-ethylene oxide)
PEDT	poly(dioxythiophene)
PEHT	polythiophene
PEO	poly(ethylene oxide)
PHTh	polyhexathiophene

PMMA	poly(methyl methacrylate)
PNMA	poly(*N*-methylaniline)
PPV	polyvinyl chloride
PPy	polypyrrole
PSMA	polystyrene-*co*-maleic anhydride
PSSQs	polysilsesquioxanes
PVB	polyvinyl butyral
QCM	quartz crystal microbalance
QD	quantum dots
RH	relative humidity
SAW	surface acoustic waves
SnO_2	tin oxide
SPR	surface plasmon resonance
TEOS	tetraethoxysilane
THF	tetrahydrofuran
TiO_2	titanium oxide
TSMRs	thickness-shear mode resonators
UV−vis	ultraviolet visible
V_2O_5	vanadium oxide
VDP	vapor deposition polymerization
VOCs	volatile organic compounds
WO_3	tungsten oxide
ZnO	zinc oxide
ZnS	zinc sulfide
ZrO_2	zirconium oxide

REFERENCES

(1). Zimmerling R; Dämmgen U; Küsters A; Grünhage L; Jäger H-J Response of a Grassland Ecosystem to Air Pollutants. IV. The chemical climate: Concentrations of Relevant Non-Criteria Pollutants (Trace Gases and Aerosols). Environ. Pollut 1996, 91, 139–147. [PubMed: 15091434]

(2). Odlyha M; Foster GM; Cohen NS; Sitwell C; Bullock L Microclimate Monitoring of Indoor Environments Using Piezoelectric Quartz Crystal Humidity Sensors. J. Environ. Monit 2000, 2, 127–131. [PubMed: 11253031]

(3). Emil J,B Jr. Indoor Pollution and its Impact on Respiratory Health. Ann. Allergy, Asthma, Immunol 2001, 87, 33–40.

(4). Becker T; Mühlberger S; Braunmühl CB-V; Müller G; Ziemann T; Hechtenberg KV. Air Pollution Monitoring Using Tin-Oxide-Based Microreactor Systems. Sens. Actuators, B 2000, 69, 108–119.

(5). Windmiller JR; Wang J Wearable Electrochemical Sensors and Biosensors: A Review. Electroanalysis 2013, 25, 29–46.

(6). Bogue R Emerald Article: Terrorism and Military Actions Pose the Ultimate Challenge to Gas Sensing. Sens. Rev 2011, 31, 6–12.

(7). Lim TC Nanosensors: Theory and Applications in Industry, Healthcare and Defense Taylor and Francis: London, 2010.

(8). Korotcenkov G Chemical Sensors: Comprehensive Sensor Technologies; Momentum Press: New York, 2011; Vol. 6.

(9). Korotcenkov G Chemical Sensors Comprehensive Sensor Technologies; Momentum Press: New York, 2011; Vol. 4.

(10). Janata J Introduction: Modern Topics in Chemical Sensing. Chem. Rev 2008, 108, 327–328. [PubMed: 18220424]

(11). Korotcenkov G Chemical Sensors; Momentum Press: New York, 2010; Vol. 1.

(12). Stetter JR; Li J Amperometric Gas Sensors-A Review. Chem. Rev 2008, 108, 352–366. [PubMed: 18201108]

(13). Blair R; Shepherd H; Faltens T; Haussmann PC; Kaner RB; Tolbert SH; Huang J; Virji S; Weiller BH Construction of a Polyaniline Nanofiber Gas Sensor. J. Chem. Educ 2008, 85, 1102.

(14). Xie D; Jiang Y; Pan W; Li D; Wu Z; Li Y Fabrication and Characterization of Polyaniline Based Gas Sensor by Ultra-Thin Film Technology. Sens. Actuators, B 2002, 81, 158–164.

(15). Jun H-K; Hoh Y-S; Lee B-S; Lee S-T; Lim J-O; Lee D-D; Huh J-S Electrical Properties of Polypyrrole Gas Sensors Fabricated Under Various Pretreatment Conditions. Sens. Actuators, B 2003, 96, 576–581.

(16). Chang JB; Liu V; Subramanian V; Sivula K; Luscombe C; Murphy A; Liu J; Frechet JM Printable Polythiophene Gas Sensor Array for Low-Cost Electronic Noses. J. Appl. Phys 2006, 100, 014506.

(17). Saxena V; Malhotra BD Prospects of Conducting Polymers in Molecular Electronics. Curr. Appl. Phys 2003, 3, 293–305.

(18). MacDiarmid AG “Synthetic Metals”: A Novel Role for Organic Polymers (Nobel Lecture). Angew. Chem., Int. Ed 2001, 40, 2581–2590.

(19). Liu T; Burger C; Chu B Nanofabrication in Polymer Matrices. Prog. Polym. Sci 2003, 28, 5–26.

(20). Inzelt G Applications of Conducting Polymers Conducting Polymers Springer: Berlin, 2012; pp 245–293.

(21). Korotcenkov G Chemical Sensors Fundamentals of Sensing Materials; Momentum Press: New York, 2011; Vol. 3.

(22). Adhikari B; Majumdar S Polymers in Sensor Applications. Prog. Polym. Sci 2004, 29, 699–766.

(23). Barisci JN; Wallace GG; Andrews MK; Partridge AC; Harris PD Conducting Polymer Sensors for Monitoring Aromatic Hydrocarbons Using an Electronic Nose. Sens. Actuators, B 2002, 84, 252–257.

(24). Bai H; Shi G Gas Sensors Based on Conducting Polymers. Sensors 2007, 7, 267–307.

(25). Haynes A; Gouma P-I Polyaniline-Based Environmental Gas Sensors for Environment, Health and Security; Baraton M-I, Ed.; Springer: Netherlands, 2009; pp 451–459.

(26). Janata J; Josowicz M Conducting Polymers in Electronic Chemical Sensors. Nat. Mater 2003, 2, 19–24. [PubMed: 12652667]

(27). Brailsford AD; Yussouff M; Logothetis EM A First Principles Model of Metal Oxide Gas Sensors for Measuring Combustibles. Sens. Actuators, B 1998, 49, 93–100.

(28). Capone S; Siciliano P; Quaranta F; Rella R; Epifani M; Vasanelli L Analysis of Vapours And Foods By Means of an Electronic Nose Based on A Sol−Gel Metal Oxide Sensors Array. Sens. Actuators, B 2000, 69, 230–235.

(29). Ehrmann S; Jüngst J; Goschnick J; Everhard D. Application of a Gas Sensor Microarray to Human Breath Analysis. Sens. Actuators, B 2000, 65, 247–249.

(30). Tsujita W; Yoshino A; Ishida H; Moriizumi T Gas Sensor Network for Air-Pollution Monitoring. Sens. Actuators, B 2005, 110, 304–311.

(31). Barsan N; Weimar U Conduction Model of Metal Oxide Gas Sensors. J. Electroceram 2001, 7, 143–167.

(32). Barsan N; Koziej D; Weimar U Metal Oxide-Based Gas Sensor Research: How to? Sens. Actuators, B 2007, 121, 18–35.

(33). Tan OK; Cao W; Hu Y; Zhu W Nano-Structured Oxide Semiconductor Materials for Gas-Sensing Applications. Ceram. Int 2004, 30, 1127–1133.

(34). Tan OK; Cao W; Hu Y; Zhu W Nanostructured Oxides by High-Energy Ball Milling Technique: Application as Gas Sensing Materials. Solid State Ionics 2004, 172, 309–316.

(35). In M; Geŕardin C; Lambard J; Sanchez C. Transition Metal Based Hybrid Organic-Inorganic Copolymers. J. Sol-Gel Sci. Technol 1995, 5, 101–114.

(36). Judeinstein P; Sanchez C Hybrid Organic−Inorganic Materials: A Land of Multidisciplinarity. J. Mater. Chem 1996, 6, 511–525.

(37). Lebeau B; Sanchez C Sol-Gel Derived Hybrid Inorganic-Organic Nanocomposites for Optics. Curr. Opin. Solid State Mater. Sci 1999, 4, 11–23.

(38). Sanchez C; Soler-Illia G.d. A. ; Ribot F; Lalot T; Mayer C; Cabuil V. Designed Hybrid Organic-Inorganic Nanocomposites from Functional Nanobuilding Blocks. Chem. Mater 2001, 13, 3061–3083.

(39). Sanchez C; Lebeau B; Chaput F; Boilot JP Optical Properties of Functional Hybrid Organic−Inorganic Nanocomposites. Adv. Mater 2003, 15, 1969–1994.

(40). Sanchez C; Soler-Illia GJ; Ribot F; Grosso D Design of Functional Nano-Structured Materials Through the use of Controlled Hybrid Organic−Inorganic Interfaces. C. R. Chim 2003, 6, 1131–1151.

(41). Mammeri F; Le Bourhis E; Rozes L; Sanchez C Mechanical Properties of Hybrid Organic−Inorganic Materials. J. Mater. Chem 2005, 15, 3787–3811.

(42). Nicole L; Boissieŕe C; Grosso D; Quach A; Sanchez C. Mesostructured Hybrid Organic−Inorganic Thin Films. J. Mater. Chem 2005, 15, 3598–3627.

(43). Sanchez C; Julián B; Belleville P; Popall M. Applications of Hybrid Organic−Inorganic Nanocomposites. J. Mater. Chem 2005, 15, 3559–3592.

(44). Grosso D; Ribot F; Boissiere C; Sanchez C Molecular and Supramolecular Dynamics of Hybrid Organic−Inorganic Interfaces for The Rational Construction of Advanced Hybrid Nanomaterials. Chem. Soc. Rev 2011, 40, 829–848. [PubMed: 21170460]

(45). Sanchez C; Belleville P; Popall M; Nicole L Applications of Advanced Hybrid Organic−Inorganic Nanomaterials: From Laboratory to Market. Chem. Soc. Rev 2011, 40, 696–753. [PubMed: 21229132]

(46). Sanchez C; Shea KJ; Kitagawa S Recent Progress in Hybrid Materials Science. Chem. Soc. Rev 2011, 40, 471–472. [PubMed: 21229133]

(47). Sanchez C; Boissiere C; Cassaignon S; Chaneac C; Durupthy O; Faustini M; Grosso D; Laberty-Robert C; Nicole L; Portehault D Molecular Engineering of Functional Inorganic and Hybrid Materials. Chem. Mater 2013, 26, 221–238.

(48). Sanchez C; Lebeau B Design and properties of Hybrid Organic−Inorganic Nanocomposites for Photonics. MRS Bull 2001, 26, 377–387.

(49). Lebeau B; Innocenzi P Hybrid Materials for Optics and Photonics. Chem. Soc. Rev 2011, 40, 886–906. [PubMed: 21212891]

(50). Tan JC; Cheetham AK Mechanical Properties of Hybrid Inorganic-Organic Framework Materials: Establishing Fundamental Structure-Property Relationships. Chem. Soc. Rev 2011, 40, 1059–1080. [PubMed: 21221446]

(51). Sanchez C; Boissière C; Cassaignon S; Chaneac C; Durupthy O; Faustini M; Grosso D; Laberty-Robert C; Nicole L; Portehault D. Molecular Engineering of Functional Inorganic and Hybrid Materials. Chem. Mater 2013, 26, 221–238.

(52). Kaushik A; Khan R; Gupta V; Malhotra BD; Ahmad S; Singh SP Hybrid Cross-Linked Polyaniline-WO_3 Nanocomposite Thin Film for NOx Gas Sensing. J. Nanosci. Nanotechnol 2009, 9, 1792–1796. [PubMed: 19435041]

(53). Nastase C; Nastase F; Vaseashta A; Stamatin I Nanocomposites based on Functionalized Nanotubes in Polyaniline Matrix by Plasma Polymerization. Prog. Solid State Chem 2006, 34, 181–189.

(54). Gómez-Romero P; Chojak M; Cuentas-Gallegos K; Asensio JA; Kulesza PJ; Casañ-Pastor N; Lira-Cantú M. Hybrid Organic–Inorganic Nanocomposite Materials For Application in Solid State Electrochemical Supercapacitors. Electrochem. Commun 2003, 5, 149–153.

(55). Shi J.-l.; Hua Z.-l.; Zhang L.-x. Nanocomposites from Ordered Mesoporous Materials. J. Mater. Chem 2004, 14, 795–806.

(56). Shchipunov YA; Karpenko TYY; Krekoten AV Hybrid Organic-Inorganic Nanocomposites Fabricated With a Novel Bio-compatible Precursor using Sol-Gel Processing. Compos. Interfaces 2005, 11, 587–607.

(57). Carotenuto G; Nicolais L; Martorana B; Perlo P Metal-Polymer Nanocomposite Synthesis: Novel ex-situ and in-situ Approaches in Metal−Polymer Nanocomposites; John Wiley & Sons, Inc.: New York, 2005; pp 155–181.

(58). Kaushik A; Kumar J; Tiwari MK; Khan R; Malhotra BD; Gupta V; Singh SP Fabrication and Characterization of Polyaniline-ZnO Hybrid Nanocomposite Thin Films. J. Nanosci. Nanotechnol 2008, 8, 1757–1761. [PubMed: 18572575]

(59). Burghard Z; Tucic A; Jeurgens LPH; Hoffmann RC; Bill J; Aldinger F Nanomechanical Properties of Bioinspired Organic−Inorganic Composite Films. Adv. Mater 2007, 19, 970–974.

(60). Godovsky D Device Applications of Polymer-Nanocomposites Biopolymers·PVA Hydrogels. Anionic Polymerisation Nanocomposites; Springer: Berlin, 2000; Vol. 153, pp 163–205.

(61). Hatchett DW; Josowicz M Composites of Intrinsically Conducting Polymers as Sensing Nanomaterials. Chem. Rev 2008, 108, 746–769. [PubMed: 18171087]

(62). Guido K Concepts for the Incorporation of Inorganic Building Blocks into Organic Polymers on a Nanoscale. Prog. Polym. Sci 2003, 28, 83–114.

(63). Mitzi DB; Chondroudis K; Kagan CR Organic-Inorganic Electronics. IBM J. Res. Dev 2001, 45, 29–45.

(64). Mitzi DB Thin-Film Deposition of Organic−Inorganic Hybrid Materials. Chem. Mater 2001, 13, 3283–3298.

(65). Sukpirom N; Lerner MM Preparation of Organic−Inorganic Nanocomposites with a Layered Titanate. Chem. Mater 2001, 13, 2179–2185.

(66). Portney NG; Singh K; Chaudhary S; Destito G; Schneemann A; Manchester M; Ozkan M Organic and Inorganic Nanoparticle Hybrids. Langmuir 2005, 21, 2098–2103. [PubMed: 15751992]

(67). Vivekchand SRC; Kam KC; Gundiah G; Govindaraj A; Cheetham AK; Rao CNR Electrical Properties of Inorganic Nanowire-Polymer Composites. J. Mater. Chem 2005, 15, 4922–4927.

(68). Kruk M; Jaroniec M Gas Adsorption Characterization of Ordered Organic−Inorganic Nanocomposite Materials. Chem. Mater 2001, 13, 3169–3183.

(69). Tran-Thi T-H; Dagnelie R; Crunaire S; Nicole L Optical Chemical Sensors Based on Hybrid Organic-Inorganic Sol-Gel Nanoreactors. Chem. Soc. Rev 2011, 40, 621–639. [PubMed: 21180764]

(70). Ferey G; Serre C; Devic T; Maurin G; Jobic H; Llewellyn PL; De Weireld G; Vimont A; Daturi M; Chang J-S Why Hybrid Porous Solids Capture Greenhouse Gases? Chem. Soc. Rev 2011, 40, 550–562. [PubMed: 21180728]

(71). Han JT; Zheng Y; Cho JH; Xu X; Cho K Stable Superhydrophobic Organic−Inorganic Hybrid Films by Electrostatic Self-Assembly. J. Phys. Chem. B 2005, 109, 20773–20778. [PubMed: 16853692]

(72). Baibarac M; mez-Romero P Nanocomposites Based on Conducting Polymers and Carbon Nanotubes: From Fancy Materials to Functional Applications. J. Nanosci. Nanotechnol 2006, 6, 289–302. [PubMed: 16573025]

(73). Pyun J; Matyjaszewski K Synthesis of Nanocomposite Organic/Inorganic Hybrid Materials Using Controlled/"Living" Radical Polymerization. Chem. Mater 2001, 13, 3436–3448.

(74). Xiao Y; Li CM Nanocomposites: From Fabrications to Electrochemical Bioapplications. Electroanalysis 2008, 20, 648–662.

(75). Gill I Bio-doped Nanocomposite Polymers: Sol−Gel Bioencapsulates. Chem. Mater 2001, 13, 3404–3421.

(76). Wen J; Wilkes GL Organic/Inorganic Hybrid Network Materials by the Sol−Gel Approach. Chem. Mater 1996, 8, 1667–1681.

(77). Schmidt H; Jonschker G; Goedicke S; Mennig M The Sol-Gel Process as a Basic Technology for Nanoparticle-Dispersed Inorganic-Organic Composites. J. Sol-Gel Sci. Technol 2000, 19, 39–51.

(78). Shchipunov YA; Karpenko T. y. Y. Hybrid Polysaccharide–Silica Nanocomposites Prepared by the Sol−Gel Technique. Langmuir 2004, 20, 3882–3887. [PubMed: 15969374]

(79). Nanu M; Schoonman J; Goossens A Inorganic Nanocomposites of n- and p-Type Semiconductors: A New Type of Three-Dimensional Solar Cell. Adv. Mater 2004, 16, 453–456.

(80). Vu Q-T; Pavlik M; Hebestreit N; Rammelt U; Plieth W; Pfleger J Nanocomposites based on Titanium Dioxide and Polythiophene: Structure and Properties. React. Funct. Polym 2005, 65, 69–77.

(81). Misra SCK; Mathur P; Srivastava BK Vacuum-Deposited Nanocrystalline Polyaniline Thin Film Sensors for Detection of Carbon Monoxide. Sens. Actuators, A 2004, 114, 30–35.

(82). Misra SCK; Mathur P; Yadav M; Tiwari MK; Garg SC; Tripathi P Preparation and Characterization of Vacuum Deposited Semiconducting Nanocrystalline Polymeric Thin Film Sensors for Detection of HCl. Polymer 2004, 45, 8623–8628.

(83). Meristoudi A; Athanasekos L; Vasileiadis M; Pispas S; Mousdis G; Karoutsos E; Alexandropoulos D; Du H; Tsigara A; Kibasi K; Perrone A; Vainos NA Nanocomposite Hybrid Photonic Media for Remote Point Sensors. J. Opt. A: Pure Appl. Opt 2009, 11, 034005.

(84). Kreno LE; Leong K; Farha OK; Allendorf M; Van Duyne RP; Hupp JT Metal−Organic Framework Materials as Chemical Sensors. Chem. Rev 2011, 112, 1105–1125. [PubMed: 22070233]

(85). Heinze J. r .; Frontana-Uribe BA; Ludwigs S. Electrochemistry of Conducting Polymers—Persistent Models and New Concepts. Chem. Rev 2010, 110, 4724–4771. [PubMed: 20557047]

(86). Rajesh Ahuja T; Kumar D Recent Progress in the Development of Nano-Structured Conducting Polymers/Nanocomposites for Sensor Applications. Sens. Actuators, B 2009, 136, 275–286.

(87). Dhand C; Arya SK; Singh SP; Singh BP; Datta M; Malhotra BD Preparation of Polyaniline/Multiwalled Carbon Nanotube Composite by Novel Electrophoretic Route. Carbon 2008, 46, 1727–1735.

(88). Shinar RSJ . Organic Electronics in Sensors and Biotechnology. Electrophoretically Deposited Polymers for Organic Electronics McGraw-Hill Professional: New York, 2009.

(89). Zhitomirsky I Electrophoretic Deposition of Organic–Inorganic Nanocomposites. J. Mater. Sci 2006, 41, 8186–8195.

(90). McDonagh C; Burke CS; MacCraith BD Optical Chemical Sensors. Chem. Rev 2008, 108, 400–422. [PubMed: 18229950]

(91). Homola J; Yee SS; Gauglitz G Surface Plasmon Resonance Sensors: Review. Sens. Actuators, B 1999, 54, 3–15.

(92). Korotcenkov G Chemical Sensors: Comprehensive Sensor Technologies; Momentum Press: New York, 2012; Vol. 5.

(93). Stevens N; Akins DL Dye-Doped Inorganic/Organic Composite Films as Fluorescence Sensors for Methanol Vapor. Sens. Actuators, B 2007, 123, 59–64.

(94). Homola J Surface Plasmon Resonance Sensors for Detection of Chemical and Biological Species. Chem. Rev 2008, 108, 462–493. [PubMed: 18229953]

(95). Bouvet M Phthalocyanine-Based Field-Effect Transistors as Gas Sensors. Anal. Bioanal. Chem 2006, 384, 366–373. [PubMed: 15933850]

(96). Torsi L; Farinola GM; Marinelli F; Tanese MC; Omar OH; Valli L; Babudri F; Palmisano F; Zambonin PG; Naso F A Sensitivity-Enhanced Field Effect Chiral Sensor. Nat. Mater 2008, 7, 412–417. [PubMed: 18425136]

(97). Arshak K; Moore E; Lyons G; Harris J; Clifford S A Review of Gas Sensors Employed in Electronic Nose Applications. Sens. Rev 2004, 24, 181–198.

(98). Caliendo C; Verardi P; Verona E; D'Amico A; Natale CD; Saggio G; Serafini M; Paolesse R; Huq SE Advances in SAW-based Gas Sensors. Smart Mater. Struct 1997, 6, 689.

(99). Lim C; Wang W; Yang S; Lee K Development of SAW-based Multi-Gas Sensor for Simultaneous Detection of CO_2 and NO_2. Sens. Actuators, B 2011, 154, 9–16.

(100). Özmen A; Tekce F; Ebeoğlu MA; Tasaltın C; Öztürk ZZ Finding the Composition of Gas Mixtures by a Phthalocyanine-Coated QCM Sensor Array and an Artificial Neural Network. Sens. Actuators, B 2006, 115, 450–454.

(101). Bakker E Electrochemical Sensors. Anal. Chem 2004, 76, 3285–3298. [PubMed: 15193109]

(102). Korotcenkov G; Han SD; Stetter JR Review of Electrochemical Hydrogen Sensors. Chem. Rev 2009, 109, 1402–1433. [PubMed: 19222198]

(103). Stradiotto NR; Yamanaka H; Zanoni MVB Electrochemical Sensors: A Powerful Tool in Analytical Chemistry. J. Br. Chem. Soc 2003, 14, 159–173.

(104). Tierney MJ; Kim HOL Electrochemical Gas Sensor with Extremely Fast Response Times. Anal. Chem 1993, 65, 3435–3440.

(105). Aswal DK; Gupta SK Science and technology of Chemiresistor Gas Sensors Nova Science Publishers: 2007.

(106). Franke ME; Koplin TJ; Simon U Metal and Metal Oxide Nanoparticles in Chemiresistors: Does the Nanoscale Matter? Small 2006, 2, 36–50. [PubMed: 17193551]

(107). Bobacka J; Ivaska A; Lewenstam A Potentiometric Ion Sensors. Chem. Rev 2008, 108, 329–351. [PubMed: 18189426]

(108). Xie X; Bakker E Non-Severinghaus Potentiometric Dissolved CO_2 Sensor with Improved Characteristics. Anal. Chem 2013, 85, 1332–1336. [PubMed: 23305117]

(109). Cha W; Tung Y-C; Meyerhoff ME; Takayama S Patterned Electrode-Based Amperometric Gas Sensor for Direct Nitric Oxide Detection within Microfluidic Devices. Anal. Chem 2010, 82, 3300–3305. [PubMed: 20329749]

(110). Ram MK; Yavuz O; Aldissi M NO_2 Gas Sensing Based on Ordered Ultrathin Films of Conducting Polymer and its Nanocomposite. Synth. Met 2005, 151, 77–84.

(111). Destaillats H; Maddalena RL; Singer BC; Hodgson AT; McKone TE Indoor Pollutants Emitted by Office Equipment: A Review of Reported Data and Information Needs. Atmos. Environ 2008, 42, 1371–1388.

(112). Yu C; Crump D A Review of the Emission of VOCs from Polymeric Materials used in Buildings. Build. Environ 1998, 33, 357–374.

(113). Molhave L Volatile Organic Compounds, Indoor Air Quality and Health. Indoor Air 1991, 1, 357–376.

(114). Hakim M; Broza YY; Barash O; Peled N; Phillips M; Amann A; Haick H Volatile Organic Compounds of Lung Cancer and Possible Biochemical Pathways. Chem. Rev 2012, 112, 5949–5966. [PubMed: 22991938]

(115). Ashley DL; Bonin MA; Cardinali FL; McCraw JM; Wooten JV Measurement of Volatile Organic Compounds in Human Blood. Environ. Health Perspect 1996, 104, 871. [PubMed: 8933028]

(116). Burn J; Henk J; Bloemen T Chemistry and Analysis of Volatile Organic Compounds in the Environment; Springer: Berlin, 1993.

(117). Ott WR; Roberts JW Everyday Exposure to Toxic Pollutants. Sci. Am 1998, 278, 86–91.

(118). Tchobanoglous G; Burton FL Wastewater Engineering. Management 1991, 7, 1–4.

(119). Potyrailo RA; Leach AM; Surman CM Multisize CdSe Nanocrystal/Polymer Nanocomposites for Selective Vapor Detection Identified from High-Throughput Screening Experimentation. ACS Combi. Sci 2012, 14, 170–178.

(120). Li W; Kim D Polyaniline/Multiwall Carbon Nanotube Nanocomposite for Detecting Aromatic Hydrocarbon Vapors. J. Mater. Sci 2011, 46, 1857–1861.

(121). Campos M; Bulhões LOS; Lindino CA Gas-sensitive Characteristics of Metal/Semiconductor Polymer Schottky Device. Sens. Actuators. A 2000, 87, 67–71.

(122). Sadek AZ; Wlodarski W; Shin K; Kaner RB; Kalantarzadeh K A Polyaniline/WO_3 Nanofiber Composite Based ZnO/64° YX $LiNbO_3$ SAW Hydrogen Gas Sensor. Synth. Met 2008, 158, 29–32.

(123). He JH; Ho CH; Chen CY Polymer Functionalized ZnO Nanobelts as Oxygen Sensors with a Significant Response Enhancement. Nanotechnology 2009, 20, 065503. [PubMed: 19417388]

(124). Arshak K; Gaidan I Development of an Array of Polymer/MnO_2/Fe_2O_3 Mixtures for use in Gas Sensing Applications. Sens. Actuators, B 2006, 118, 386–392.

(125). Arshak K; Gaidan I NiO/Fe_2O_3Polymer Thick Films as Room Temperature Gas Sensors. Thin Solid Films 2006, 495, 286–291.

(126). Vaddiraju S; Gleason KK Selective Sensing Of Volatile Organic Compounds using Novel Conducting Polymer−Metal Nanoparticle Hybrids. Nanotechnology 2010, 21, 125503. [PubMed: 20203352]

(127). Sayago I; Fernández MJ; Fontecha JL; Horrillo MC; Vera C; Obieta I; Bustero I New Sensitive Layers for Surface Acoustic Wave Gas Sensors Based on Polymer and Carbon Nanotube Composites. Sens. Actuators, B 2012, 175, 67–72.

(128). Tatavarty R; Hwang ET; Park J-W; Kwak J-H; Lee J-O; Gu MB Conductive Quantum Dot-Encapsulated Electrospun Nanofibers from Polystyrene and Polystyrene-Co-Maleic Anhydride Copolymer Blend as Gas Sensors. React.Funct. Polym 2011, 71, 104–108.

(129). Mondal SP; Bera S; Narender G; Ray SK CdSe Quantum Dots-Poly(3-Hexylthiophene) Nanocomposite Sensors for Selective Chloroform Vapor Detection at Room Temperature. Appl. Phys. Lett 2012, 101, 173108.

(130). Sharma S; Nirkhe C; Pethkar S; Athawale AA Chloroform Vapour Sensor based on Copper/Polyaniline Nanocomposite. Sens. Actuators, B 2002, 85, 131–136.

(131). Ma X; Wang M; Li G; Chen H; Bai R Preparation of Polyaniline−TiO_2 Composite Film with in Situ Polymerization Approach and its Gas-Sensitivity at Room Temperature. Mater. Chem. Phys 2006, 98, 241–247.

(132). Hierlemann A; Bodenhöfer K; Fluck M; Schurig V; Göpel W Selective Detection of Nitrogen and Oxygen Containing Volatile Organic Compounds: Use Of Metal-Modified Polysiloxanes As Sensor Coatings. Anal. Chim. Acta 1997, 346, 327–339.

(133). Wang YD; Djerdj I; Antonietti M; Smarsly B Polymer-Assisted Generation of Antimony-Doped SnO2 Nanoparticles with High Crystallinity for Application in Gas Sensors. Small 2008, 4, 1656–1660. [PubMed: 18819131]

(134). Wang J; Matsubara I; Murayama N; Woosuck S; Izu N The Preparation of Polyaniline Intercalated MoO3 Thin Film and its Sensitivity to Volatile Organic Compounds. Thin Solid Films 2006, 514, 329–333.

(135). Itoh T; Matsubara I; Shin W; Izu N Synthesis and Characterization of Layered Organic/Inorganic Hybrid Thin Films Based on Molybdenum Trioxide with Poly(N-methylaniline) for VOC sensor. Mater. Lett 2007, 61, 4031–4034.

(136). Itoh T; Matsubara I; Shin W; Izu N; Nishibori M Preparation of Layered Organic−Inorganic Nanohybrid Thin Films of Molybdenum Trioxide with Polyaniline Derivatives for Aldehyde Gases Sensors of Several Tens ppb Level. Sens. Actuators, B 2008, 128, 512–520.

(137). Lu J; Park BJ; Kumar B; Castro M; Choi HJ; Feller J-F Polyaniline Nanoparticle−Carbon Nanotube Hybrid Network Vapour Sensors with Switchable Chemo-Electrical Polarity. Nanotechnology 2010, 21, 255501. [PubMed: 20508309]

(138). de Julián Fernández C; Manera MG; Spadavecchia J; Maggioni G; Quaranta A; Mattei G; Bazzan M; Cattaruzza E; Bonafini M; Negro E; Vomiero A; Carturan S; Scian C; Mea GD; Rella R; Vasanelli L; Mazzoldi P Study of the Gas Optical Sensing Properties of Au-Polyimide

Nanocomposite Films Prepared by Ion Implantation. Sens. Actuators, B 2005, 111–112, 225–229.

(139). Savage NO Gas Sensing Composites of Metal Oxides with Vapor-Deposited Polypyrrole. Sens. Actuators, B 2009, 143, 6–11.

(140). Barkade SS; Naik JB; Sonawane SH Ultrasound Assisted Miniemulsion Synthesis of Polyaniline/Ag Nanocomposite and its Application for Ethanol Vapor Sensing. Colloids Surf., A 2011, 378, 94–98.

(141). Kumar B; Feller J-F; Castro M; Lu J Conductive Bio-Polymer Nano-Composites (CPC): Chitosan-Carbon Nanotube Transducers Assembled via Spray Layer-by-Layer for Volatile Organic Compound Sensing. Talanta 2010, 81, 908–915. [PubMed: 20298872]

(142). Athawale AA; Bhagwat SV; Katre PP Nanocomposite of Pd−Polyaniline as a Selective Methanol Sensor. Sens. Actuators, B 2006, 114, 263–267.

(143). Han L; Andrady AL; Ensor DS Chemical Sensing Using Electrospun Polymer/Carbon Nanotube Composite Nanofibers with Printed-on Electrodes. Sens. Actuators, B 2013, 186, 52–55.

(144). Feller JF; Lu J; Zhang K; Kumar B; Castro M; Gatt N; Choi HJ Novel Architecture of Carbon Nanotube Decorated Poly(Methyl Methacrylate) Microbead Vapour Sensors Assembled by Spray Layer by Layer. J. Mater. Chem 2011, 21, 4142–4149.

(145). Lvova L; Mastroianni M; Pomarico G; Santonico M; Pennazza G; Di Natale C; Paolesse R; D'Amico A Carbon Nanotubes Modified with Porphyrin Units for Gaseous Phase Chemical Sensing. Sens. Actuators, B 2012, 170, 163–171.

(146). Evans CD; Monteith DT; Fowler D; Cape JN; Brayshaw S Hydrochloric Acid: An Overlooked Driver of Environmental Change. Environ. Sci. Technol 2011, 45, 1887–1894. [PubMed: 21288016]

(147). Tripathy SK; Woo JY; Han C-S Highly Selective Colorimetric Detection of Hydrochloric Acid Using Unlabeled Gold Nanoparticles and an Oxidizing Agent. Anal. Chem 2011, 83, 9206–9212. [PubMed: 22074405]

(148). Jang J; Bae J Carbon Nanofiber/Polypyrrole Nanocable as Toxic Gas Sensor. Sens. Actuators, B 2007, 122, 7–13.

(149). Cano M; Castillero P; Roales J; Pedrosa JM; Brittle S; Richardson T; González-Elipe AR; Barranco A A transparent TMPyP/TiO2 Composite Thin Film as an HCl Sensitive Optochemical Gas Sensor. Sens. Actuators, B 2010, 150, 764–769.

(150). Timmer B. r.; Olthuis W; Berg A. v. d. Ammonia Sensors and Their Applications-A Review. Sens. Actuators, B 2005, 107, 666–677.

(151). Kowalchuk GA; Stephen JR Ammonia-oxidizing Bacteria: A Model for Molecular Microbial Ecology. Annu. Rev. Microbiol 2001, 55, 485–529. [PubMed: 11544365]

(152). Kristensen H; Wathes C Ammonia and Poultry Welfare: A review. World's Poultry Sci. J 2000, 56, 235–245.

(153). Venditti I; Fratoddi I; Russo MV; Bearzotti A A Nanostructured Composite Based on Polyaniline and Gold Nanoparticles: Synthesis and Gas Sensing Properties. Nanotechnology 2013, 24, 155503. [PubMed: 23518508]

(154). Lobotka P; Kunzo P; Kovacova E; Vavra I; Krizanova Z; Smatko V; Stejskal J; Konyushenko EN; Omastova M; Spitalsky Z; Micusik M; Krupa I Thin Polyaniline and Polyaniline/Carbon Nanocomposite Films for Gas Sensing. Thin Solid Films 2011, 519, 4123–4127.

(155). Tai H; Jiang Y; Xie G; Yu J; Chen X Fabrication and Gas Sensitivity of Polyaniline−Titanium Dioxide Nanocomposite Thin Film. Sens. Actuators, B 2007, 125, 644–650.

(156). Tai H; Jiang Y; Xie G; Yu J Preparation, Characterization and Comparative NH3-sensing Characteristic Studies of PANI/Inorganic Oxides Nanocomposite Thin Films. J. Mater. Sci. Technol 2010, 26, 605–613.

(157). Van Hieu N; Dung NQ; Tam PD; Trung T; Chien ND Thin Film Polypyrrole/SWCNTs Nanocomposites Based NH_3 Sensor Operated at Room Temperature. Sens. Actuators, B 2009, 140, 500–507.

(158). Hong L; Li Y; Yang M Fabrication and Ammonia Gas Sensing of Palladium/Polypyrrole Nanocomposite. Sens. Actuators, B 2010, 145, 25–31.

(159). Lim J-H; Phiboolsirichit N; Mubeen S; Deshusses MA; Mulchandani A; Myung NV Electrical and Gas Sensing Properties of Polyaniline Functionalized Single-Walled Carbon Nanotubes. Nanotechnology 2010, 21, 075502.

(160). Jian J; Guo X; Lin L; Cai Q; Cheng J; Li J Gas-Sensing Characteristics of Dielectrophoretically Assembled Composite Film of Oxygen Plasma-Treated SWCNTs and PEDOT/PSS Polymer. Sens. Actuators, B 2013, 178, 279–288.

(161). Jiang S; Chen J; Tang J; Jin E; Kong L; Zhang W; Wang C Au Nanoparticles-Functionalized Two-Dimensional Patterned Conducting PANI Nanobowl Monolayer for Gas Sensor. Sens. Actuators, B 2009, 140, 520–524.

(162). Chang Q; Zhao K; Chen X; Li M; Liu J Preparation of Gold/Polyaniline/Multiwall Carbon Nanotube Nanocomposites and Application in Ammonia Gas Detection. J. Mater. Sci 2008, 43, 5861–5866.

(163). Zhang T; Mubeen S; Yoo B; Myung NV; Deshusses MA A gas Nanosensor Unaffected by Humidity. Nanotechnology 2009, 20, 255501. [PubMed: 19487798]

(164). Gong J; Li Y; Hu Z; Zhou Z; Deng Y Ultrasensitive NH_3 Gas Sensor from Polyaniline Nanograin Enchased TiO_2 Fibers. J. Phys. Chem. C 2010, 114, 9970–9974.

(165). Tao W-H; Tsai C-H H_2S Sensing Properties of Noble Metal Doped WO_3 Thin Film Sensor Fabricated by Micromachining. Sens. Actuators, B 2002, 81, 237–247.

(166). Geng L; Wang S; Zhao Y; Li P; Zhang S; Huang W; Wu S Study of the Primary Sensitivity of Polypyrrole/r-Fe_2O_3 to Toxic Gases. Mater. Chem. Phys 2006, 99, 15–19.

(167). Raut BT; Chougule MA; Nalage SR; Dalavi DS; Mali S; Patil PS; Patil VB CSA doped Polyaniline/CdS Organic–Inorganic Nanohybrid: Physical and Gas Sensing Properties. Ceram. Int 2012, 38, 5501–5506.

(168). Shirsat MD; Bangar MA; Deshusses MA; Myung NV; Mulchandani A Polyaniline Nanowires-Gold Nanoparticles Hybrid Network based Chemiresistive Hydrogen Sulfide Sensor. Appl. Phys. Lett 2009, 94, 083502–3.

(169). Starke TKH; Coles GSV; Ferkel H High Sensitivity NO2 Sensors for Environmental Monitoring Produced Using Laser Ablated Nanocrystalline Metal Oxides. Sens. Actuators, B 2002, 85, 239–245.

(170). Fleming WJ Overview of Automotive Sensors. Sens. J., IEEE 2001, 1, 296–308.

(171). Menil F; Coillard V; Lucat C Critical Review of Nitrogen Monoxide Sensors for Exhaust Gases of Lean Burn Engines. Sens. Actuators, B 2000, 67, 1–23.

(172). Prakash S; Rajesh S; Singh SR; Karunakaran C; Vasu V Electrochemical Incorporation of Hemin in a ZnO−PPy Nanocomposite on a Pt Electrode as NOx Sensor. Analyst 2012, 137, 5874. [PubMed: 23113320]

(173). Geng L; Zhao Y; Huang X; Wang S; Zhang S; Huang W; Wu S The Preparation and Gas Sensitivity Study of Polypyrrole/Zinc Oxide. Synth. Met 2006, 156, 1078–1082.

(174). Xu M; Zhang J; Wang S; Guo X; Xia H; Wang Y; Zhang S; Huang W; Wu S Gas Sensing Properties of SnO2 Hollow Spheres/Polythiophene Inorganic−Organic Hybrids. Sens. Actuators, B 2010, 146, 8–13.

(175). Sadek AZ; Wlodarski W; Shin K; Kaner RB; Kalantarzadeh K A Layered Surface Acoustic Wave Gas Sensor Based on a Polyaniline/In_2O_3 Nanofibre Composite. Nanotechnology 2006, 17, 4488–4492.

(176). Do J-S; Chang W-B Amperometric Nitrogen Dioxide Gas Sensor Based on Pan/Au/Nafion Prepared by Constant Current and Cyclic Voltammetry Methods. Sens. Actuators, B 2004, 101, 97–106.

(177). Hoherčáková Z; Opekar F Au/PVC Composite-A new Material for Solid-State Gas Sensors: Detection of Nitrogen Dioxide in the Air. Sens. Actuators, B 2004, 97, 379–386.

(178). Nguyen DT; Nguyen MT; Ho GT; Nguyen TN; Reisberg S; Piro B; Pham MC Design of Interpenetrated Network MWCNT/Poly(1,5-DAN) on Interdigital Electrode: Toward NO_2 Gas Sensing. Talanta 2013, 115, 713–717. [PubMed: 24054652]

(179). Gedney N; Cox P; Betts R; Boucher O; Huntingford C; Stott P Detection of a Direct Carbon Dioxide Effect in Continental River Runoff Records. Nature 2006, 439, 835–838. [PubMed: 16482155]

(180). Neethirajan S; Jayas D; Sadistap S Carbon Dioxide (CO_2) Sensors for the Agri-Food Industry-A Review. Food Bioprocess Technol 2009, 2, 115–121.

(181). Star A; Han TR; Joshi V; Gabriel JC; Gruner G Nanoelectronic Carbon Dioxide Sensors. Adv. Mater 2004, 16, 2049–2052.

(182). Kim JH; Lee YM Gas Permeation Properties of Poly(Amide-6-B-Ethylene Oxide)−Silica Hybrid Membranes. J. Membr. Sci 2001, 193, 209–225.

(183). Rodenas T; Luz I; Prieto G; Seoane B; Miro H; Corma A; Kapteijn F; L. i. Xamena FX; Gascon J. Metal-Organic Framework Nanosheets in Polymer Composite Materials for Gas Separation. Nat. Mater 2015, 14, 48–55. [PubMed: 25362353]

(184). Kang WR; Lee AS; Park S; Park S-H; Baek K-Y; Lee KB; Lee S-H; Lee J-H; Hwang SS; Lee JS Free-Standing, Polysilsesquioxane-Based Inorganic/Organic Hybrid Membranes for Gas Separations. J. Membr. Sci 2015, 475, 384–394.

(185). Raub JA; Mathieu-Nolf M; Hampson NB; Thom SR Carbon Monoxide Poisoning-A Public Health Perspective. Toxicology 2000, 145, 1–14. [PubMed: 10771127]

(186). Ernst A; Zibrak JD Carbon Monoxide Poisoning. N. Eng. J. Med 1998, 339, 1603–1608.

(187). Densakulprasert N; Wannatong L; Chotpattananont D; Hiamtup P; Sirivat A; Schwank J Electrical Conductivity of Polyaniline/Zeolite Composites and Synergetic Interaction with CO. Mater. Sci. Eng., B 2005, 117, 276–282.

(188). Ram MK; Yavuz O; Lahsangah V; Aldissi M CO Gas Sensing from Ultrathin Nano-Composite Conducting Polymer Film. Sens. Actuators, B 2005, 106, 750–757.

(189). Jin G-P; Peng X; Ding Y-F; Liu W-Q; Ye J-M Electrodeposition of Platinum−Nickel Alloy Nanocomposites on Polyaniline-Multiwalled Carbon Nanotubes for Carbon Monoxide Redox. J. Solid State Electrochem 2009, 13, 967–973.

(190). Chen Z; Lu C Humidity Sensors: A Review of Materials and Mechanisms. Sens. Lett 2005, 3, 274–295.

(191). Lee C-Y; Lee G-B Humidity Sensors: A Review. Sens. Lett 2005, 3, 1–15.

(192). Rittersma ZM Recent achievements in Miniaturised Humidity Sensors-A Review of Transduction Techniques. Sens. Actuators, A 2002, 96, 196–210.

(193). Kumar A; Zhang P; Vincent A; McCormack R; Kalyanaraman R; Cho HJ; Seal S Hydrogen Selective Gas Sensor in Humid Environment Based on Polymer Coated Nanostructured Doped Tin Oxide. Sens. Actuators, B 2011, 155, 884–892.

(194). Mickelson W; Sussman A; Zettl A Low-Power, Fast, Selective Nanoparticle Based Hydrogen Sulfide Gas Sensor. Appl. Phys. Lett 2012, 100, 173110.

(195). Wu T-T; Chen Y-Y; Chou T-H A High Sensitivity Nanomaterial Based SAW Humidity Sensor. J. Phys. D: Appl. Phys 2008, 41, 085101.

(196). Tandon RP; Tripathy MR; Arora AK; Hotchandani S Gas and Humidity Response of Iron Oxide-Polypyrrole Nanocomposites. Sens. Actuators, B 2006, 114, 768–773.

(197). Power AC; Betts AJ; Cassidy JF Silver Nanoparticle Polymer Composite Based Humidity Sensor. Analyst 2010, 135, 1645–1652. [PubMed: 20514383]

(198). Su P-G; Huang L-N Humidity Sensors Based on TiO_2 Nanoparticles/Polypyrrole Composite Thin Films. Sens. Actuators, B 2007, 123, 501–507.

(199). Su P-G; Wang C-P Flexible Humidity Sensor based on TiO_2 Nanoparticles-Polypyrrole-Poly-[3-(Methacrylamino)Propyl] Trimethyl Ammonium Chloride Composite Materials. Sens. Actuators, B 2008, 129, 538–543.

(200). Patil D; Seo Y-K; Hwang YK; Chang J-S; Patil P Humidity Sensing Properties of Poly(o-anisidine)/WO_3 Composites. Sens. Actuators, B 2008, 128, 374–382.

(201). Parvatikar N; Jain S; Khasim S; Revansiddappa M; Bhoraskar SV; Prasad MVNA Electrical and Humidity Sensing Properties of Polyaniline/WO_3 Composites. Sens. Actuators, B 2006, 114, 599–603.

(202). Su P-G; Huang S-C Humidity Sensing and Electrical Properties of a Composite Material of SiO_2 and poly-[3-(methacrylamino)propyl] Trimethyl Ammonium Chloride. Sens. Actuators, B 2005, 105, 170–175.

(203). Litao L; Xiongying Y; Kang W; Zhaoying Z; Dongjin L; Tianhong C Humidity Sensitivity of Carbon Nanotube and Poly (Dimethyldiallylammonium Chloride) Composite Films. Sens. J. IEEE 2009, 9, 1308–1314.

(204). Li Y; Yang MJ; She Y Humidity Sensors Using In Situ Synthesized Sodium Polystyrenesulfonate/ZnO Nanocomposites. Talanta 2004, 62, 707–712. [PubMed: 18969352]

(205). Fuke MV; Kanitkar P; Kulkarni M; Kale BB; Aiyer RC Effect of Particle Size Variation of Ag Nanoparticles in Polyaniline Composite on Humidity Sensing. Talanta 2010, 81, 320–326. [PubMed: 20188926]

(206). Liu L; Ye X; Wu K; Zhou Z; Lee D; Cui T Humidity Sensitivity of Carbon Nanotube and Poly (Dimethyldiallylammonium Chloride) Composite Films. Sens. J., IEEE 2009, 9, 1308–1314.

(207). Timm RA; Falla MPH; Huila MFG; Peres HEM; Ramirez-Fernandez FJ; Araki K; Toma HE Vanadium oxide-Porphyrin Nanocomposites as Gas Sensor Interfaces for Probing Low Water Content in Ethanol. Sens. Actuators, B 2010, 146, 61–68.

(208). Arshak K; Adley C; Moore E; Cunniffe C; Campion M; Harris J Characterisation of Polymer Nanocomposite Sensors for Quantification of Bacterial Cultures. Sens. Actuators, B 2007, 126, 226–231.

(209). Zhan S; Li D; Liang S; Chen X; Li X A Novel Flexible Room Temperature Ethanol Gas Sensor based on SnO_2 Doped Poly-Diallyldimethylammonium Chloride. Sensors 2015, 13, 4378–4389.

(210). Kruefu V; Wisitsoraat A; Tuantranont A; Phanichphant S C_2H_5OH Gas Sensing Based on Poly(3-hexylthiophene)/Nb-Loaded ZnO Nanocomposite Films. Mol. Cryst. Liq. Cryst 2014, 599, 1–7.

(211). Nasirian S; Moghaddam HM Hydrogen Gas Sensing Based on Polyaniline/Anatase Titania Nanocomposite. Int. J. Hydrogen Energy 2014, 39, 630–642.

(212). Tai H; Li X; Jiang Y; Xie G; Du X The Enhanced Formaldehyde-Sensing Properties of P3HT-ZnO Hybrid Thin Film OTFT Sensor and Further Insight into its Stability. Sensors 2015, 15, 2086–2103. [PubMed: 25608214]

(213). Murugan C; Subramanian E; Padiyan DP Enhanced Sensor Functionality of In-Situ Synthesized Polyaniline-SnO_2 Hybrids Toward Benzene and Toluene Vapors. Sens. Actuators, B 2014, 205, 74–81.

(214). Murugan C; Subramanian E; Padiyan DP p-n Heterojunction Formation in Polyaniline-SnO_2 Organic-Inorganic Hybrid Composite Materials Leading to Enhancement in Sensor Functionality Toward Benzene and Toluene Vapors at Room Temperature. Synth. Met 2014, 192, 106–112.

(215). Nia PM; Lorestani F; Meng WP; Alias Y A Novel Non-enzymatic H_2O_2 Sensor Based on Polypyrrole Nanofibers-Silver Nanoparticles Decorated Reduced Graphene Oxide Nanocomposites. Appl. Surf. Sci 2015, 332, 648–656.

(216). Bochenkov VE; Stephan N; Brehmer L; Zagorskii VV; Sergeev GB Sensor Activity of Thin Polymer Films Containing Lead Nanoparticles. Colloid. Surf., A 2002, 198–200, 911–915.

(217). Talwar V; Singh O; Singh RC ZnO Assisted Polyaniline Nanofibers and its Application as Ammonia Gas Sensor. Sens. Actuators, B 2014, 191, 276–282.

(218). Wang L; Huang H; Xiao S; Cai D; Liu Y; Liu B; Wang D; Wang C; Li H; Wang Y; Li Q; Wang T Enhanced Sensitivity and Stability of Room-Temperature NH3 Sensors Using Core-Shell CeO2 Nanoparticles@Cross-linked PANI with p-n Heterojunctions. ACS Appl. Mater. Interface 2014, 6, 14131–14140.

(219). Pandey S; Goswami GK; Nanda KK Nanocomposite Based Flexible Ultrasensitive Resistive Gas Sensor for Chemical Reactions Studies. Sci. Rep 2015, 3.

(220). Su P-G; Peng Y-T Fabrication of a Room-Temperature H_2S Gas Sensor Based on PPy/WO_3 Nanocomposite Films by In-Situ Photopolymerization. Sens. Actuators, B 2014, 193, 637–643.

(221). Bai S; Zhang K; Sun J; Zhang D; Luo R; Li D; Liu C Polythiophene-WO_3 Hybrid Architectures For Low-Temperature H_2S Detection. Sens. Actuators, B 2014, 197, 142–148.

(222). Fedoruk GG; Sagaidak DI; Misevich AV; Pochtenny AE Electrical and Gas Sensing Properties of Copper Phthalocyanine–Polymer Composites. Sens. Actuators, B 1998, 48, 351–355.

(223). Tiwari A; Gong S Electrochemical Synthesis of Chitosan-co-polyaniline/$WO_3 \cdot nH_2O$ Composite Electrode for Amperometric Detection of NO_2 Gas. Electroanalysis 2008, 20, 1775–1781.

(224). Nalage SR; Mane AT; Pawar RC; Lee CS; Patil VB Polypyrrole-NiO Hybrid Nanocomposite Films: Highly Selective, Sensitive, and Reproducible NO_2 Sensors. Ionics 2014, 20, 1607–1616.

(225). Navale S; Khuspe G; Chougule M; Patil V Room Temperature NO_2 Gas Sensor Based on PPy/α-Fe_2O_3 Hybrid Nanocomposites. Ceram. Int 2014, 40, 8013–8020.

(226). Mane A; Navale S; Sen S; Aswal D; Gupta S; Patil V Nitrogen Dioxide (NO_2) Sensing Performance of P-Polypyrrole/N-Tungsten Oxide Hybrid Nanocomposites at Room temperature. Org. Electron 2015, 16, 195–204.

(227). Tsigara A; Mountrichas G; Gatsouli K; Nichelatti A; Pispas S; Madamopoulos N; Vainos NA; Du HL; Roubani-Kalantzopoulou F Hybrid Polymer/Cobalt Chloride Humidity Sensors Based on Optical Diffraction. Sens. Actuators, B 2007, 120, 481–486.

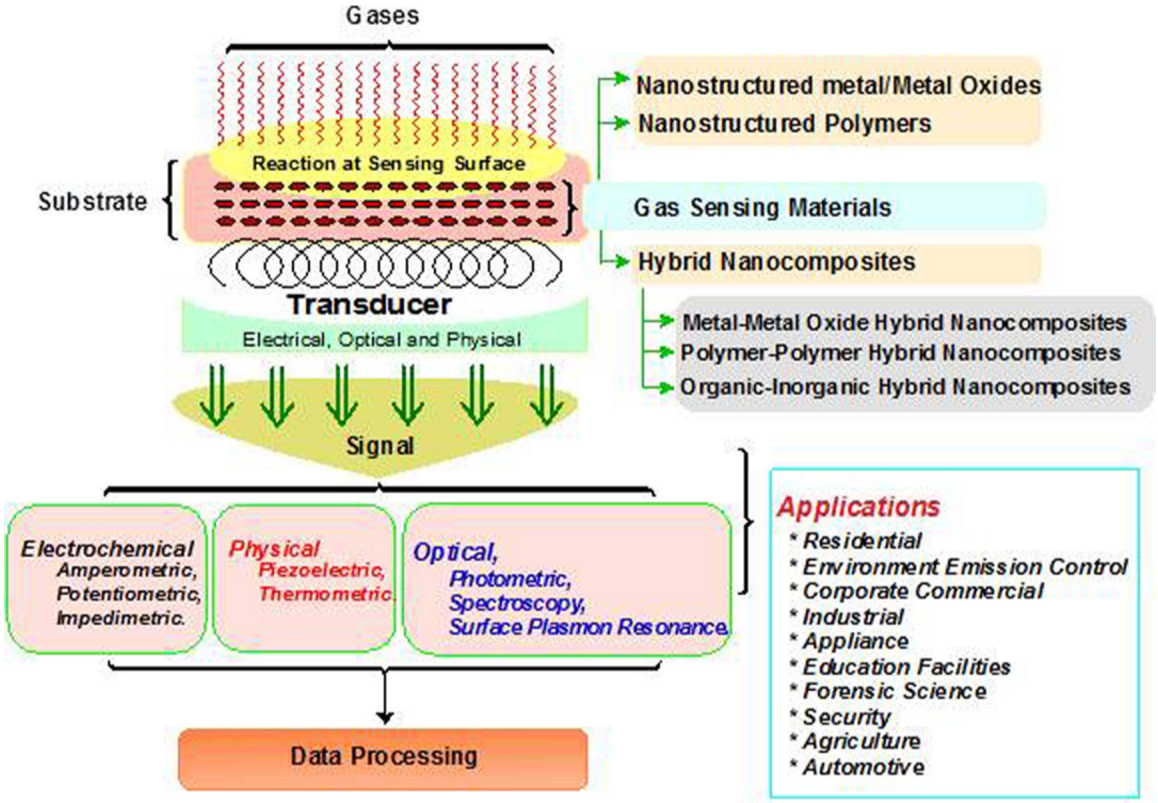

Figure 1.
Schematic of gas sensor fabrication techniques.

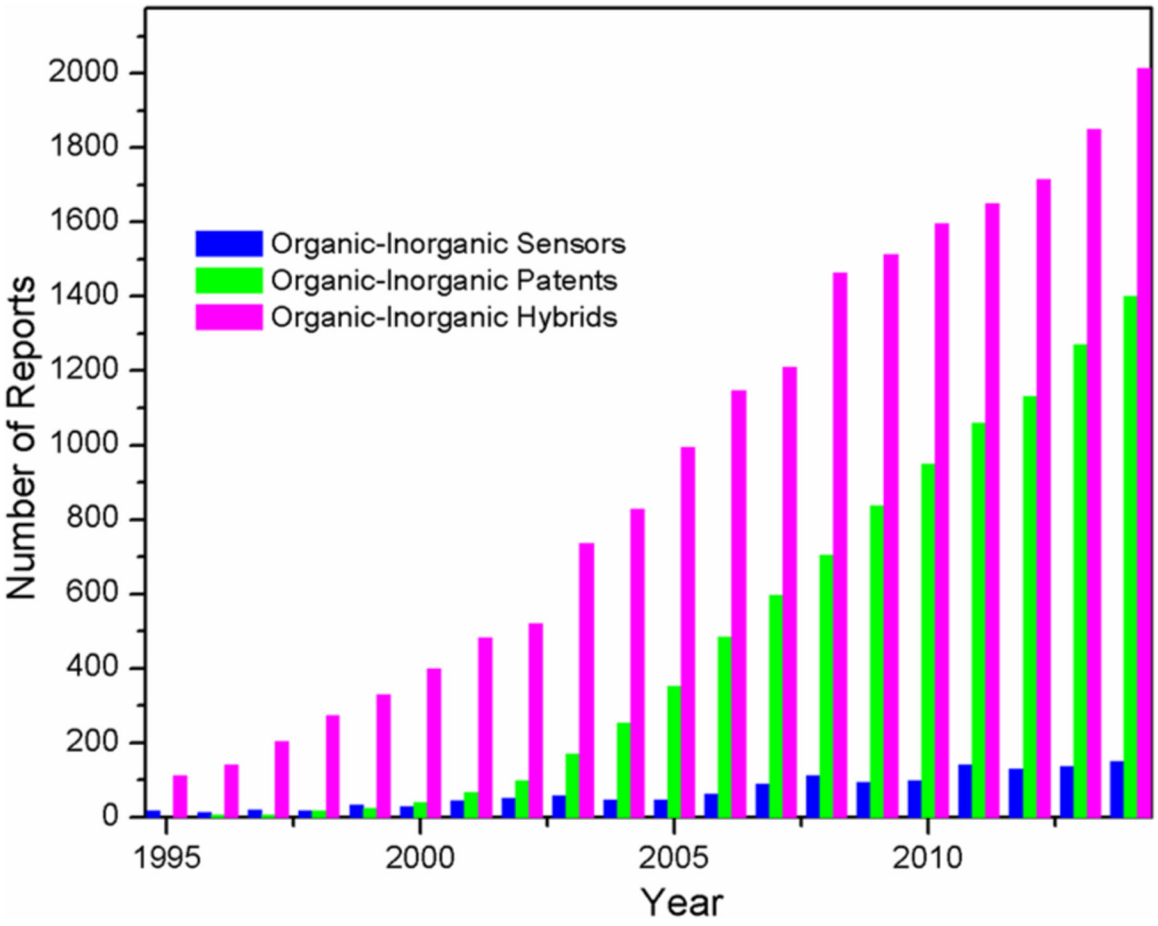

Figure 2.
Yearly publications and patents in the field of organic–inorganic hybrid nanocomposites. (Source: web of science and world intellectual property organization.)

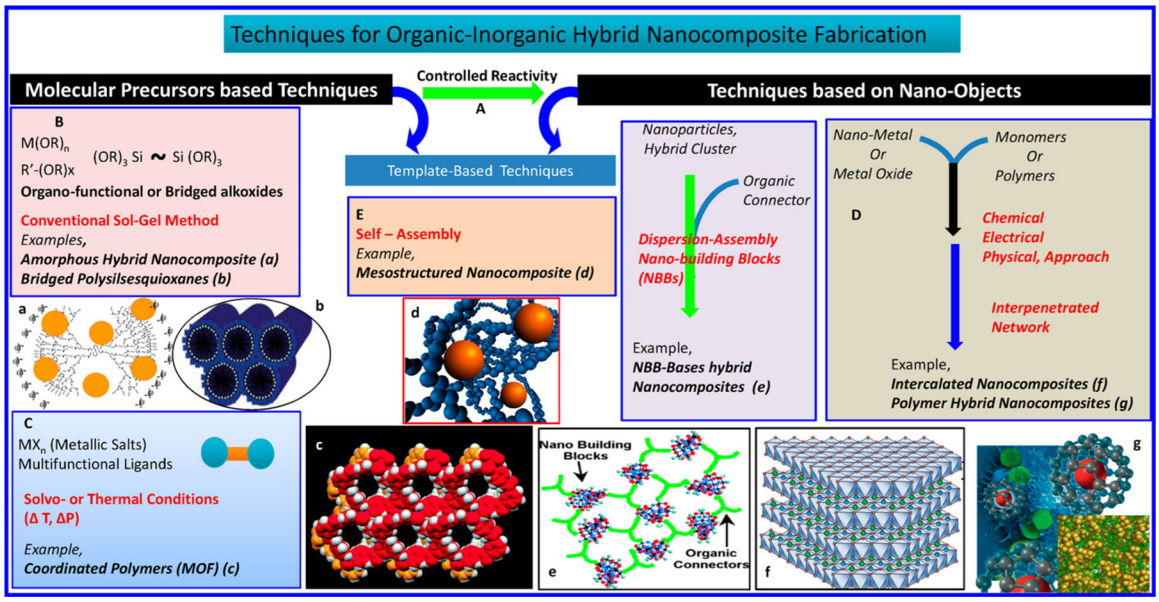

Figure 3.

Various strategies adopted for the synthesis of organic−inorganic hybrid nanocomposites along with schematic representation.

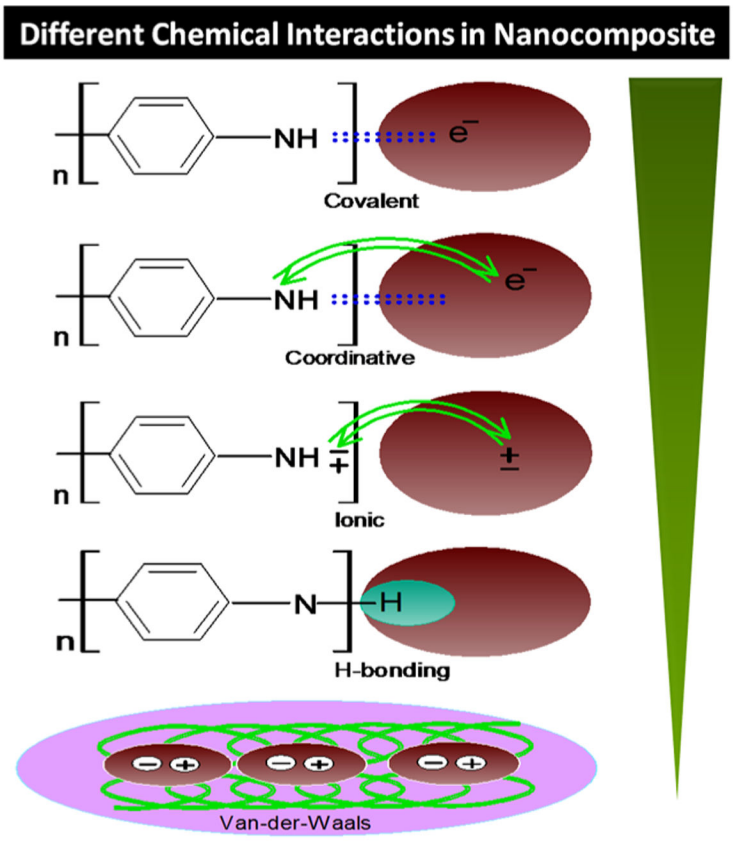

Interaction	Strength [kJ/mol]	Range	Characteristics
Covalent	350	Short	Predominantly Irreversible
Coordinative	50-250	Short	Directly
Ionic	50-200	Long	Non-Selective
Hydrogen	5-65	Short	Selective Directional
Van-der-Waals	50	Short	Non-Directional, Non-Directional

Figure 4.

Types of chemical/physical interactions during the fabrication of organic−inorganic hybrid nanocomposites.

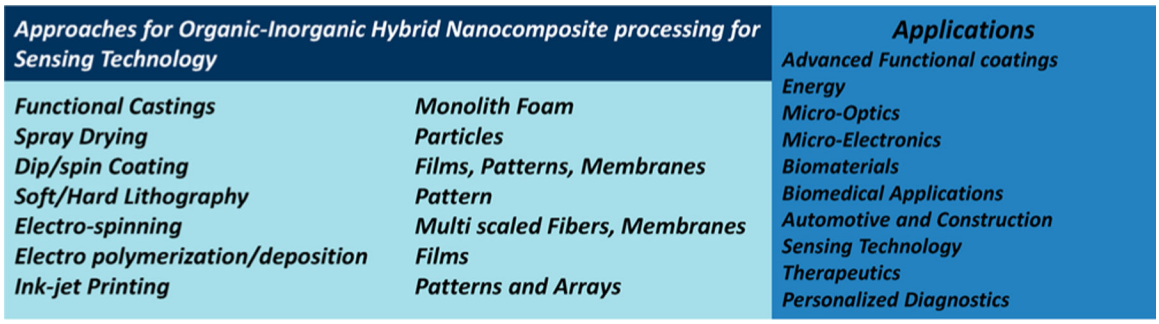

Figure 5.

Appropriate approaches for the processing of organic–inorganic hybrid nanocomposites for various applications.

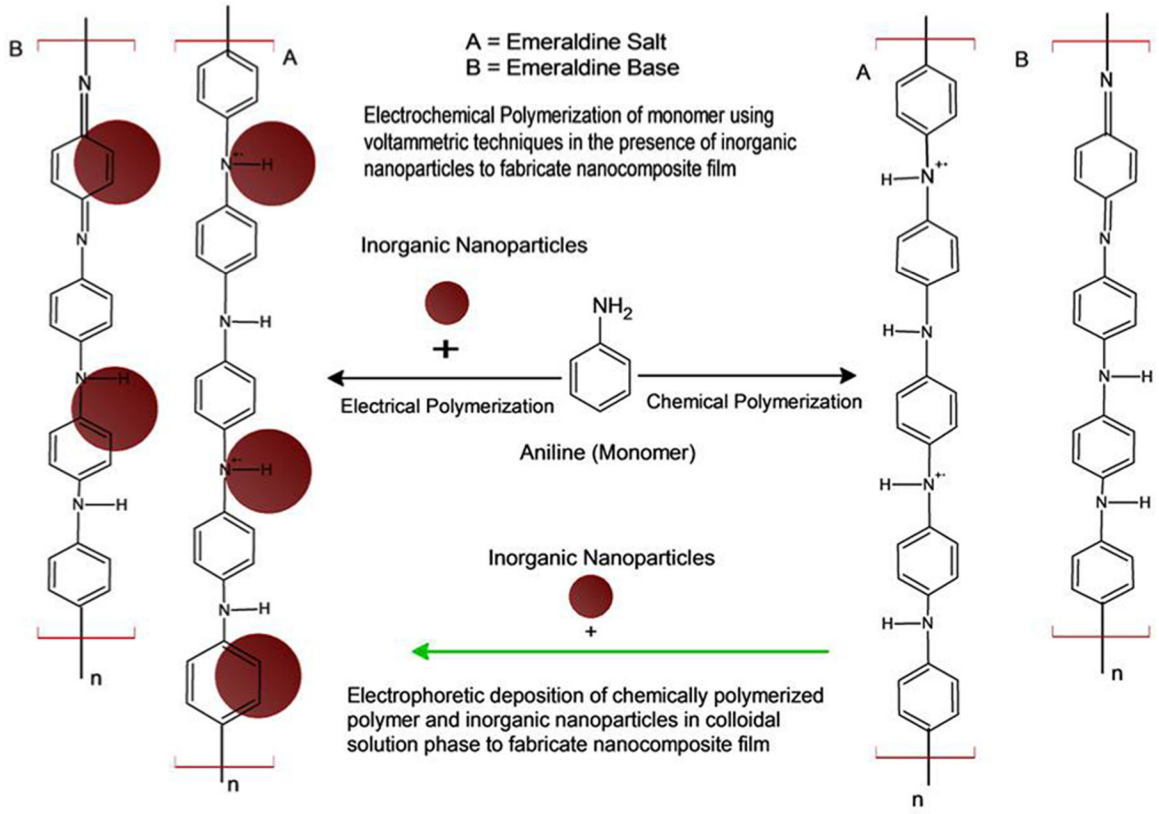

Figure 6.

Electrical polymerization and electrophoretic deposition of organic−inorganic hybrid nanocomposites.

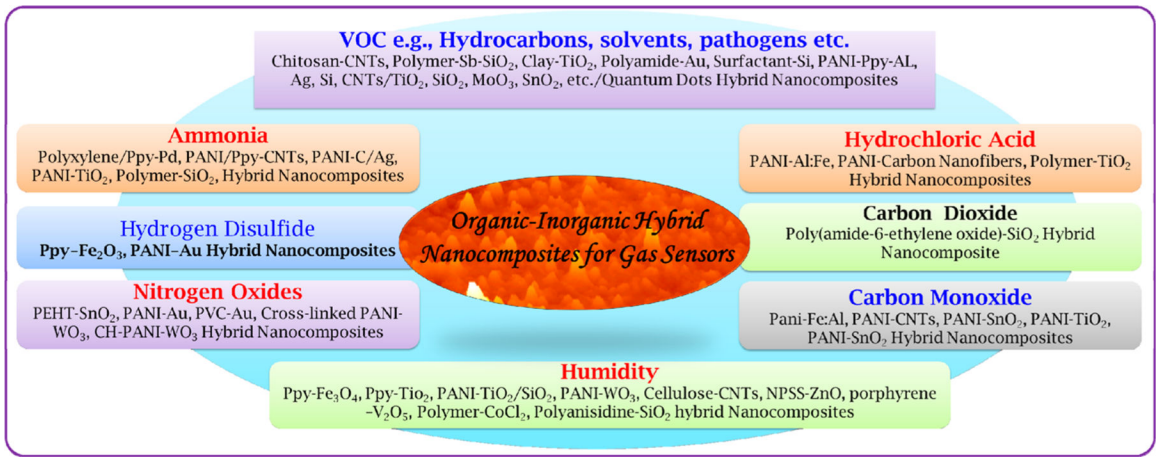

Figure 7.
Organic−inorganic hybrid nanocomposites used for gas sensing applications.

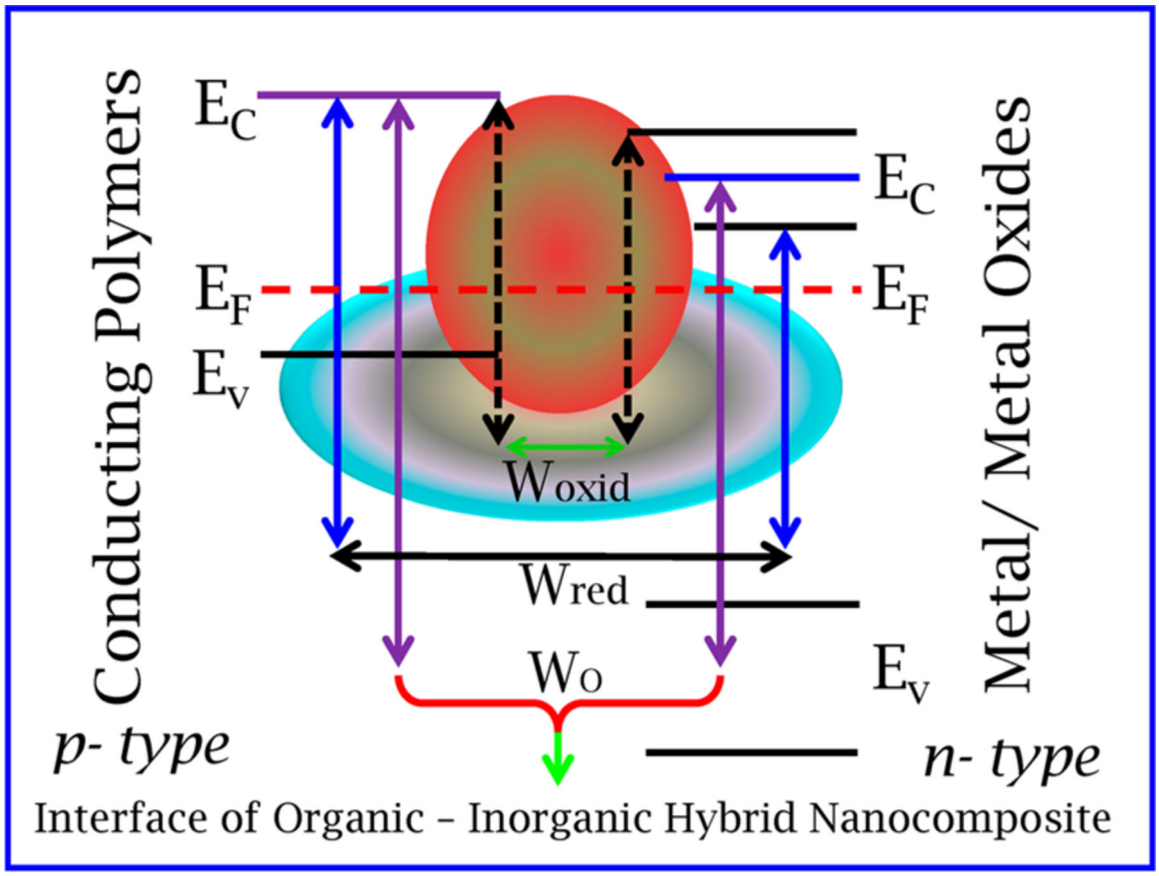

Figure 8.
Energy band gap diagram of organic−inorganic hybrid nanocomposites on gas exposure.

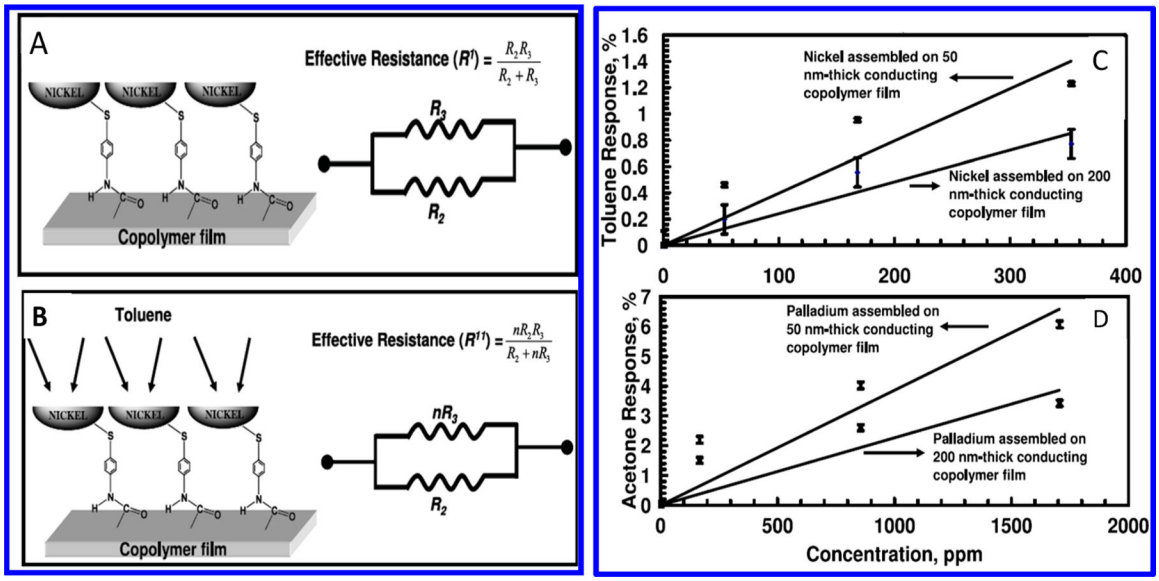

Figure 9.

Pictorial representation of Ni-poly(EDT-*co*-TAA) before and after exposure to toluene (A and B); variation of the response of Ni-poly(EDT-*co*-TAA) hybrid toluene concentration (C); and (D) variation of the response of Pd-poly(EDT-*co*-TAA) hybrids to acetone concentration. Reprinted with permission from ref 126. Copyright 2010 Institute of Physics.

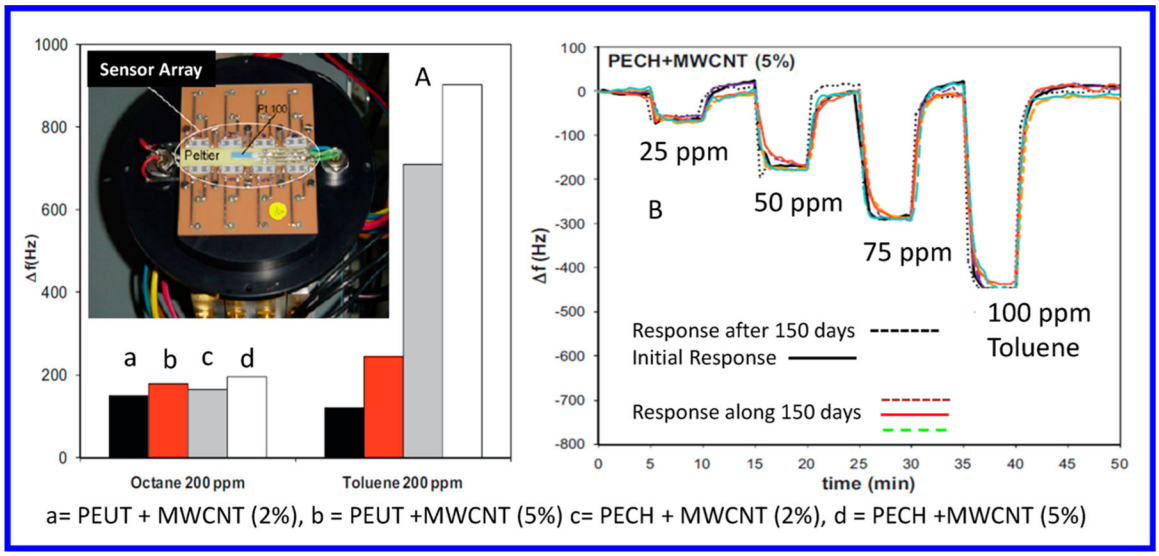

Figure 10.

Inset in (A), the sensor array in the measuring cell and the oscillator circuits, (A) sensing responses at 200 ppm of octane and toluene at room temperature. (B) Testing of repeatability of the S4 sensors exposed to different concentrations of toluene over 5 months at room temperature. Reprinted with permission from ref 127. Copyright 2012 Elsevier.

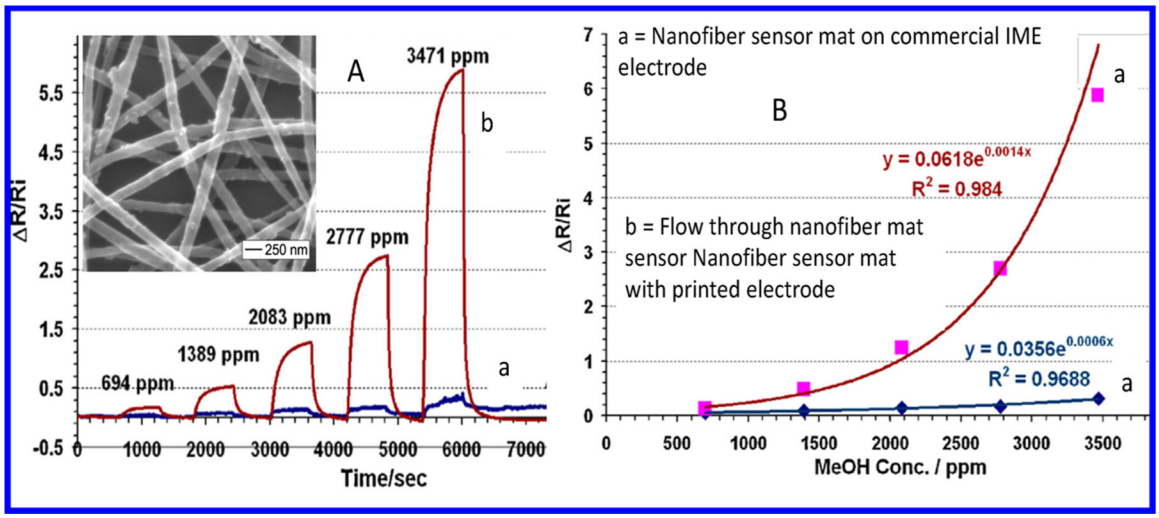

Figure 11.

Inset in (A) SEM image of typical electrospun SWCNT-PMMA composite nanofibers. (A) Comparison of the sensor response profile of a flow-through sensing material with a printed electrode and a nonflow-through sensing mat on commercial IME electrodes, and (B) comparison of the sensitivities. Reprinted with permission from ref 143. Copyright 2013 Elsevier.

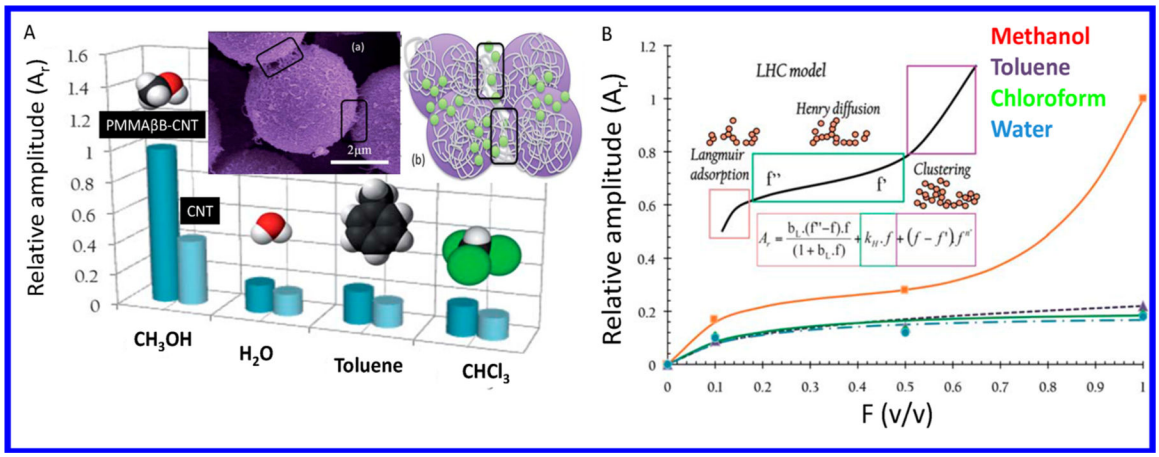

Figure 12.

Inset (A) SEM image of MCNT-PMMA hybrid (a), schematic presentation of bridging of PMMA and (b) in a MWCNT random network. (A) Selectivity of a MWCNT-PMMA and CNT random network when exposed to methanol, water, toluene, and chloroform vapors. (B) Effect of analyte concentration on MWCNT-PMMA response amplitude Ar for methanol, water, toluene, and chloroform vapors. Reprinted with permission from ref 144. Copyright 2011 Royal Society of Chemistry.

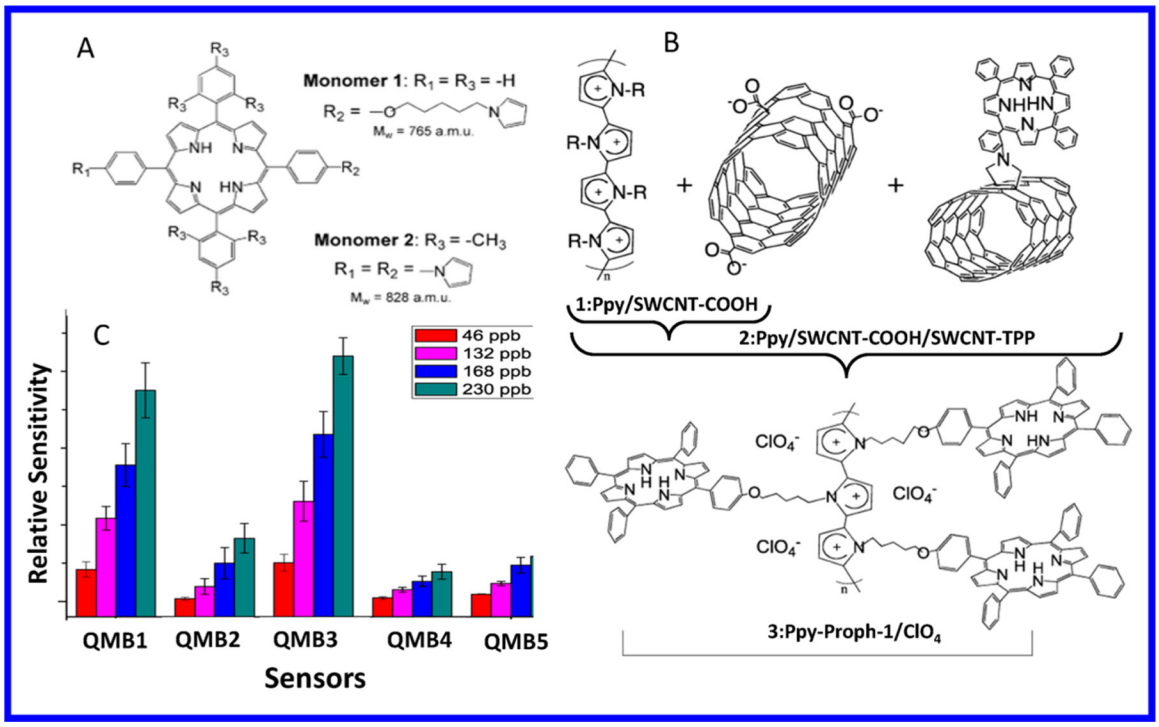

Figure 13.

(A and B) Chemical structure of TPP and Pr monomers 1 and 2, schematic representation of QMB coatings, where R in PPy backbone corresponds to H or monomer 2 substituents, and the relative sensitivity to 1-butanol for QMBs modified with SWCNT−Pr electro-polymers. (C) Relative response study of all 5 QCM gas sensors as a function of gas concentration. Reprinted with permission from ref 145. Copyright 2012 Elsevier.

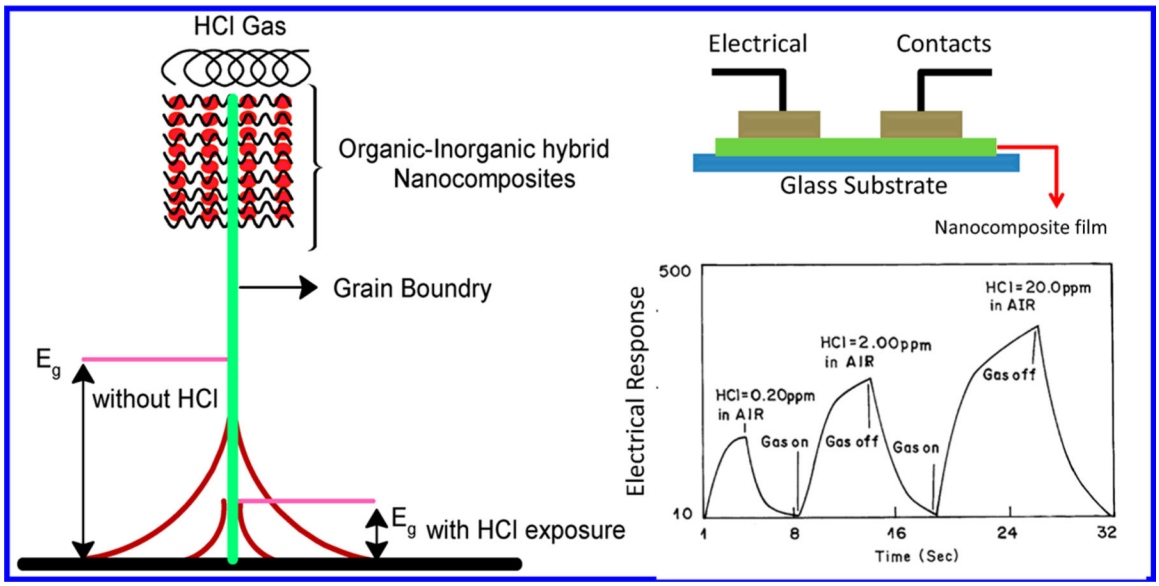

Figure 14.

Effect of HCl gas on a organic−inorganic hybrid nanocomposite, schematic of gas sensor fabrication, and gas sensing response of a nanocomposite as a function of HCl concentration. Reprinted with permission from ref 82. Copyright 2004 Elsevier.

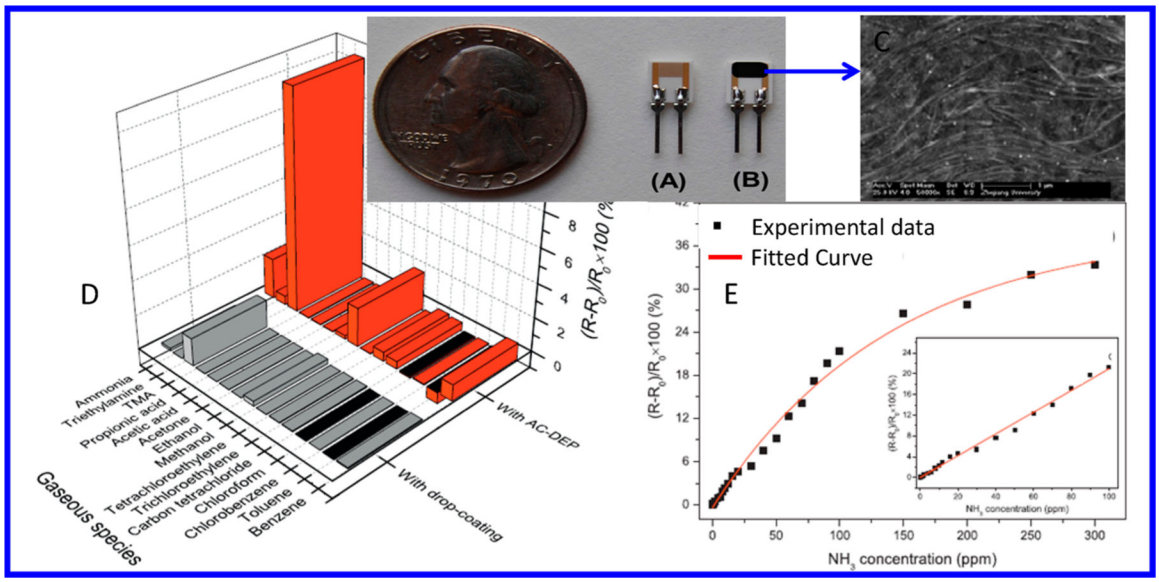

Figure 15.

Microelectrodes before (A) and after (B) the deposition of the AC-DEP-assembled PEDOT/PSS-SWCNTs composite film, (C) FE-SEM images of the PEDOT/PSS-SWCNTs composite films doped with SWCNTs (5 mg/mL), (D) selective responses of the drop-coated and AC-DEP-assembled PEDOT/PSSSWCNTs composite films to various vapors at 10 ppm, and (E) the calibration of the sensor response to NH_3 gas at 2–300 ppm and the linear response range (insert). Reprinted with permission from ref 160. Copyright 2013 Elsevier.

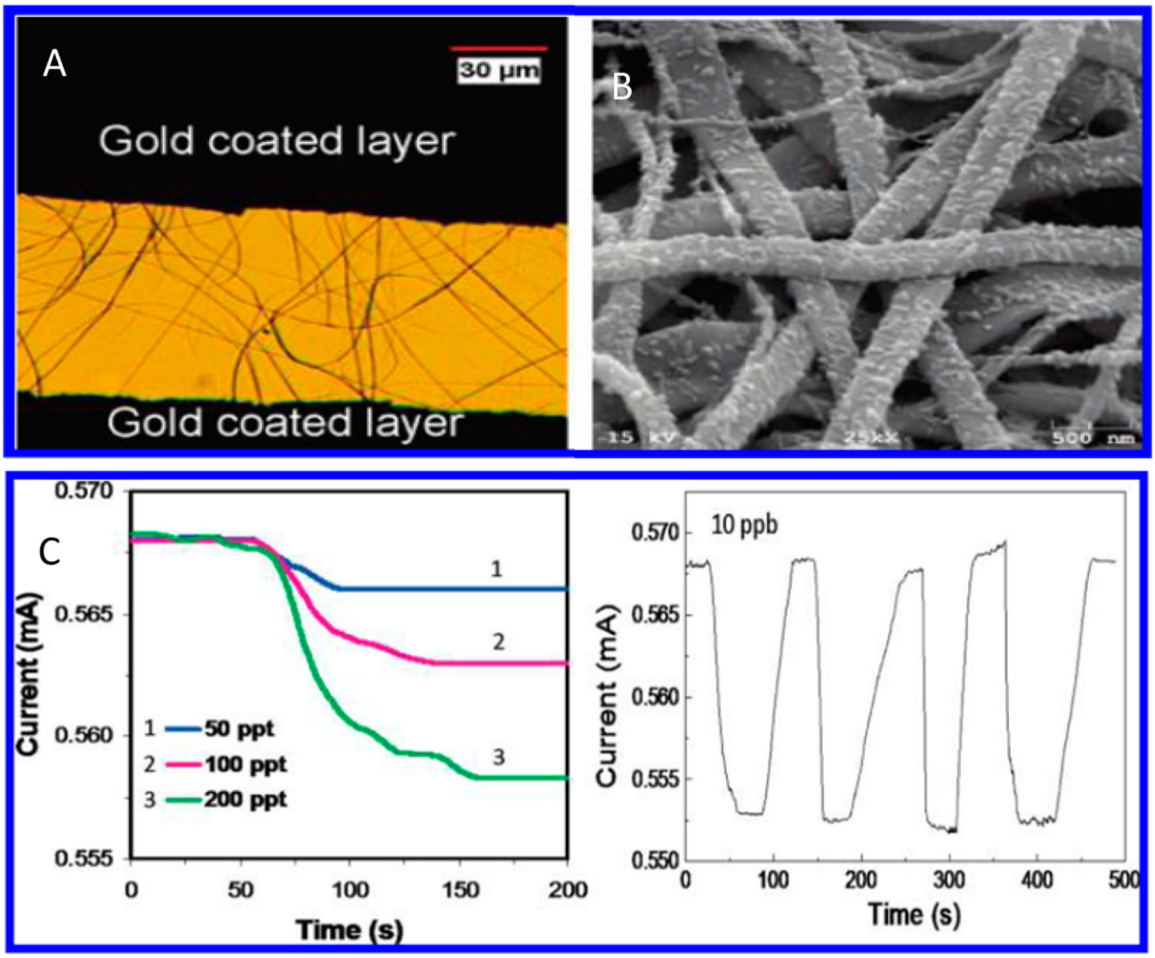

Figure 16.

(A) Optical microscope image of the sensor and (B) TiO_2 microfibers encased with PANI nanograins. (C) Current responses of a sensor made of TiO_2 microfibers encased with PANI nanograins to different concentrations of NH_3 gas as a function of time (left) and reproducibility of the sensor exposed to 10 ppb NH_3 gas (right). Reprinted with permission from ref 164. Copyright 2010 American Chemical Society.

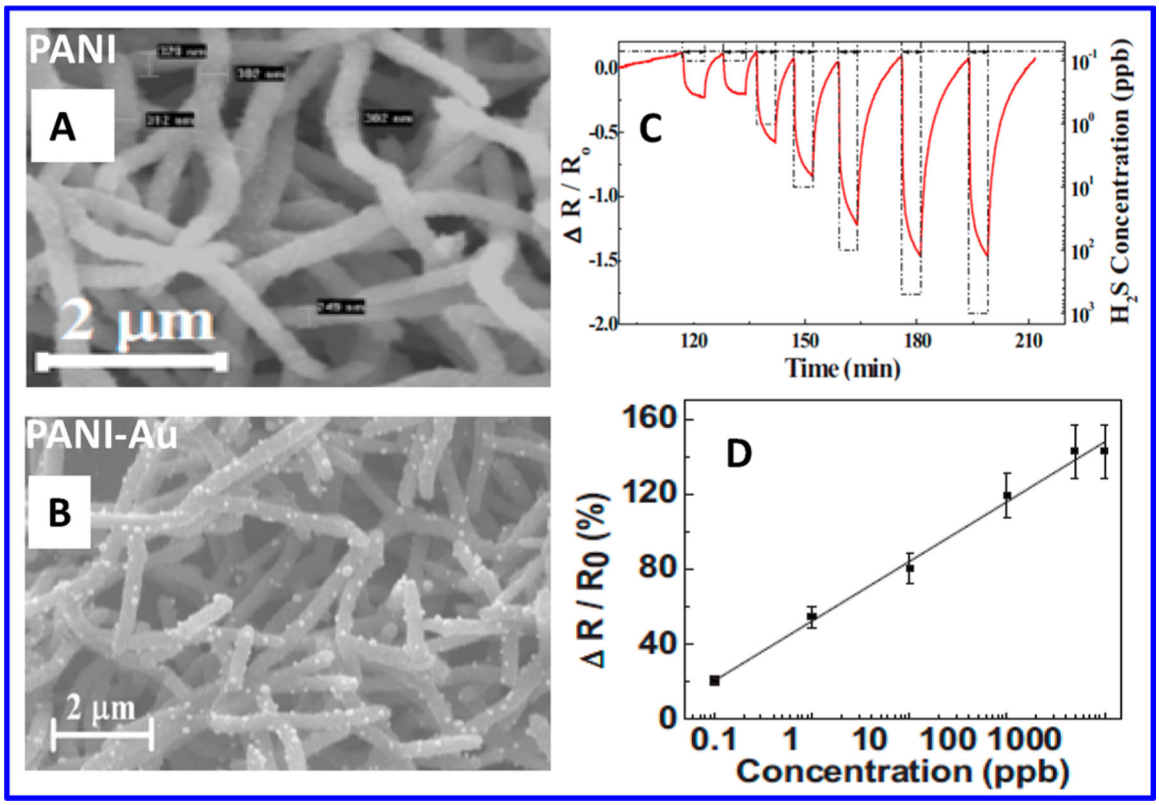

Figure 17.

(A) SEM image of a PANI nanowire network grown on Au IDE at the end of second step. (B) SEM image of a gold nanoparticle-functionalized PANI nanowire network across gold microelectrodes. (C) Response and recovery behavior of sensor as a function of 0.1 ppb, 1 ppb, 10 ppb, 100 ppb, 500 ppb, and 1 ppm of H_2S gas. (D) Response R/R_0% of a gold-nanoparticle-functionalized PANI nanowire-network-based chemiresistive sensor as a function of H_2S concentration. Reprinted with permission from ref 168. Copyright 2009 American Institute of Physics.

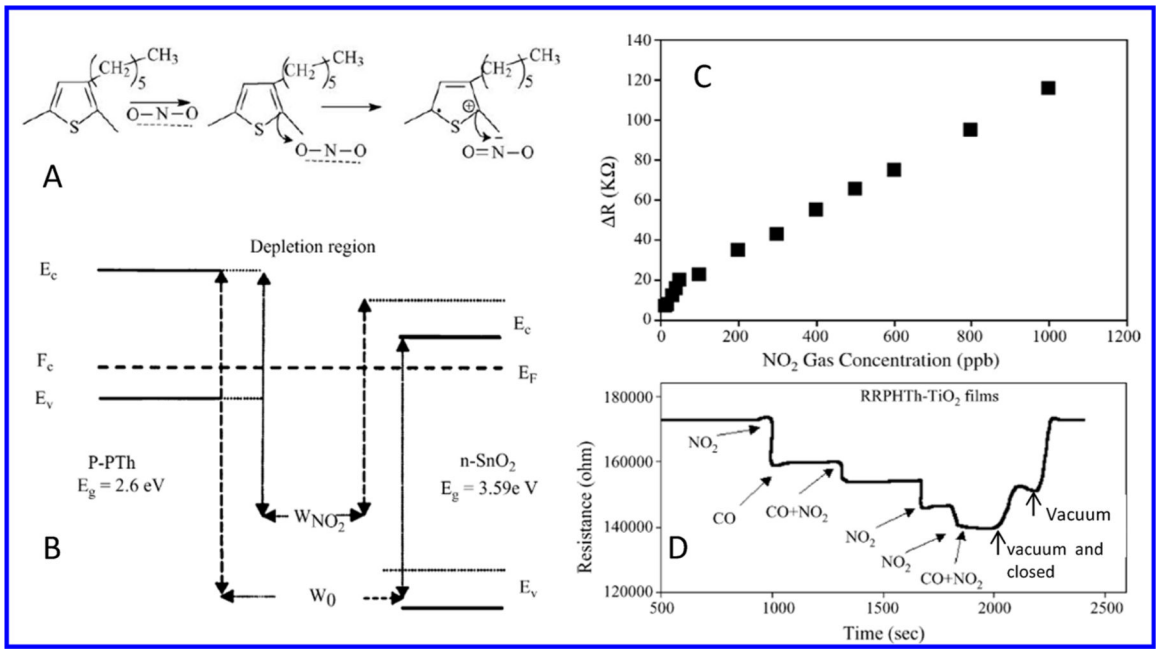

Figure 18.

(A) Schematic of the NO_2 reaction with PHTh conducting polymer, (B) energy band of hetero p−n junction with and without NO_2 exposure, (C) resistance change of a RRPHTh−SnO_2 nanocomposite vs NO_2 gas concentration, and (D) resistance change vs time by CO + NO_2 gas concentration in RRPHTh−TiO_2 films. Reprinted with permission from ref 110. Copyright 2005 Elsevier.

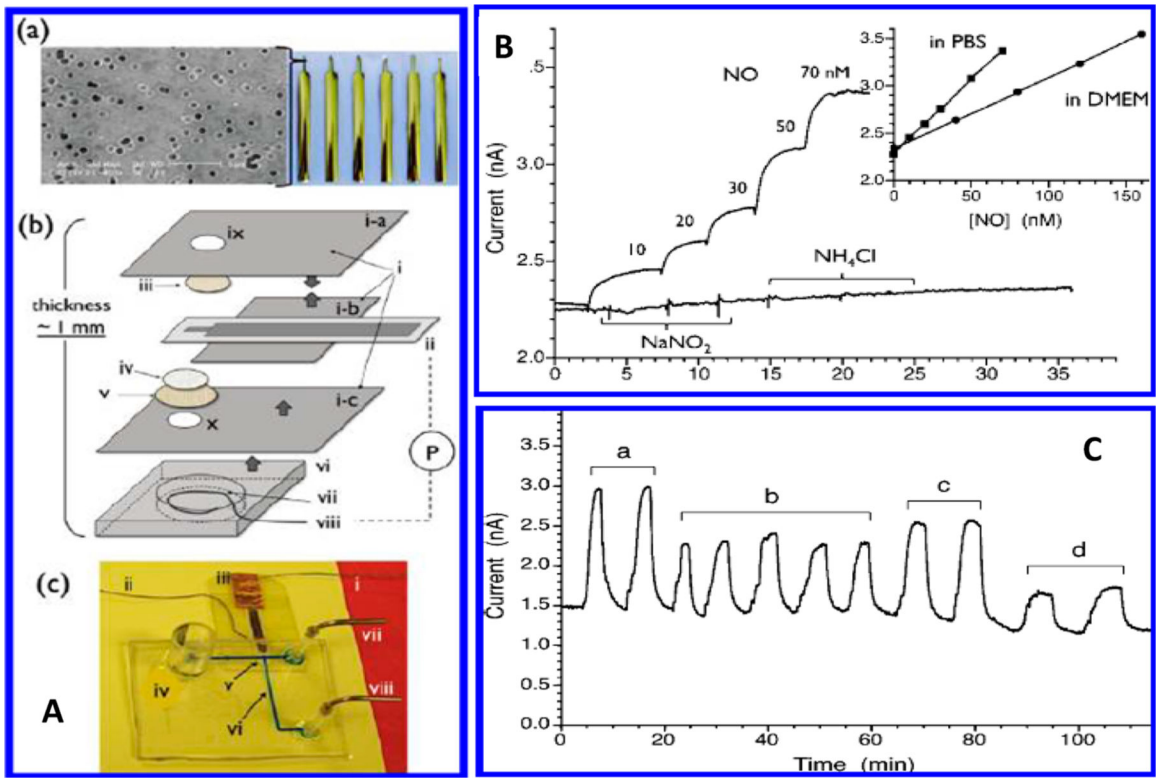

Figure 19.

(A) SEM image of electrode and stepwise fabrication of fluidic-based gas sensor, (B) NO sensor response curves exhibiting selectivity over nitrite and ammonia, both species added three times separately; 1, 2, and 3 mM concentrations were obtained after each injection; (inset) NO calibration plots in two different media, and (C) amperometric response of the microfluidic NO detector with flowing test solutions containing different levels of NO; flow rate 50 μL/min, (a) 350 nM, (b) 100 nM, (c) 200 nM, and (d) 40 nM. Reprinted with permission from ref 109. Copyright 2010 American Chemical Society.

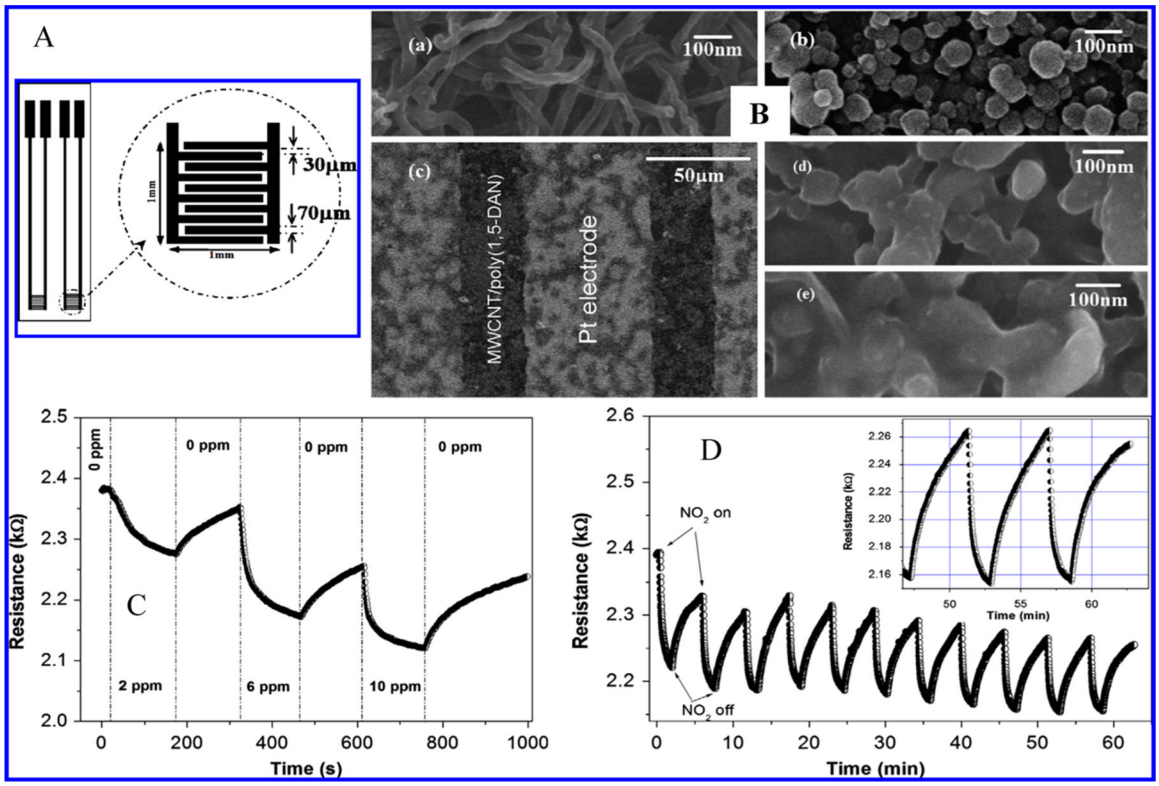

Figure 20.

(A) Structure of the IDE electrode, (B) SEM images: MWCNT (a), poly(1,5-DAN) (b), surface of the film IDE/MWCNT/poly(1,5-DAN), and (c) surface morphologies of MWCNT/poly(1,5-DAN) at 10 cycles (d) and at 25 cycles (e). (C) Response of the IDE/MWCNT/poly(1,5-DAN) film formed with 10 polymerization cycles to different concentrations of NO_2. (D) Response−recovery cycles of the IDE/MWCNT/poly(1,5-DAN) film formed with 10 polymerization cycles to 5 ppm of NO_2 and pure air; the inset depicts the last cycles. Reprinted with permission from ref 178. Copyright 2013 Elsevier.

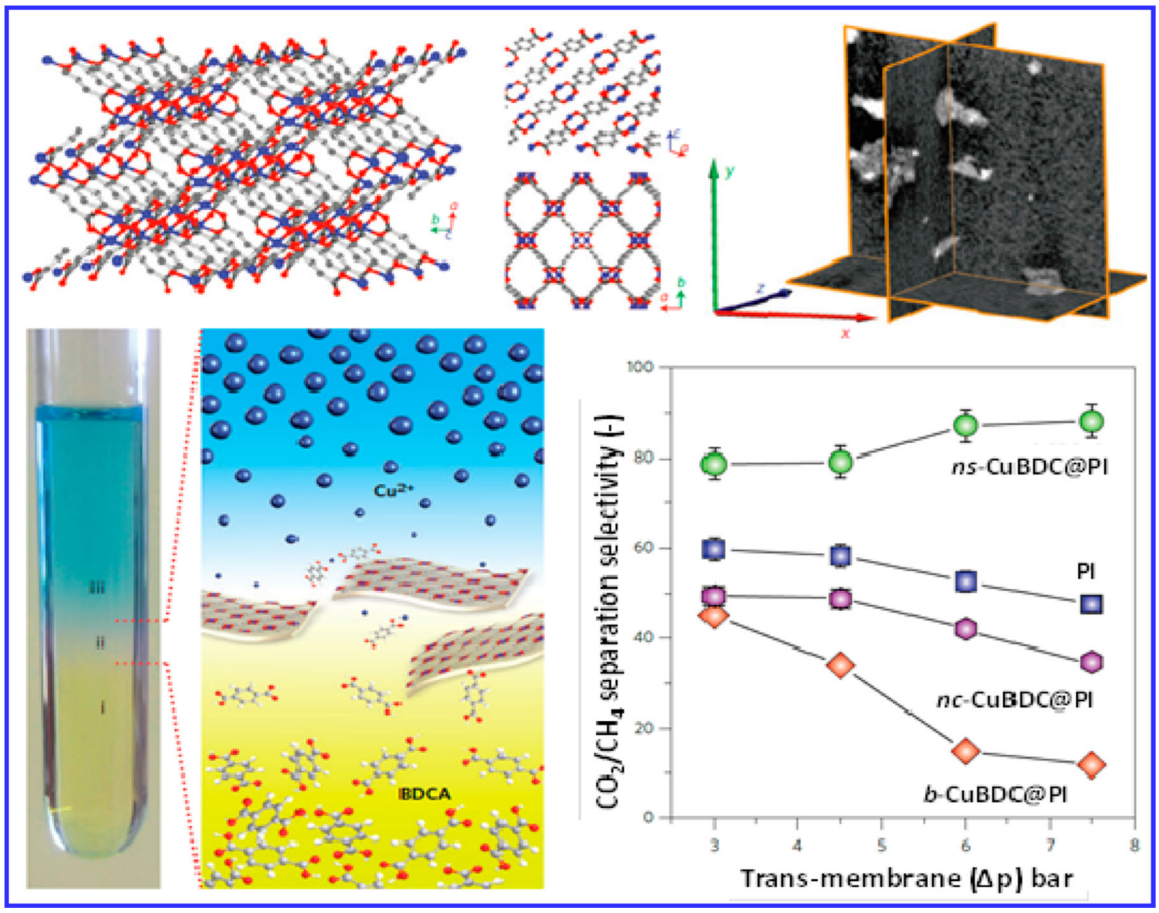

Figure 21.

(A) 3D crystalline structure of CuBDC MOF. (B) Spatial arrangement of different liquid layers during the synthesis of CuBDC MOF nanosheets, (i) corresponds to a benzene 1,4-dicarboxylic acid (BDCA) solution, (ii) the solvent spacer layer, and (iii) solution of Cu_2C ions, respectively. (C) 3D-reconstructed FIB−SEM tomogram of a MOF−polymer composite. (D) CO_2 separation performance of a MOF membrane with reference to a standard membrane of polyamide (PI).[183] Reprinted with permission from ref 183. Copyright 2014 Nature Publishing Group.

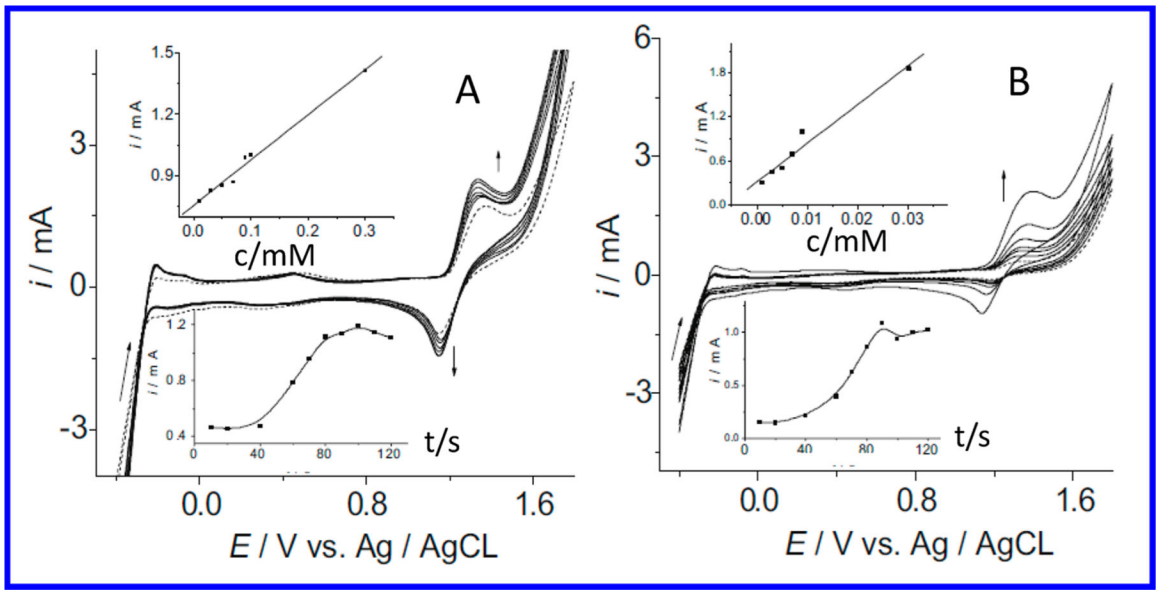

Figure 22.

(A) CVs of CO (0.01, 0.03, 0.05, 0.07, 0.09, 0.3, 0.5, and 0.7 mM) at Pt/PAN/MWCNTs/WGE; the upper inset depicts the dependence of reduction peak currents of CO on the concentration. The lower inset shows the accumulation effect of 0.1 mM CO at Pt/PAN/MWCNTs/WGE. (B) CVs of CO (1.0, 3.0, 5.0, 7.0, 9.0, 30.0, and 50.0 μm) at Pt−Ni/PAN/MWCNTs/WGE made in solution concentration ratio of Pt−Ni of 1:1 using constant potential and CV step; the upper inset shows the dependence of oxidation peak currents of CO on the concentration. The lower inset shows the accumulation effect of 0.1 mM CO at Pt−Ni/PAN/MWCNTs/WGE. Buffer: 0.5 M $HClO_4$. Scan: 50 mV s^{-1}. Reprinted with permission from ref 189. Copyright 2009 Elsevier.

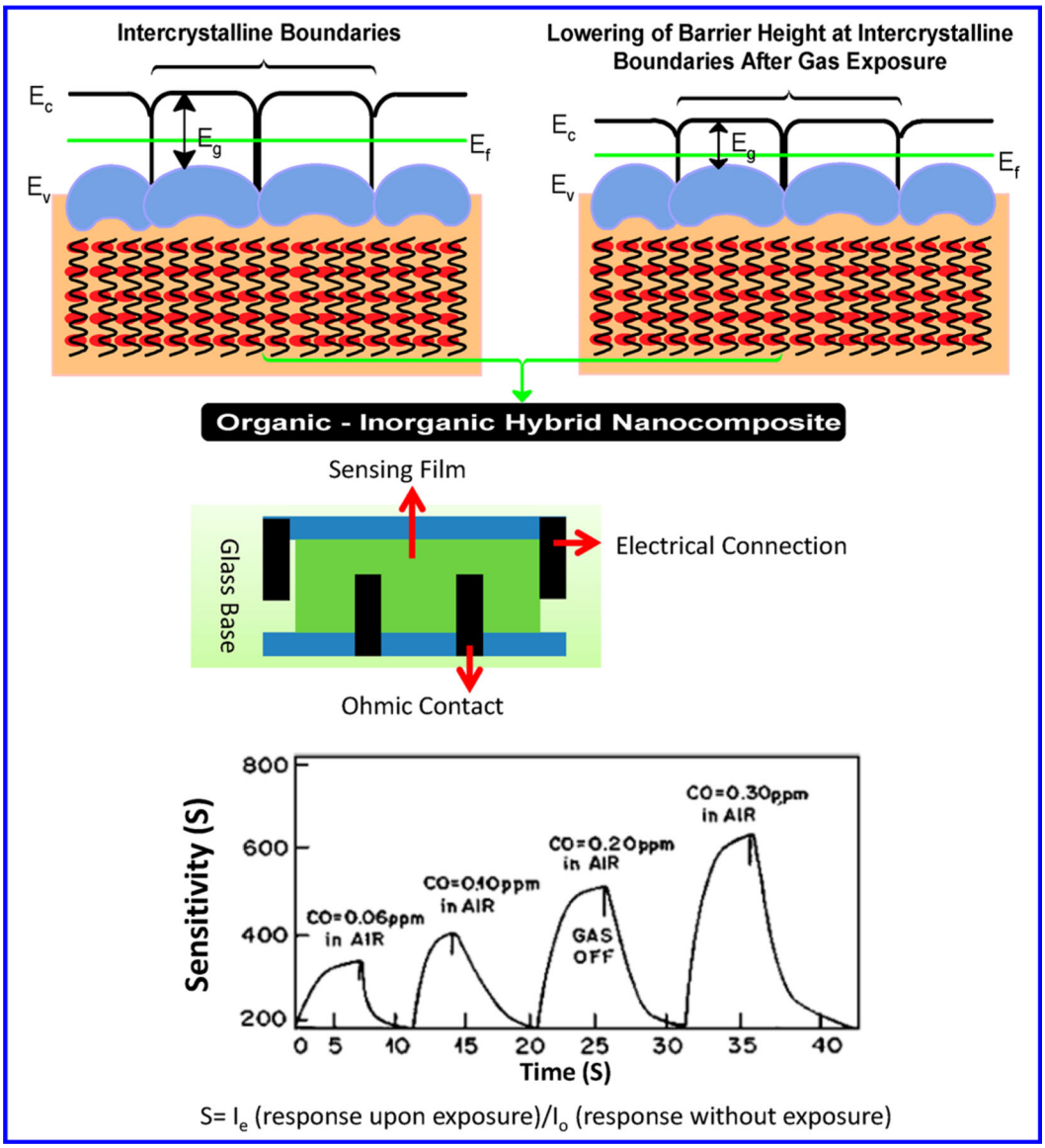

Figure 23.

Effect of CO gas on an organic−inorganic hybrid nanocomposite surface. Reprinted with permission from ref 81. Copyright 2004 Elsevier.

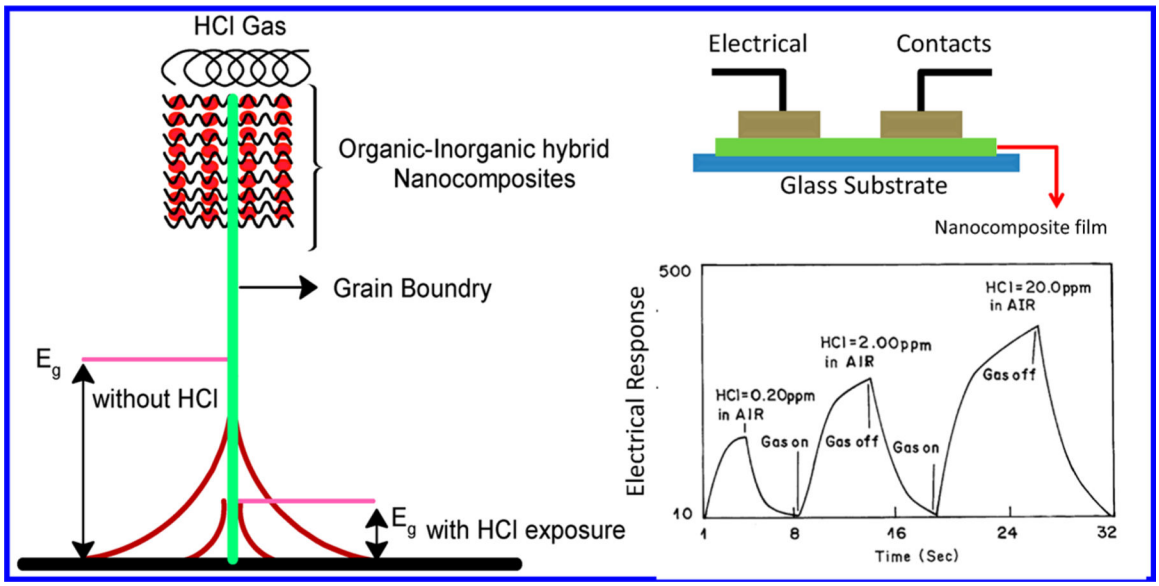

Figure 24.

(A) Schematic structures of the Co(III)VXG and Co(IV)VXG host−guest materials. (B) Wireframe structural representation of the cationic Co(IV)TRPyP and Co(III)TRPyP species. The respective chloride salts were used for the preparation of the host−guest nanocomposites with VXG. (C) AFM images of Co(III)VXG (a) and Co(IV)VXG (b) films on mica substrates in a more densely packed region and at the Co(III)VXG film edge. (D) Plot of R/R_0 as a function of the percentage of water (v/v) in ethanol/water mixtures, for IDE Co(III)VXG and Co(IV)VXG sensors. Inset: plot of ln(1 – R/R_0) vs (% water). Reprinted with permission from ref 207. Copyright 2010 Elsevier.

Table 1.

Gas Sensing Characteristics of Various Hybrid Nanocomposite Systems

sensing platform	sensing characteristics	ref
[NSP] PANI-CNF	[A] food-borne pathogens	208
[R] resistance change	*Bacillus cereus*, *Vibro Parahemolyticus* and *Salmonella*	
[FT] film via drop-coating	[Rm] operate at room temperature and better than metal oxides	
[NSP] PANI-Al diodes	[A] CH_3OH	121
[R] I−V/C-V change	[Rm] CH_4 decreases the reverse bias current and increases barrier height	
[FT] electrochemically		
[NSP] dye-doped silica	[A] CH_3OH	93
[R] fluorescence intensity	[DL] 150 ppm	
[FT] self-assembled sol–gel	[Rm] interaction of gas generates the energy transfer complex and intensity decreases on increasing dose	
[NSP] polysiloxanes-Zn/Ni/Eu	[A] mixtures of VOCs	132
[R] frequency shift	[L] 20–40 ppb	
[FT] spin coated onto quartz crystal	[DL] 0.3 ppb [Rm] good detection range but has sensitivity problems	
[NSP] Cu-PANI	[A] $CHCl_3$	130
[R] resistance change	[L] 10–100 ppm	
[FT] chemical oxidative polymerization	[DL] 10 ppm [S] 1.5–3.5 [Rm] resistance changes due to protonation and deprotonation	
[NSP] PVB-Fe_2O_3, PVB-MnO_2	[A] mixtures of VOCs	124
[R] resistance change	[L] 0–5000 ppm	
[FT] chemical oxidative polymerization	[S] sensor of composition 75 Fe_2O_3/25 MnO_2 mol %; shows maximum sensitivity to propanol and toluene [Rm] sensor is not sensitive to CH_3CH_2OH, $CHCl_3$ or C_6H_{14}	
[NSP] PVB-NiO_2/Fe_2O_3	[A] mixtures of VOCs	125
[R] resistance change	[DL] 4000 ppm for $C_6H_5CH_3$ and CH_3CH_2OH	
[FT] self-casting	[Rs] 30 s for CH_3CH_2OH and 40s $C_6H_5CH_3$ [Rs] 45 for CH_3CH_2OH and 48 for $C_6H_5CH_3$ [Rm] response is crystalline-size-dependent but shows response to many VOCs	
[NSP] Au-polyamide	[A] VOCs	138
[R] optical sensor	[DL] 6000 ppm for CH_3OH, 6000 ppm for CH_3CH_2OH	

Chem Rev. Author manuscript; available in PMC 2023 May 31.

sensing platform	sensing characteristics	ref
[FT] glow discharge vapor deposition	[Rm] Au-polyamide (5×10^{16} Au^{+} cm^{-2}) implanted film exhibits interesting optical properties but uses complex technique for response measurement.	
[NSP] PPy-MoO_3	[A] CH_3CH_2OH	139
[R] resistance change	[DL] 0.3%	
[FT] vapor polymerization	[Rs] 2100 s [Rm] resistance of nanocomposite increases on increasing gas dose but operation at high temperature is a major issue	
[NSP] PANI-Ag	[A] CH_3CH_2OH	140
[R] resistance change	[L] 20–225 ppm	
[FT] ultrasound-assisted in situ polymerization then spin-coating	[DL] 100 ppm [Rs] 5–6 min [Rm] response and reaction time is Ag concentration dependent	
[NSP] chitosan-CNTs	[A] CH_3CH_2OH	141
[R] change in conduction	[L] 0–100%	
[FT] layer-by-layer deposition	[DL] high response at 70% [Rm] diffusion of gas leads to tunneling	
[NSP] PDDAC-SnO_2	[A] CH_3CH_2OH	209
[R] change in resistance	[L] 10–200 ppm	
[FT] patterning onto IDEs	[DL] 10 ppm [SL] 60 d [Rs] 88 s [Rm] room-temperature operation, selective and stable sensor; suitable for device fabrication	
[NSP] P3HT/Ng-ZnO	[A] CH_3CH_2OH	210
[R] change in resistance	[L] 50–1000 ppm	
[FT] drop casting	[DL] 50 ppm [Rs] 11 s [Rm] P3HT:0.75 mol % Nb/ZnO sensor exhibited room-temperature sensing; stability and selectivity need to be explored	
[NSP] PANI-Pd	[A] aliphatic alcohols	142
[R] resistance change	[S] 8.9×10^5 Ω/ppm for propanol	
[FT] oxidative polymerization	[DL] 10 ppm [SL] 110 d [Rs] 2 to 12 s [Rm] sensing mechanism depend on size of gas molecule, which affects the barrier height in diffusion	
[NSP] PANI-MoO_3	[A] HCHO and CH_3CHO	134
[R] electrical resistivity	[D] 50 ppm	
[FT] chemical vapor deposition	[T] 30 °C [Rm] PANI used for signal amplification, and gas exposure affects the charge conduction in nanocomposites	
[NSP] PNMA-MoO_3	[A] HCHO and CH_3CHO	135

sensing platform	sensing characteristics	ref
[R] electrical resistivity	[L] 1–10 ppm	
[FT] chemical vapor deposition	[Rm] response is dependent on interlayer space and detailed analysis of sensing characteristics is lacking	
[NSP] PoANIS-MoO_3	[A] HCHO and CH_3CHO	136
[R] electrical resistivity	[Rm] fabricated sensor has less impurity and exhibits relative sensing performance	
[FT] chemical vapor deposition		
[NSP] PANI-TiO_2	[A] $N(C_2H_5)_3$	131
[R] electrical resistivity	[S] 5.14×10^{-7} mol mL^{-1}	
[FT] spin-coating onto interdigitated electrode	[Rs] 3 min [Rm] protonation- and deprotonation-based sensing, also dependent on TiO_2 concentration; sensing characteristics could be improved	
[NSP] PANI-WO_3	[A] H_2	122
[R] surface acoustic wave	[DL] 7 kHz for 1% H_2	
[FT] sol−gel technique	[L] 0–1% [Rm] sensor is sensitive and reproducible at room temperature over an interval of 5 d; other parameters are not related	
[NSP] PANI-anantase TiO_2	[A] H_2	211
[R] change in resistance	[S] 1.63	
[FT] chemical oxidative polymerization	[L] 0.4–1.0 vol % [DL] 0.8 vol % [Rs] 83 s, [Rv] 130 s [Rm] I−V of sensor exhibited an ohmic characteristic; band gap theory on gap adsorption and desorption is proposed in this work; the stability, selectivity and industrial applications should be explored	
[NSP] PP-AN-ZnO_2	[A] O_2	123
[R] conduction change	[S] 16.6 ppm	
[FT] plasma polymerized	[T] 150 °C [Rs] 3 s [Rm] UV exposure generates photocurrents resulting in increased free electron−hole pair that reduces the electron depletion region	
[NSP] polymer-Sb-SnO_2	[A] HCHO	133
[R] conduction change	[L] 10–50 ppm	
[FT] template sol−gel	[T] 136 °C [DL] 10 ppm [Rm] shows better sensing parameters	
[NSP] P3HT-ZnO-based OTFT	[A] HCHO	212
[R] change in resistance	[L] 10–150 ppm	
[FT] spray deposition	[DL] 4 ppm [SL] 15 d	

sensing platform	sensing characteristics	ref
	[Rs] [Rm] OTFT-based room-temperature HCHO sensor; sensitivity, response time, and sensitivity was not explained	
[NSP] PANI-CNTs	[A] HCHO, $CHCl_3$, CH_3OH, $C_6H_5CH_3$, H_2O	137
[R] chemoresistive	with flow rate 100 cm^3 min^{-1} to 50 ppm	
[FT] oxidative dispersive polymerization	[Rm] effect of precursor concentration of VOC sensor has been discussed but this research lacks selective detection of VOCs	
[NSP] Pd/Ni-poly(EDOT-*co*-TAA)	[A] CH_3COCH_3 and $C_6H_5CH_3$	126
[R] resistance change	[L] 0–1800 ppm	
[FT] wet chemical route	[DL] 50 ppm for CH_3COCH_3 in case of Pd based sensor [DL] 10 ppm for $C_6H_5CH_3$ in case of Ni based sensor [Rs] 60–70 s for CH_3COCH_3 [Rs] 200–300 s for $C_6H_5CH_3$ [Rm] fabricated sensor is thickness-dependent (optimized thickness ~50 nm)	
[NSP] PANI-SnO_2	[A] C_6H_6 and $C_6H_5CH_3$	213
[R] thermogravimetric	PANI-SnO_2 (40%) nanocomposite exhibited maximum response to C_6H_6 (16.9%) and $C_6H_5CH_3$ (19.5%)	
[FT] in situ chemical oxidative polymerization	[Rm] presented research work is only a proof of the concept	
[NSP] PANI-SnO_2	[A] C_6H_6 and $C_6H_5CH_3$	214
[R] change in voltage	PANI-SnO_2 (40 wt %)-based sensor (10% sensor efficiency) was found more sensitive for C_6H_6	
[FT] physical grinding	[Rm] sensing performance was not explored.	
[NSP] PANI-MWCNTs	[A] hydrocarbons	120
[R] resistance change	[DL] ppm level and maximum sensitivity at 1000 ppm	
[FT] electrochemical polymerization	[Rm] polarity of the aromatic hydrocarbons was found to be responsible for the response; however, sensing parameters could be improved	
[NSP] MWCNTs-PMMA	[A] chloroform, methanol, toluene, and water	144
[R] resistance change	[Rm] sensor is selective for methanol; CNT network in PMMA resulted in a high surface area, increasing conducting network sensitivity by ~240%	
[FT] layer-by-layer deposition		
[NSP] CdSe-ZnSe and PS−PSMA	[A] THF and DMF	128
[R] resistance change	[L] 0–1000 ppm	
[FT] electrospun technique	[Rs] ~1 s [SL] 6 months [Rm] sensor found to be sensitive to chloroform and THF	
[NSP] PPy-Ag-GO	[A] H_2O_2	215
[R] amperometric	[S] 0.085 (S/N of 3)	
[FT] electrochemical polymerization	[L] 0.1–5 mM [DL] 1.009 mM	

Chem Rev. Author manuscript; available in PMC 2023 May 31.

sensing platform	sensing characteristics	ref
	[SL] 21 d [Rs] [Rm] sensor is nonenzymatic and found to be selective	
[NSP] Fe:Al-PANI	[A] HCl	82
[R] resistance change	[L] 0.1–80 ppm	
[FT] vacuum evaporation deposition	[Rs] ~10 s [S] 400–8000 [Rm] exploration of vacuum-evaporation-deposited nanostructured films for gas sensor applications; sensing mechanism was explained on the basis of the energy band gap theory	
[NSP] CNF-PPy	[A] NH_3 and HCl	148
[R] resistance change	[L] 10–50 ppm	
[FT] vapor deposition polymerization	[DL] 10 ppm for NH_3 and 20 ppm for HCl [Rm] sensor is reproducible and reversible; sensing characteristics are thickness-dependent and based on protonation and deprotonation	
[NSP] TiO_2-TMPyP	[A] HCl	149
[R] resistance change	[T] 80 °C	
[FT] glancing-angle physical deposition technique	[DL] 0.1 ppm [Rs] 51 s [Rv] 300 s [DL] 10 ppm for NH_3 and 20 ppm for HCl [Rm] sensor exhibits enhanced sensing characteristics	
[NSP] poly(*p*-xylene)-Pb	[A] NH_3	216
[R] resistance change	[Rm] current change was measured at 13 ppm with time	
[FT] vacuum deposition technique		
[NSP] PPy-SWCNTs	[A] NH_3	157
[R] electrical resistance	[L] 10–800 ppm	
[FT] chemical polymerization	[Rs] 22 s [Rv] 38 s [T] 25 °C [Rm] fabrication parameters were optimized for 150 ppm of NH_3	
[NSP] PPy-Pd	[A] NH_3	158
[R] electrical resistance	[L] 50–2000 ppm	
[FT] vapor phase polymerization	[Rs] 14 s [Rv] 148 s for 1000 ppm [Rm] response magnitude ~13.9–58.9; sensor is selective and response is dependent on size and concentration of Pd	
[NSP] PANI-Au	[A] NH_3	161
[R] electrical resistance	[L] 0–1600 ppm	

Chem Rev. Author manuscript; available in PMC 2023 May 31.

sensing platform	sensing characteristics	ref
[FT] self-assembled onto polystyrene sheet	[Rs] 5 s [Rv] 7 s for 100 ppm [Rm] response results were found to be enhanced	
[NSP] PANI-CNT	[A] NH_3	159
[R] electrical resistance	[DL] 50 ppb	
[FT] self-assembled onto polystyrene sheet	[L] 0–100 ppm [Rm] sensing mechanism is based on protonation and deprotonation and obtained response is improved but stability is an issue here	
[NSP] Au/CNT-PANI	[A] NH_3	162
[R] electrical resistance	[DL] 200 ppb	
[FT] in situ polymerization	[L] 200 ppb to 10 ppm [SL] a few days [Rm] sensor is reproducible and sensitive	
[NSP] PANI-TiO_2	[A] NH_3	156
[R] electrical resistance	[DL] 23 ppm	
[FT] self-assembled onto interdigited electrode of Si	[L] 23–114 ppm [SL] 30 days [Rm] TiO_2 nanoparticles result in improved electrical and morphological properties in nanocomposites resulting in enhanced sensing	
[NSP] PANI-TiO_2	[A] NH_3	164
[R] electrical resistance	[DL] 50 ppt	
[FT] layer-by-layer self-assembly	[L] 23–114 ppm [SL] 30 days [Rm] TiO_2 nanoparticles improve the electrical (via affecting conduction) and morphological properties in nanocomposites, resulting in enhanced sensing	
[NSP] PANI-TiO_2/SnO_2/In_2O_3	[A] NH_3	156
[R] electrical resistance	[DL] 23 ppm	
[FT] in situ self-assembled	[L] 23–114 ppm [SL] 30 days [Rm] PANI-TiO_2 nanocomposite found to be suitable for NH_3 sensing	
[NSP] PANI-MWCNT/SWCNT	[A] NH_3	154
[R] electrical resistance	[DL] 0.5 ppm	
[FT] in situ self-assembled	[Rm] this report focused on material science prospects and applications in gas sensor development	
[NSP] PANI-ZnO	[A] NH_3	217
[R] change in resistance	[L] 25–100 ppm	
[FT] template approach	[Rm] sensing material preparation was optimized to perform NH_3 sensing	

sensing platform	sensing characteristics	ref
[NSP] CeO_2@PANI	[A] NH_3	218
[R] change in resistance response	[L] 60.5–50 ppm	
[FT] change in resistance	[DL] 25 ppm [SL] 15 d [Rs] 57 s [Rm] researchers explored related band gap diagram; developed sensor was found to be sensitive, repeatable, and selective	
[NSP] guar gum-Ag	[A] NH_3	219
[R] change in current	[S] 1.5 fold	
[FT] wet chemistry routes	[L] 500 ppt to 1300 ppm [DL] 500 ppt [SL] 90 d [Rs] 50 s [Rm] sensor exhibited lowest detection limit	
[NSP] PPy-Fe_2O_3	[A] H_2S	173
[R] electrical resistance	[Rm] PPy-Fe_2O_3 annealed at 150 °C and found to be sensitive to H_2S	
[FT] in situ self-assembled		
[NSP] PPy-Au	[A] H_2S	168
[R] chemoresistive	[DL] 0.1 ppb	
[FT] electrochemical polymerization	[L] 0.1–100 ppb [Rm] fabricated sensor exhibits superior characteristics to those of PANI-based sensing; however, sensing mechanism is not well explained	
[NSP] PPy-WO_3	[A] H_2S	220
[R] relative change in resistance	[S] 83%	
[FT] in situ polymerization	[L] 100 ppb [DL] 100–1000 ppb [SL] 54 d [Rs] 6 min, [Rv] 210 min [Rm] PPy-WO_3 (0.5 g doping) showed better sensing than PPy and WO_3 based sensors	
[NSP] PETH-WO_3	[A] H_2S	221
[R]	[L] 5–200 ppm	
[FT] nanosheet of WO_3 synthesized using hydrothermal	[DL] 2 ppm	
nanocomposite synthesized using in situ polymerization	[Rv] 15 s [Rm] developed sensor exhibited low detection limit and extremely rapid recovery time; the sensitivity and shelf life of sensor was not discussed	
[NSP] Cu phthalocyanine-polymer	[A] NO_2	222
[R] adsorption resistive	[Rm] this report explains that the nanocomposite system shows improved properties over that of parent material	
[FT] plasma-activated or laser vacuum technique		

sensing platform	sensing characteristics	ref
[NSP] PEDT-SnO_2	[A] NO_2	110
[R] resistance change	[L] 10–800 ppb and 100–200 ppm	
[FT] layer-by-layer deposition	[S] more than 2 order [Rm] SnO_2-based composite shows better properties than TiO_2-based sensor due to excellent change in conductivity at room temperature; however, there is scope to improve sensing performance	
[NSP] PANI-Au-Nafion	[A] NO_2	176
[R] amperometric	[L] 0–100 ppm	
[FT] CV technique	[S] 3.04 μA/ppm [Rm] this electrochemical sensor exhibits high BET surface and could be used as an electronic nose	
[NSP] PVC-Au	[A] NO_2	177
[R] solid-state electrochemical	[L] 0.6–2.6 ppm (v/v)	
[FT] self coating	[S] 333 nA/ppm [DL] 50 ppb [Rs] 50 s [SL] 30 days [Rm] this sensor exhibits better properties than Nafion-based sensor for NO_2 detection	
[NSP] polymer-Au/ITO	[A] NO_2	109
[R] amperometric	[DL] 1 nM and working potential is very low	
[FT] self coating	[Rm] sensor can be attached to microfluidic devices to detect pathogens and for drug testing	
[NSP] CLPANI-WO_3	[A] NO_2	52
[R] resistance	[S] 4	
[FT] vacuum evaporation deposition	[Rm] mainly focused on nanocomposite fabrication; this report is lacking in detailed discussion of sensing parameters	
[NSP] CH-*co*-PANI-WO_3	[A] NO_2	223
[R] resistance	[L] 100–500 ppb	
[FT] electrochemical polymerization	[Rs] 8 s [SL] 84 days [Rm] this report lacks description of the related sensing mechanism	
[NSP] PPy-NiO	[A] NO_2	224
[R] resistance response	[L] 10–100 ppm	
[FT] spin coating	[DL] 10 ppm [SL] 30 d [Rs] 129–49 s at 100 ppm [Rm] PPy-NiO (50%) exhibited highest sensitivity	
[NSP] PPy-αFe_2O_3	[A] NO_2	225
[R] resistance change	[S] 56%	

Chem Rev. Author manuscript; available in PMC 2023 May 31.

sensing platform	sensing characteristics	ref
[FT] spin coating	[L] 10–100 ppm [DL] 10 ppm [SL] 40 d [Rs] 89 s, [Rv] 4205 s [Rm] sensing performance was compared with PPy- and WO_3-based NO_2 sensors	
[NSP] PPy-WO_3	[A] NO_2	226
[R] impedance change	[L] 5–100 ppm	
[FT] solid state synthesis	[DL] 5 ppm [SL] 20 d [Rm] response-recovery time and sensitivity of presented sensor is not discussed	
[NSP] PPy-ZnO_2	[A] NO_x	173
[R] resistance	[Rm] PPy (10%)-ZnO shows maximum sensitivity at 1000 ppm.	
[FT] electrochemical polymerization		
[NSP] polythiophene-SnO_2	[A] NO_2	174
[R] resistance	[L] 0–200 ppm	
[FT] in situ chemical oxidative polymerization	[T] 90 °C [Rm] sensor is very selective, improved properties are due to the high surface area of the hybrid nanocomposite	
[NSP] PEBAX-SiO_2	[A] CO_2	182
[R] resistance	[Rm] this sensor explains the effect of CO_2 on the activation energy on nanocomposite	
[FT] sol−gel technique		
[NSP] PANI-Fe:Al	[A] CO_2	81
[R] resistance	[L] 0.006–0.3 ppm	
[FT] vacuum evaporation technique	[Rs] 10 s [S] 400–600 [Rm] this is a very promising sensor for technological applications, wherein CO_2 reduces the barrier height at the intercrystalline grain boundary	
[NSP] PANI-SiO_2 and PANI-TiO_2	[A] CO_2	188
[R] resistivity change	[L] 0–1000 ppm	
[FT] coating onto interdigitated electrode	[S] 400–600 [Rs] 20 s [Rv] 250 s [Rm] this sensor was found to be suitable for online monitoring of CO_2	
[NSP] PANI-zeolite	[Rm] research explains the effect of pore size on sensing	187
[R] resistivity change		
[FT] heterogeneous mixing		
[NSP] PANI-Pt/Ni	[A] CO_2	189

sensing platform	sensing characteristics	ref
[R] resistivity change	[L] 0.001–0.7 mM for oxidation peak	
[FT] electrochemical polymerization	[L] 1–50 mM for reduction current [Rm] maximum sensitivity observed at 0.01 mM and the enhanced electrocatalytic property is due to bifunctional catalysis	
[NSP] PPy-Fe_3O_4	[A] H_2O	196
[R] resistivity change	[Rm] this composite shows maximum sensitivity for humidity but also less sensitivity to CO_2, N_2, and O_2; selectivity is a major issue	
[FT] electrochemical polymerization		
[NSP] PANI-TiO_2	[A] H_2O	135
[R] activation energy	[Rs] 20 s	
[FT] electrochemical polymerization	[Rv] 40 s [T] 35 °C [Rm] the sensor shows improved sensitivity	
[NSP] PMAPTAC/PPy-Fe_3O_4	[A] H_2O	136
[R] resistivity change	[Rm] the fabricated sensor shows further enhanced sensitivity and flexibility	
[FT] electrochemical polymerization		
[NSP] NaPSS-ZnO	[A] H_2O	204
[R] impedance	[L] 11–97%	
[FT] electrochemical polymerization	[DL] 2% [Rs] 20 s [Rm] obtained sensing is improved. ZnO facilitates the adsorption and desorption of gas on nanocomposite surface	
[NSP] PANI-Ag	[A] H_2O	205
[R] optical fiber based	[L] 5–95%	
[FT] chemical oxidative polymerization	[Rs] 30 s [Rv] 90 s [Rm] sensor exhibits reversible behavior at 1% humidity	
[NSP] PANI-WO_3	[A] H_2O	201
[R] resistivity	[L] 10–95%	
[FT] heterogeneous mixture pallet	[Rs] 30 s [Rv] 90 s [Rm] humidity increases the conductivity of the nanocomposite due to increased hole concentration; detailed studies of R_s, hysteresis, etc. are lacking	
[NSP] POA−WO_3	[A] humidity	200
[R] resistivity	[SL] 30 d	
[FT] heterogeneous mixture pallet	[Rm] optimized nanocomposite shows % response factor as 353 at 85% humidity; however studies of other parameters are not discussed	
[NSP] polyMAPTAC−SiO_2	[A] H_2O	202

sensing platform	sensing characteristics	ref
[R] electrical resistance	[L] 10–90%	
[FT] sol−gel technique	[S] the obtained response magnitude is 3 orders higher than polymer [Rm] the activation energy for conduction was found to be reduced when OH is adsorbed onto nanocomposite	
[NSP] PEP−$CoCl_2$	[A] H_2O	227
[R] electrical resistance	[Rm] this sensor was used for real-time analysis and exhibits reversible behavior and longer stability	
[FT] spin-coated electrodes		
[NSP] PDDA−CNT	[A] H_2O	203
[R] electrical resistance	[L] 20–98%	
[FT] layer-by-layer self-assembly	[Rm] fabricated sensor lacks detailed analysis of sensing characteristics	
[NSP] $[Ru(bipy)_2Cl]^+$−V_2O_5 xerogel	[A] H_2O	207
[R] electrical resistance	[L] 0–10%	
[FT] spin-coated electrodes	[T] 23 °C [Rm] sensor used for low levels of humidity detection	

Chem Rev. Author manuscript; available in PMC 2023 May 31.